5. Blast design management

Helsinki Conference Proceedings 2019, R. Holmberg et al

Influence of the loading and support conditions on the ultimate capacity of columns to resist the effects of near - field explosions

F. Dinu
Department of Steel Structures and Structural Mechanics, Politehnica University Timisoara, Romania
Laboratory of Steel Structures, Romanian Academy, Timisoara Branch, Romania

I. Marginean
Department of Steel Structures and Structural Mechanics, Politehnica University Timisoara, Romania

R. Laszlo, E. Ghicioi & A. Kovacs
Department Safety of Explosives and Pyrotechnical Articles, National Institute for Research and Development in Mine Safety and Protection to Explosion – INSEMEX Petroşani, Romania

ABSTRACT: Explosions may have severe consequences on the integrity of structural or non-structural elements of a building. Being considered events with a low probability of occurrence, they are not considered directly in the design, except in certain special situations (accidental design situations). In the case of deliberate attacks, placing explosive devices at short distances or even attached to building elements can cause major local failures. Local failure and potential loss of load carrying capacity are dependent on local conditions in the structural elements (load and end support conditions, mechanical properties of material). The paper presents the results of recent research carried out on the response of steel building frames under blast loading. The data of the experimental testing, combined with the numerical modelling, allowed to investigate the local failure mechanism in the elements and the global response of the structure to the applied blast load.

1 INTRODUCTION

The capacity of a structure to resist a variety of extreme events without being damaged to an extent disproportionate to the original cause is called robustness and is required by design codes and standards. Raising awareness concerning these risks requires adequate measures during the design and construction of building structures. Explicit analysis and design that accounts for the possibility of an explosion can pose difficulties (compared to other types of design), both in terms of load assessment (i.e. the maximum value of the resultant pressure, or its variation, on elements or structures) and the effects on materials and elements, such as the effect of the loading rate on the mechanical characteristics of steel or explosion–structure interaction. As the stand-off

distance from the explosion decreases, the effects on the building become more complex. In such a case, the use of numerical analysis may lead to more accurate results, especially when results are validated by experimental data. As very few experimental studies have been carried out on the resistance to blast of framed buildings, there is a high interest in such investigations. A more convenient approach is the Alternate load path method (APM), where for simplicity it is assumed that one column is lost due to explosion, then the capacity for carrying the redistributed loads is checked. However, it is not yet well established if APM is representative of all types of explosive threats.

The paper presents the results of recent research carried out in the FRAMEBLAST project (2017-2018) on the safety of building structures under extreme actions. A two-bay, two-span, and two-story steel frame building was tested for different blast loading conditions to evaluate the consequences of near field explosions on the structural elements. The experimental data were combined with the numerical modelling to investigate the residual capacity of steel columns and the potential for progressive collapse resulting from such extreme loading. Numerical modelling was done with Extreme Loading for Structures ELS.

2 EXPERIMENTAL BLAST TESTING

The steel frame building model has been constructed in an explosive testing site. The steel frame building has two bays, two spans, and two stories (Figure 1). The bays and spans measure 4.5 m and 3.0 m, respectively, while stories are 2.5 m high each. The structural system is made of moment resisting frames on the x-direction (transversal direction), while on the y-direction

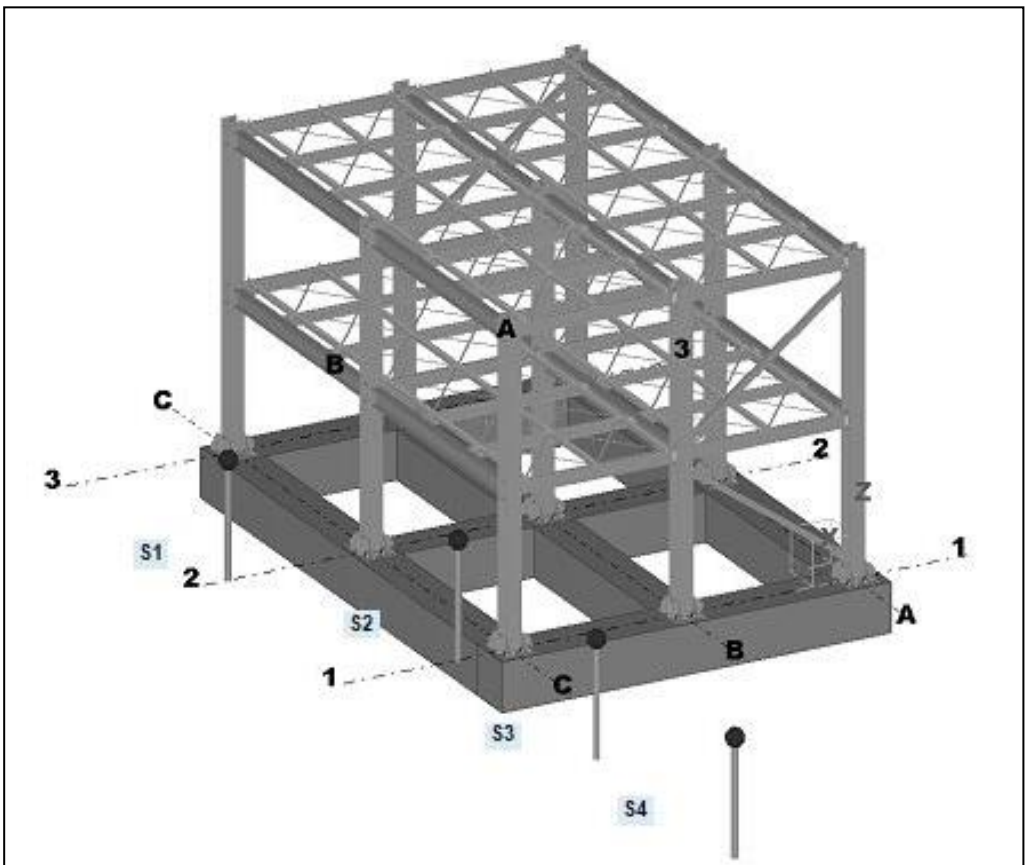

Figure 1a. Overview of the steel frame specimen - 3D geometry, with the position of pressure sensors S1-S4.

(longitudinal direction) concentrically braces are introduced in each frame. The secondary beams are spaced at 1.5 m intervals. The extended end-plate bolted beam-to-column connections at the moment resisting frames are designed as fully rigid and fully restrained connections using M24 gr.10.9 bolts on a 16 mm thick end plate. Secondary beam-to-column connections and secondary beam-to-main beam connections are pinned. The column bases are welded to steel plates bolted to reinforced concrete girders that constitute the foundations of the structure. These connections are fully rigid and restrained. The design of the structure was done considering the seismic design condition, combining the permanent actions (dead load D = 5 kN/m2), the variable actions (live load L = 4 kN/m2) and the seismic action (low seismicity, horizontal acceleration = 0.10 g). Horizontal and vertical tying requirements for accidental design situation were also verified using EN 1991-1-7 provisions.

The design resulted in HEB260 section for columns, IPE270 section for main beams, IPE200 section for secondary beams between columns, and IPE180 section for intermediate secondary beams. Note that structural steel in beams, columns, and plates is S275 (yield strength of 275 N/mm2) and bolts are class 10.9 (ultimate strength of 1000 N/mm2).

Four pairs of sensors have been used for pressure measurements at four different locations near the structure (see Figure 1a):

- 1st location: 2.5 m from the middle perimeter column C2, and collinear with the explosive charge (S1);
- 2nd location: in front of the corner column C1 and in line with the explosive charge (S2);
- 3rd location: 4.5 m away from the 2nd location and in line with the explosive charge (S3);
- 4th location: 4.5 m away from the 3rd location and in line with the explosive charge (S4).

Strain gauges were arranged on the structural elements to measure the history of strains in the elements, that is, columns (web, flanges), beams (web, flanges) and the end plates of the beams at the beam-column joints. A total station was also used to measure global deflections in 20 different locations. 14 tracking marks were tagged on the front frame (R1 to R14), and six on the left side

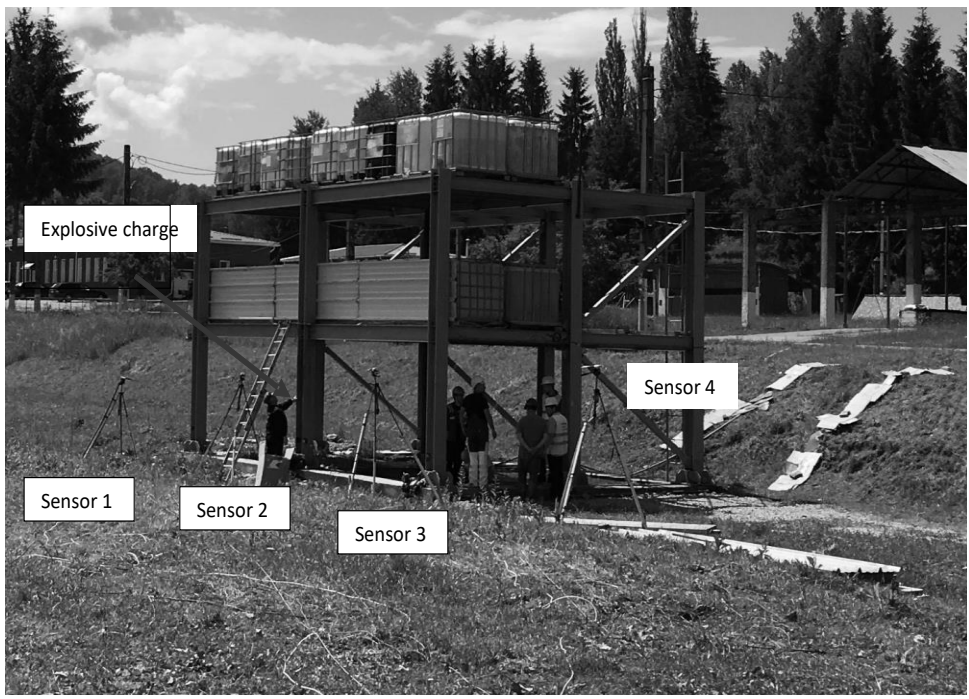

Figure 1b. Overview of the steel frame specimen, photo before testing.

frame (L1 to L6). Two high-speed cameras were used to record and analyse the blasting events. Before testing, gravity loads with an equivalent load of 7.5 kN / m2 were placed on the floors. Note that the loads were added only on the first bay (B-C/1-3). During the loading process, strains and deflections were measured in the points indicated in the previous section. With the structure loaded, eight blast tests were performed on the structure, but only the first 6 tests are reported here. The details are given in Table 1.

Table 1. Blast testing, with mass and position for charges E1 to E6.

Test name	Charge mass [g]	Distance, D [mm]	Height, H [mm]
E1	286	500	1750
E2	572	500	1750
E3	1144	500	1750
E4	2288	500	1750
E5	2288	200	1750
E6	2574	200	1750

Note:
- Distance D is measured from the front face of the central perimeter column C2
- Height H is measured from the column base plate

Tests E1 and E2 did not produce any plastic deformations in the steel members (column, beams). Following the E3 test, residual deformations were measured at the level of the column web and flanges. Test E5 produced the first fracture in the column web (Figure 2a). Residual out of plane deformations were also recorded (Figure 2b). Test E6 completely removed a large part of the column web and caused large distortions of the section and continuity plates in the beam-column joint above the point of detonation (Figure 2c). Figure 3 presents the wave propagation around the structure for tests E6.

3 NUMERICAL MODELLING OF SITE EXPLOSION

The numerical analyses were performed using Extreme Loading for Structures (ELS) software. The experimental data obtained from the blast tests were used to calibrate the numerical model, see Figure 4. ELS uses a non-linear solver based on AEM and allows the automatic detection and computation of yielding, hardening, failure of materials, separation of elements, contact at

Figure 2a. Central column after test E5, front view.

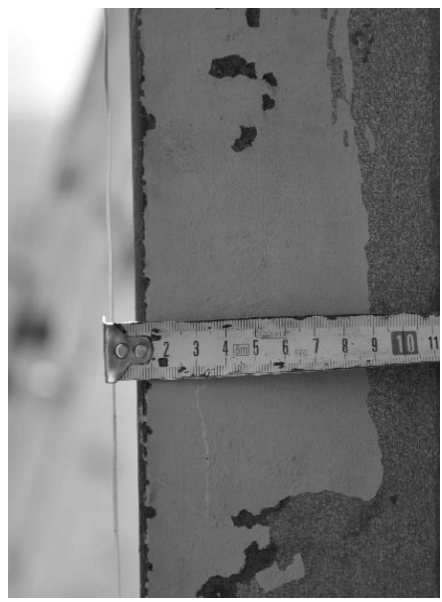

Figure 2b. Central column after test E5, side view.

Figure 2c. Central column after test E6, front view.

impact, buckling / post-buckling, crack propagation, membrane action, and P-Δ effect. In the AEM modelling technique, the structural elements are modelled as small solid elements connected by normal and shear springs that follow the constitutive law of the corresponding material (Figure 5a, & 5b). These elements are considered rigid and the displacement one to the other is expressed through the springs, which will generate stresses and strains. The material volume property of these springs is represented by the interface spring tributary surface and distance between the centroids of the elements (Figure 5c). The rigid AEM elements have six degrees of freedom (three for translations and three for rotations), and no simplification are made on their possible displacements and consequently on springs deformations, see Figure 6. Two neighbouring elements can be separated once the springs connecting them are ruptured. Fully nonlinear path-dependent constitutive models were used for materials, see Figure 7. Structural steel S275 was assigned for all steel elements (beams, columns, plates) and class 10.9 bolts were used for connections. The dynamic effects in the material were modelled based on the maximum strain rates derived from the numerical simulation, that is, 300 s-1. Figure 8 shows a detailed view of the

Figure 3a. Shock wave propagation E6.

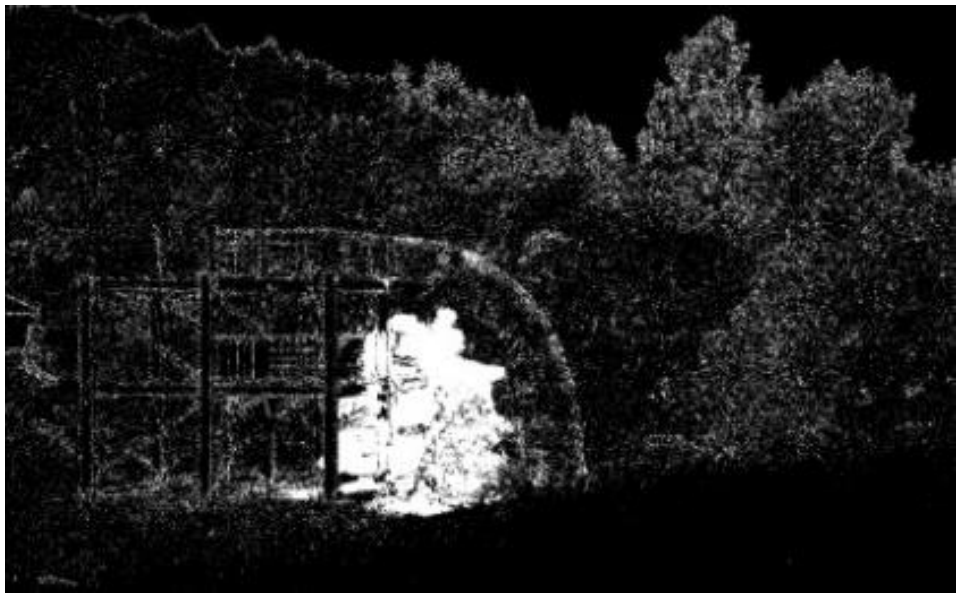

Figure 3b. Shock wave propagation, test E6.

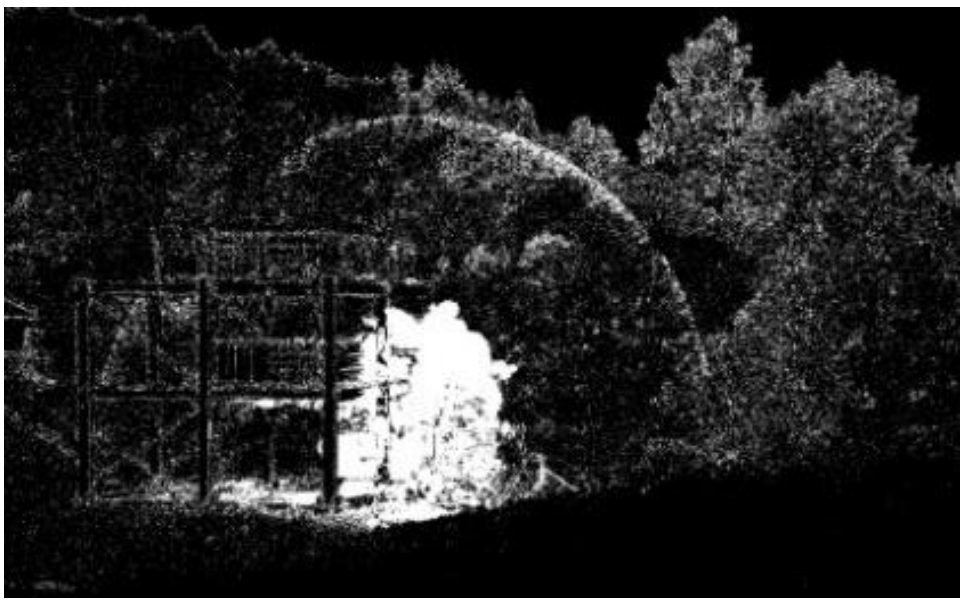

Figure 3c. Shock wave propagation, test E6.

AEM model, with the position of small elements (1 to 9) located in the column fracture zone. The elevation of the blast charge is also indicated in the figure.

The pressure histories measured at the four points indicated in Figure 1b were used for the calibration of the pressure load in the numerical model. Figure 9 shows the pressure histories,

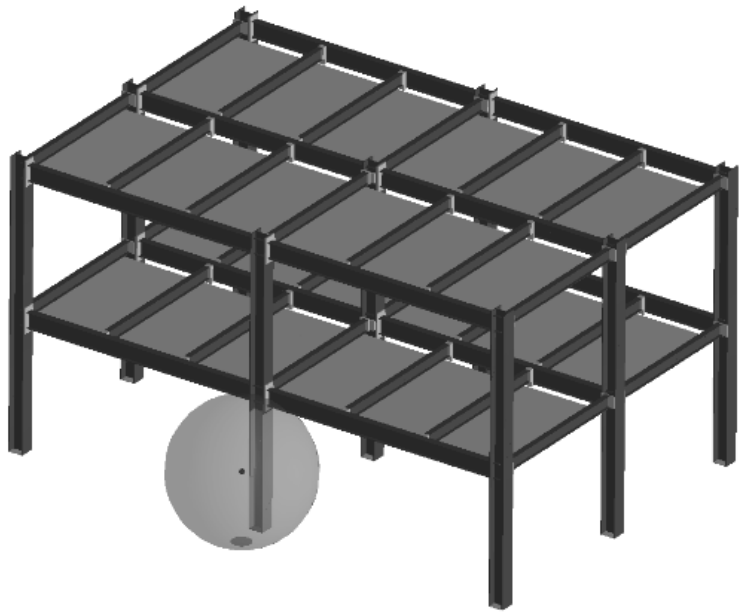

Figure 4. Three-dimensional numerical model developed using ELS ([14]).

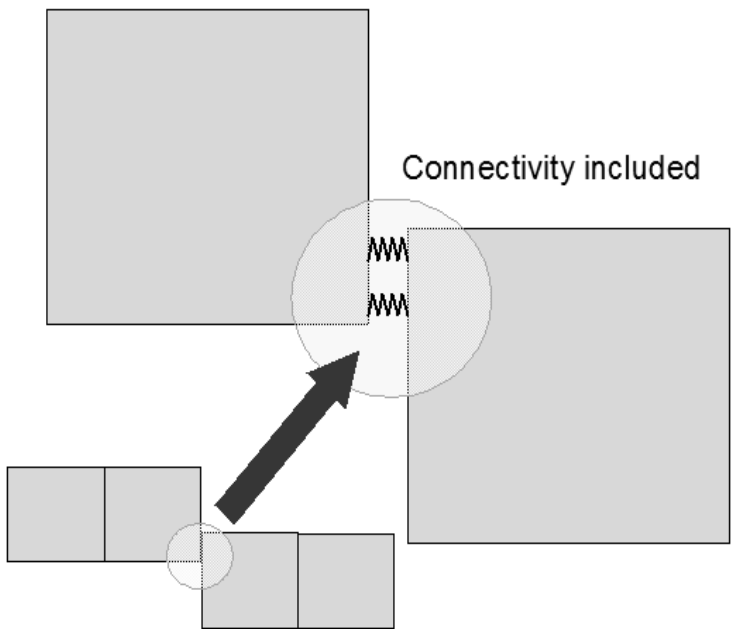

Figure 5a. Modelling connectivity with AEM and spring generation on element faces - partial connectivity.

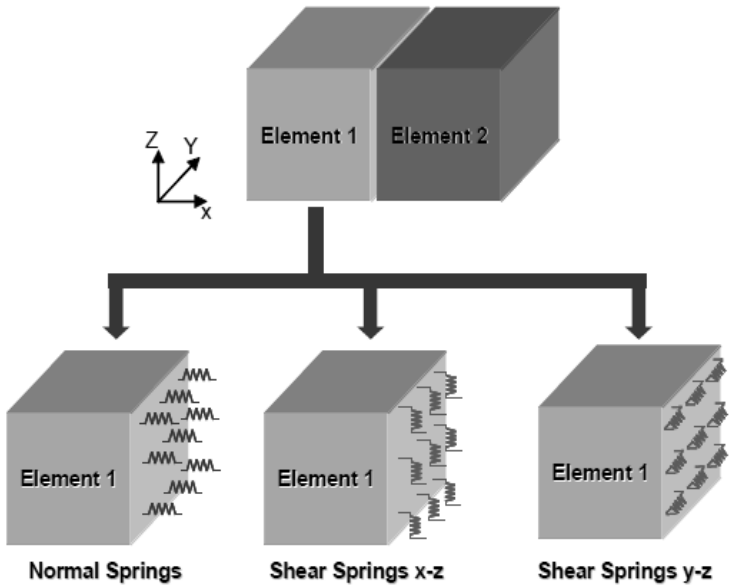

Figure 5b. Modelling connectivity with AEM and spring generation on element faces - connectivity matrix spring.

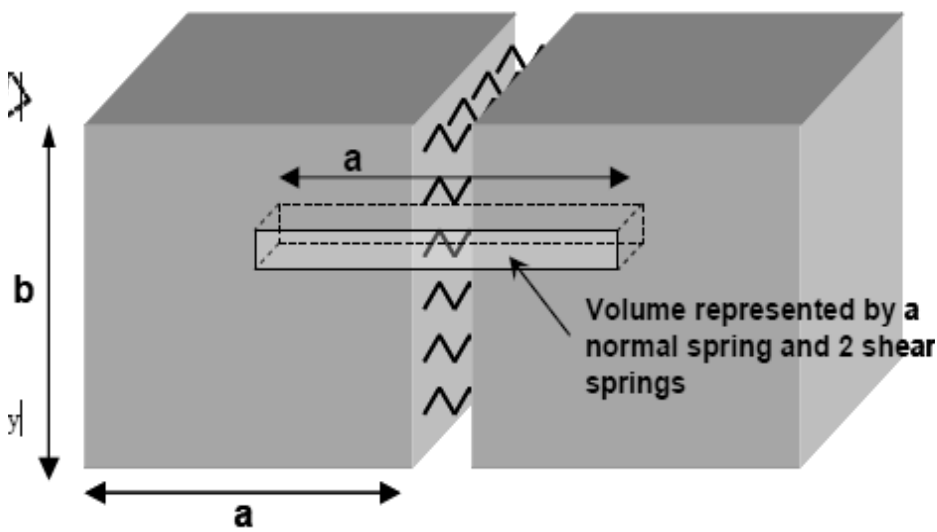

Figure 5c. Modelling connectivity with AEM and spring generation on element faces - spring distribution and tributary area.

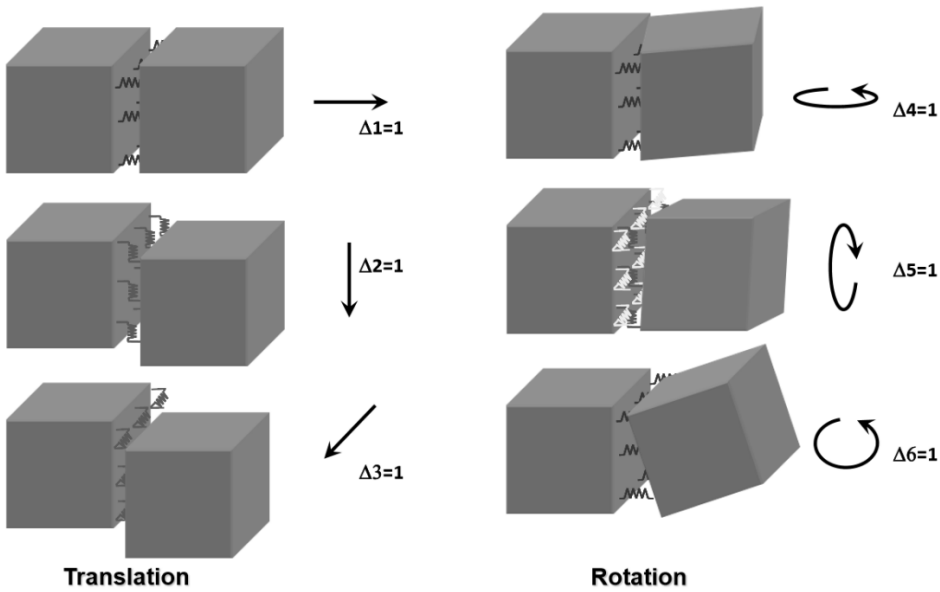

Figure 6. Relative displacements of AEM elements.

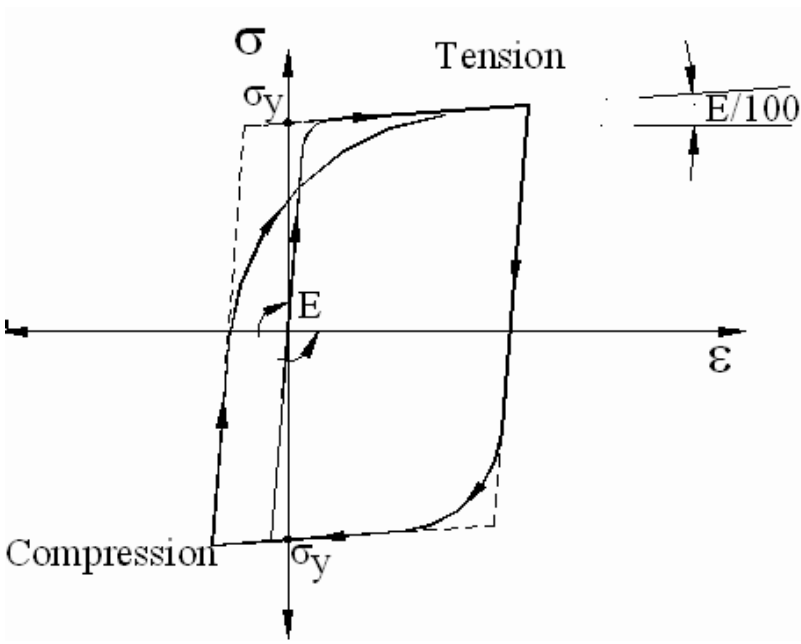

Figure 7. Constitutive model for steel under axial stresses used in ELS.

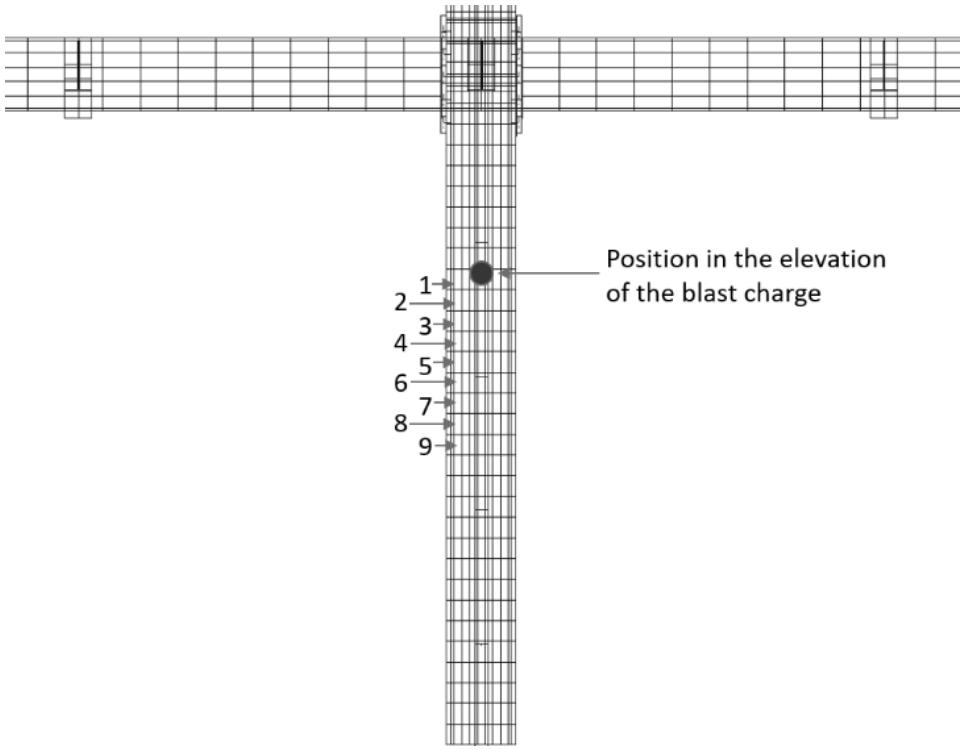

Figure 8. Detailed view with AEM model, with the position of small elements (1 to 9) and elevation of the blast charge.

experimental vs. numerical, for test E5. For clarity, pressures S1, S2 and S3, S4 are presented on separate graphs. It may be seen the pressure is well approximated at points 2, 3, and 4, the only significant difference is at point 1, possibly due to some local effects or sampling rate in the data acquisition system. Note that only the positive phase is modelled in ELS.

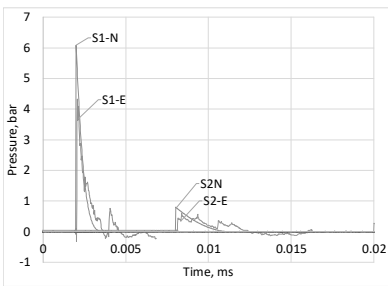

Figure 9a. Pressure history at points S1 to S4, experimental (E) vs numerical (N), test E5.

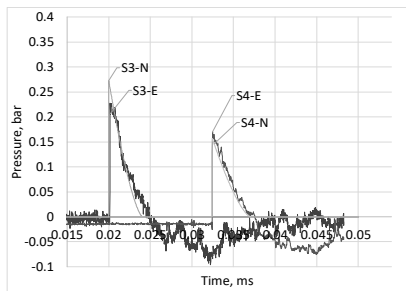

Figure 9b. Pressure history at points S1 to S4, experimental (E) vs numerical (N), test E5.

Figure 10 shows the main phases of deformation in the column. As seen, the strains are highly localized in the web toe of the fillet, symmetrically above and below the centre of the explosion. The partial fracture of the web is initiated at 0.3 ms from start and extends over a length nearly double the height of the column.

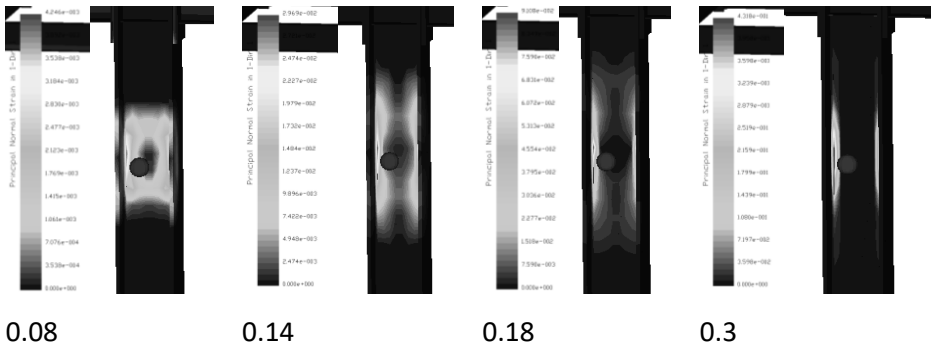

Figure 10. Evolution of the out of plane deformations in the column, test E5 (deformations in mm, time in ms).

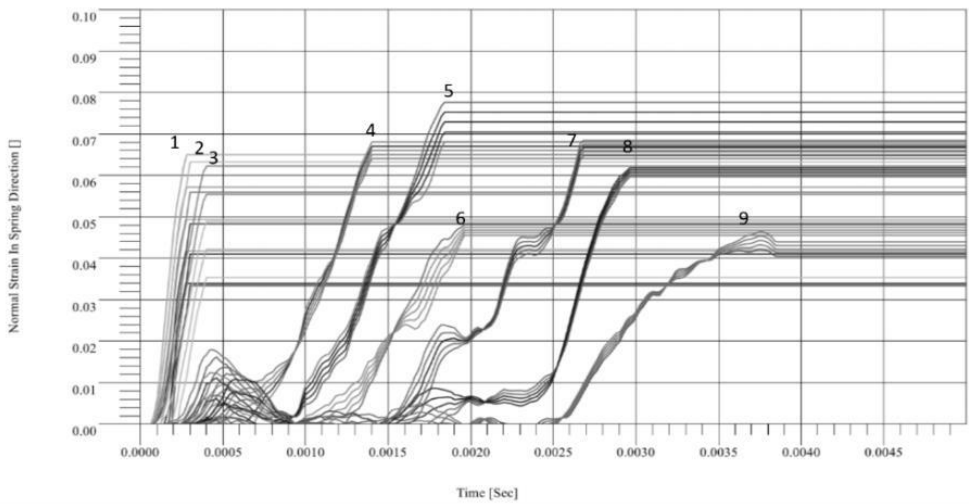

Figure 11a. Strain history in springs, fibres F1 to F9: a) normal strain.

The initiation and propagation of fracture is complex and is caused by the combined bending and shear. Thus, Figure 11 shows the evolution of strains (normal strain and resultant shear strain) in time at nine points from the web toe of the fillet in the central column, beneath the centre of explosion (see also Figure 8). Note that similar effects are expected at similar locations above the point of explosion. As seen from the figure, the normal and shear strains get the fastest increase rate in the group of springs 1,2, and 3, and the fracture is caused by the attainment of the ultimate shear strain, before the full development of the normal strains. The deformations extend also to points 4, 5, and 6, then last to points 7, 8, and 9, which all develop fracture from shear.

4 CONCLUSIONS

Explosions produced near buildings pose a special threat to structural integrity and implicitly to occupant safety. The ability of a structure to withstand such action depends both on the capacity of the most affected elements and on the ability of the structure to limit the extent of damage and to avoid progressive collapse. Increasing the safety distance is the most effective measure to reduce the damage level in the

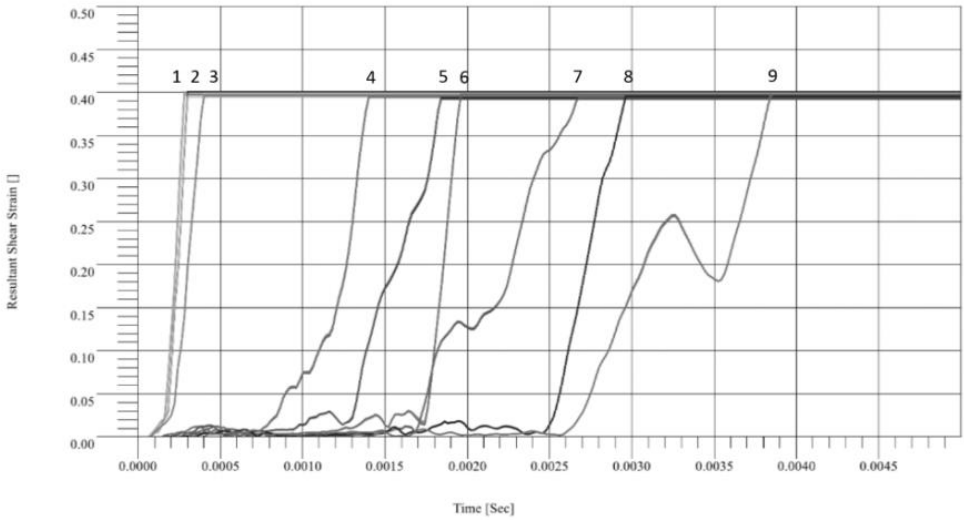

Figure 11b. Strain history in springs, fibres F1 to F9: b) resultant shear strain.

structure. The interaction between the shock wave and the structure results in a significant increase in the maximum pressure and implicitly in the state of strains in the structure. For this reason, a two-bay, two-span, and two-story steel frame building model was tested for different blast loading conditions to evaluate the consequences of near-field explosions on the structural elements. The results of the blast tests showed that the interaction between the shock wave and the structure may result in a significant increase in the maximum pressure and implicitly in the level of deformations in the structure. Also, increasing the safety distance is the most effective measure of damage reduction in the structure. The specific instrumentation (pressure, strains, video) provided extensive data that allowed to calibrate the numerical models and to go deeper into the blast-structure interaction process and sequences of failure.

REFERENCES

Adam J. M., Parisi F., Sagaseta J. & Lu X. 2018. Research and practice on progressive collapse and robustness of building structures in the 21st century. *Eng. Struct*., vol. 173, Oct. 2018, pp. 122–149.

Applied Science International 2018. *Extreme loading for structures theoretical manual*, Version 6. 2018.

Chen, C.H., Zhu Y.F., Yao, Y., Huang, Y. & Long X. 2016. An evaluation method to predict progressive collapse resistance of steel frame structures. *J. Constr. Steel. Res*., vol. 122, Jul. 2016, pp. 238–250.

Dinu F., Dubina D. & Marginean I. 2015, Improving the structural robustness of multi-story steel-frame buildings. *Structure and Infrastructure Engineering*, vol. 11, no. 8, Aug. 2015, pp. 1028–1041.

Dinu F., Marginean I., Dubina D. & Petran I. 2016, Experimental testing and numerical analysis of 3D steel frame system under column loss. *Eng. Struct.*, vol. 113, Apr. 2016 pp. 59–70.

Dinu F., Marginean I., Dubina D., Kovacs A. & Ghicioi E. 2017, Experimental testing and numerical modelling of steel frames under close-in detonations. *Procedia Engineering*, vol. 210, Jan. 2017 pp. 377–385.

Dinu F., Marginean I. & Dubina D. 2017. Experimental testing and numerical modelling of steel moment-frame connections under column loss. *Eng. Struct*., vol. 151, Nov. 2017, pp. 861–878.

Dinu F., Marginean I., Dubina D. Khalil A. & De Iuliis E. 2018. Factors affecting the response of steel columns to close-in detonations. *12th International Conference on Advances in Steel-Concrete Composite Structures* (ASCCS

2018), Universitat Politècnica de València, València, Spain, June 27-29, 2018.

EN 1991-1-7 2006. Eurocode 1 - Actions on structures - Part 1-7 : General actions - Accidental actions. European Committee for Standardisation CEN, 2006.

El-Tawil S., Li H., & Kunnath S. 2014, Computational simulation of gravity-induced progressive collapse of steel-frame buildings: current trends and future research needs. *J. Struct. Eng*., vol. 140, Aug. 2014, no. 8.

Experimental validation of the response of a full-scale frame building subjected to blast load frameblast. UEFISCDI, Executive Agency for Higher Education, Research, Development and Innovation Funding, 2018.

Mazurkiewicz L., Malachowski J. & Baranowski P. 2015. Blast loading influence on load carrying capacity of I-column. *Engineering Structures*, vol. 104, Dec. 2015. pp. 107–115.

Tagel-Din H.S. & Meguro K. 2000. Applied element method for dynamic large deformation analysis of structures. *JSCE,* vol. 661, pp. 1–10.

Tagel-Din H.S. & Meguro K. 2000. Applied element method for simulation of nonlinear materials: theory and application for RC structures. *JSCE,* vol. 17, pp. 137–148.

UFC 4-023-03 2016. Design of buildings to resist progressive collapse. Department of Defense DoD.

Zhang J., Jiang J., Xu S. & Wang Z. 2018. An investigation of the effect of semi-rigid connections on sudden column removal in steel frames. *Structures,* vol. 13, pp. 166–177.

Helsinki Conference Proceedings 2019, R. Holmberg et al

Intelligent design software for open bench blasting

M.S. Zhao, H.B. Yu, Q. Liu & X.G. He
Poly Xinlian Blasting Engineering Co., Ltd., Guiyang, Guizhou, China

G.X. Zhang
Poly Explosive Hami Co., Ltd., Hami, Xinjiang, China

J. Liu
Institute of Safety and Disaster Prevention Engineering, Hohai University, Nanjing, Jiangsu, China

ABSTRACT: With the increasing demand for safety and environmental protection, intelligent bench blasting design is urgently needed in the field of blasting engineering. Based on the Voronoi grid technology, the designs of blast hole layout and initiation sequence are proposed, and the corresponding software modules are developed to improve the accuracy of blasting hole layout and the energy efficiency of explosives. Based on the plane image processing technology, the algorithm of the size distribution on the muck pile surface is proposed, and the module for boulder yield analytic statistics is developed through the image binary conversion and the outline recognition technique. Based on the combination of optimisation theory, linear programming and fuzzy mathematics, the blasting effect comprehensive evaluation module is developed. The design software is developed by using VC platform, STL template library and OpenGL graphic library. The on-site evaluation results of the software show that it is of high evaluation accuracy and high evaluation efficiency, which can realise the automotive hole layout and network design, effectively reducing the harmful effects of blasting vibration, and providing the technical support for blasting parameter optimisation.

1 INTRODUCTION

Bench blasting is a common method for open pit mining and large-scale earthwork excavation. Its blasting quality and blasting construction safety are closely related to blasting parameters. The present bench blasting design has several main technical limitations. The method of blasting design based on experience and engineering analogy cannot meet the requirements of blasting refinement. The existing computer-aided blasting design software and blasting parameter optimisation method can only complete a certain part of blasting design, but penetrate the whole process of blasting design, parameter optimisation and effect evaluation. For a given blasting design, there is a lack of easy applied software for evaluating and predicting the harmful effects of blasting vibration. And it lacks of effective comprehensive evaluation system for blasting

effect, so it cannot quantitatively evaluate the effect of blasting engineering, which does not meet the requirements of blasting refinement. The orderly advancement of intelligent, digital and scientific blasting construction has become inevitable. This blasting design software is developed for on-site application. It takes the adaptive blasthole arrangement of hole-by-hole blasting, automatic determination of detonation sequence and calculation of charge amount as the main objectives. It develops the explosion block size distribution statistical module and the vibration waveform prediction module, and use optimisation model to analyse the blasting effect of hole-by-hole blasting.

2 DEVELOPMENT OF THE DESIGN SOFTWARE FOR OPEN-PIT BLASTING

2.1 Design method of blasthole layout and initiation sequence

2.1.1 Blasthole self-adaptive layout

The adaptive blasthole layout algorithm rules are as follows: (a) Measure the coordinates of the top line and the corresponding bottom line, calibrate the free boundary by the two lines, i.e. the free face of the bench blasting. The free boundary can be regarded as one free boundary or two free boundaries according to the angle between the two line segments corresponding to the measuring point. That is, if the angle between the two line segments connected to a measuring point in the blasting area is less than or equal to 90º, it would be considered as two free boundaries, which are identified by 1 and 2 respectively. Or it would be considered as one free boundary, identified by 1. The purpose of dividing the free boundary into two is to facilitate the search for the first detonated blasthole; when there is only one free boundary, the first detonated blasthole is randomly formulated. (b) Since the scale of each blasting is determined according to the production task and the capacity of the shovel, it can only be part of a bench. Therefore, in the adaptive blasthole layout algorithm, the boundary line of the rock mass needing to be blasted and that needing to be retained should also be made out, which is referred to herein as the infinite boundary, identified by -1 (see Figure 1).

After the free boundary and the infinite boundary are marked, the blasting parameters are entered, including the hole pattern, the hole diameter, the step height, the explosive unit consumption, the charge density, and the rock density. The hole pattern can be square or triangular, the hole diameter is determined by the site rock drilling equipment, the step height is determined by the mining design plan, the explosive unit consumption is selected according to the experience and adjusted based on the field test blast, and the charge density is determined by the explosive properties, and the rock density is determined by field mechanics tests. Based on the blasting parameters, the resistance line distance, hole spacing and ultra-deep in the blasting design can be calculated. Push back the free boundary at the specified row spacing to obtain a series of

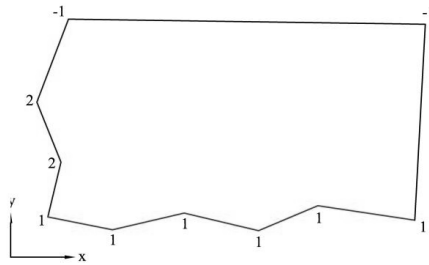

Figure 1. The identification method of free boundary and infinite boundary.

contours for arranging the blastholes. The back-pushing method for the free boundary is: Calculate the normal vector of the two line segments connected to each measuring point (pointing to the inner side of the explosion zone), move each line segment back to the distance of the row spacing according to the direction of the

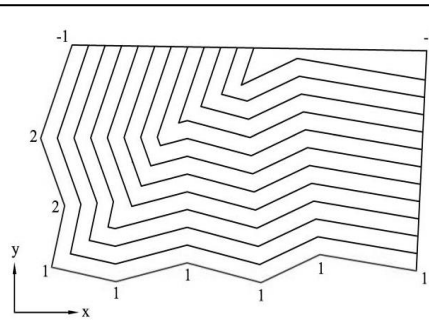

Figure 2. The back-pushing method of free boundary.

normal vector, and then calculate the intersection of each line segment after the backward movement. The contour lines of the free boundary

are moved back, and repeat the above process until the backward contour fills the entire explosion area (see Figure 2).

When the backward free boundary contours cover the whole explosion area, the blasthole can be arranged on each of the contour lines. Take the intersection of each contour line and the infinite boundary as the starting point and make a circle with the hole spacing as the diameter. There would be 1 or 2 intersections of the circle and the contour. Take the intersection farther to the starting point as the position of a blasthole when there are 2 intersections. Repeating on each contour line in turn, the blasthole layout would be completed in the blast zone (see Figure 3).

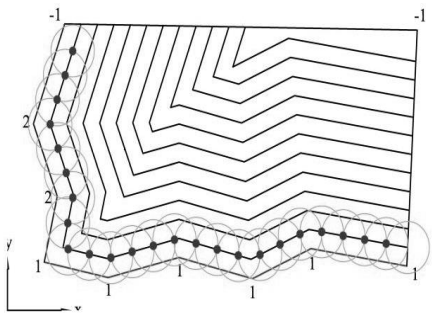

Figure 3. The position of blastholes on the back-pushed contour.

During the back pushing of the free boundary, polygon intersections, i.e. redundant points, may occur. In order to eliminate redundant points, the convex hull algorithm in computational geometry is used, that is, only the points on the outer contour of the scatter system are preserved, so as to eliminate the redundant points. The flow chart of the adaptive blasthole arrangement algorithm is shown in Figure 4.

2.1.2 Determination of initiation sequence based on the Voronoi stochastic grid technique

Based on the measured geological data and the determined parameters of each group of holes, the Voronoi mesh technology is used to make the Voronoi random meshing on the two-dimensional plane with each blasthole as the centre. The reference point of each Voronoi unit is the position of the blasthole. The area each Voronoi unit contains is approximately considered as the destruction area of each blasthole. Based on the blasting free face and the minimum resistance line, the initiation sequence of each blasthole is determined (see Figure 5).

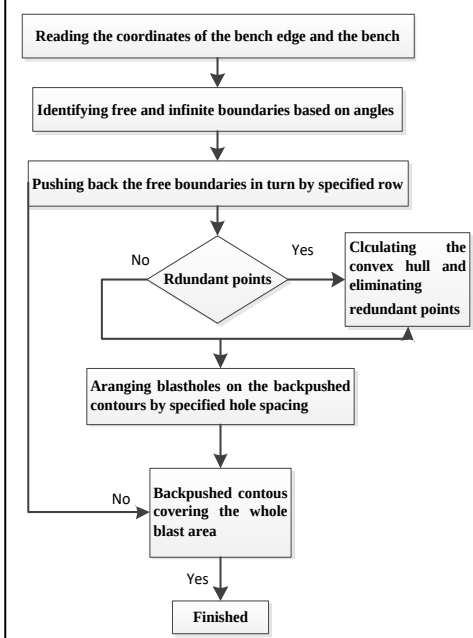

Figure 4. Flow chart of adaptive blasthole layout algorithm.

After a blasthole's detonation, the principles of determining the next blasthole to be detonated are: (a) Whether it has the minimum resistance line; (b) whether, with the current resistance line, it has the same throwing direction as the previous blasthole or not; (c) whether the blastholes in the subsequent blast meets the above two conditions. According to the above conditions, in each time step of the initiation sequence, all the holes are searched, compared and calculated and finally the initiation sequence scheme is obtained. The final initiation sequence is determined not only by the initiation principle of the Voronoi grid, but also by the inter-hole and inter-row delay time. After the Voronoi grid is divided and the blasting sequence of each blasthole is determined, it is necessary to adjust the initiation sequence based on the time difference between the holes and the rows.

2.2 Blasting block size analysis and vibration prediction

2.2.1 Surface block size distribution algorithm based on planar image processing technology

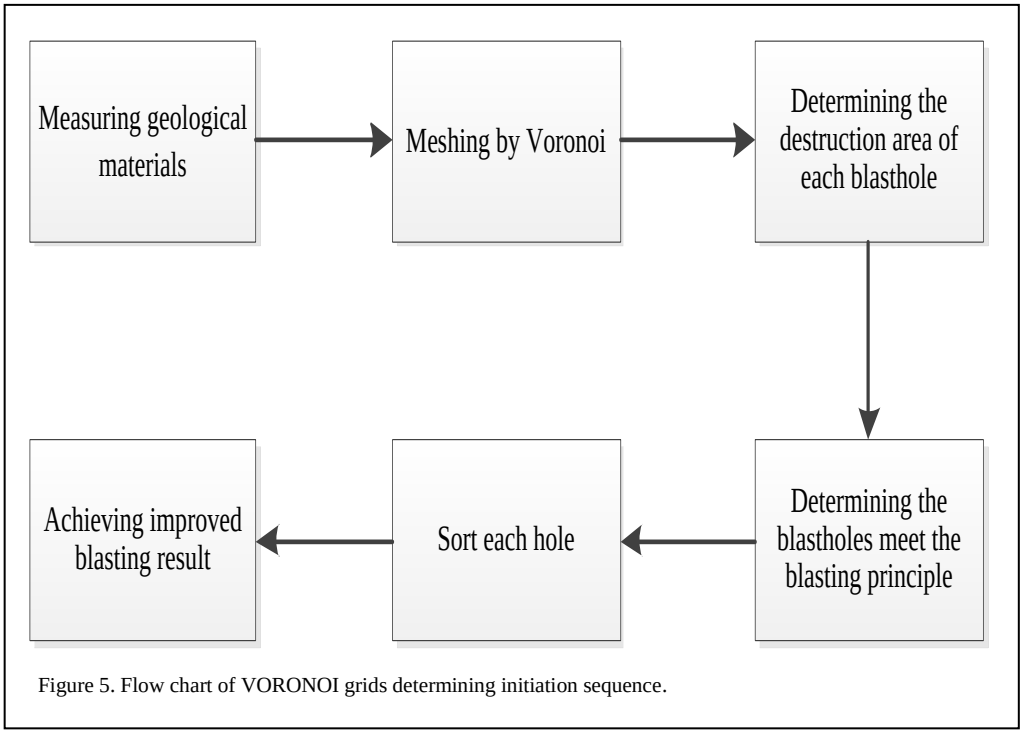

Figure 5. Flow chart of VORONOI grids determining initiation sequence.

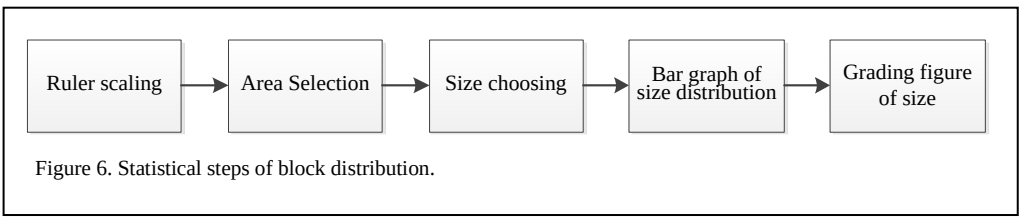

Figure 6. Statistical steps of block distribution.

Based on the Image processing technology, like image digitisation, image coding, image compression, image enhancement and restoration, image enhancement, image restoration, and image analysis, a large two-dimensional array could be received by the set of a more rationalised threshold and the local adaptive binarisation of images. Extract the details in the binarised image, and finally identify the features of the target shape by contour recognition. Statistical steps are shown in Figure 6.

2.2.2 Blasting Vibration Prediction Based on Anderson Model

The simulation and prediction of seismic waves is a very complicated task. At present, various models proposed by scholars at home and abroad focus on some aspect of blasting vibration, like the maximum amplitude of vibration, or a single parameter such as the main frequency of vibration. There are certain limitations in using numerical methods such as finite element, prediction methods based on statistics models, complete time history models, etc. It is urgent to establish a comprehensive, accurate and convenient vibration prediction model.

According to the characteristics of bench blasting, the Anderson prediction model based on superposition time domain waveform is improved by using the nonlinear prediction method of step blasting vibration effect of Volterra functional series. The Anderson model is improved based on the seismic scale factor of the bench blasting. The Volterra nonlinear system model, the improved Anderson model and the calculation program for structural response prediction are developed. According to the improved Anderson model and the vibration waveform predicted by the nonlinear Volterra functional series model, the vibration

mode decomposition response spectrum method, time history analysis method and transfer function method are developed to predict the change rules with time of vibration effect like internal force, shear force and displacement of the building structure.

2.3 Determination of blasting effect evaluation system based on optimisation theory

2.3.1 Analysis of factors influencing blasting effect

Both bulk rate and looseness affect the efficiency and cost of subsequent mining operations. The main indicators of blasting quality evaluation are bulk rate and pile looseness. The factors affecting the blasting pile size are: a) geological structure, like joint fissures, number of faults, degree of fracture, etc.; b) blasting parameters: blasthole spacing, minimum resistance line, explosive unit consumption, etc.; c) charging method: charging structure, charge density, charge amount, clogging method, etc.; d) detonation method: detonation type, initiation sequence and delay time; e) explosive performance: detonation pressure, explosion pressure, etc. Looseness is the proportion of the void volume of the explosive pile to the total volume of the pile. The looseness being too small will affect the efficiency of the shovel and directly increase the cost of mining.

The blasting block rate is the result of the comprehensive influence of various factors. Among them, the blasthole spacing, the minimum resistance line, and the explosive unit consumption takes a large proportion in accounting for the bulk rate. Therefore, find the connection between these aspects and the block rate and finally determine the optimal value of each factor.

2.3.2 Determination of evaluation system based on optimisation theory

In the aspect of the characteristics of blasting, it is necessary first to ensure the safety of the blasting, and secondly to make the blasting achieve the optimal effect and feasible in economy. In the evaluation index of the blasting effect, what the engineers concern most are the indicators such as the block rate and the root rate.

It is feasible to comprehensively judge the merits and demerits of the blasting parameter system from the three aspects of rationality, safety and economy. The importance of each item is determined in the form of weight. In the actual evaluation, safety, technicality and economy are taken as constraints, and the blasting effect is used as the evaluation target. Based on this, the evaluation system of Table 1 is proposed. The constraint and objective function are described by linguistic variables, and according to the actual experience and reasoning, plus the principle of highlighting the advantages and disadvantages of the scheme, the linguistic variables are transformed into corresponding membership degrees, as shown in Table 2.

Table 1. The evaluation system of weight.

Evaluation index (large item)	Weight	Evaluation index (small item)	Weight
Safety and reliability	0.4	Effect	0.4
		Flyrock	0.3
		Vibration	0.2
		Dust	0.1
Technical Rationality	0.4	Bulk	0.4
		Root	0.4
		Forward and backward	0.1
		Operation difficulty	0.1
Economic benefit	0.2	Explosive unit consumption	0.5
		Blasting output per meter hole	0.2
		supporting materials	0.1
		Blasting materials	0.2

It can be seen from Table 2 that the evaluation of the parameter system is a decision with multiple objectives, levels and constrains. The evaluation value of each test is calculated by the convex fuzzy programming principle, and finally the parameters corresponding to the optimal blasting scheme are obtained.

2.3.3 Optimisation of blasting design parameters

In practice, the main indexes to evaluate the blasting effect are block rate, root rate, block evenness rate and pile looseness. In the case that the type of explosive, the inclination

Table 2 Constraint and target language variables and corresponding membership.

	Extremely poor	Very poor	Poor	Fair	Good	Very good	Excellent
Safety and reliability membership	0	0.1	0.2	0.5	0.6	0.8	1
Technical Rationality membership	0	0.1	0.2	0.5	0.6	0.8	1
Economic benefit membership	0	0.1	0.2	0.5	0.6	0.8	1

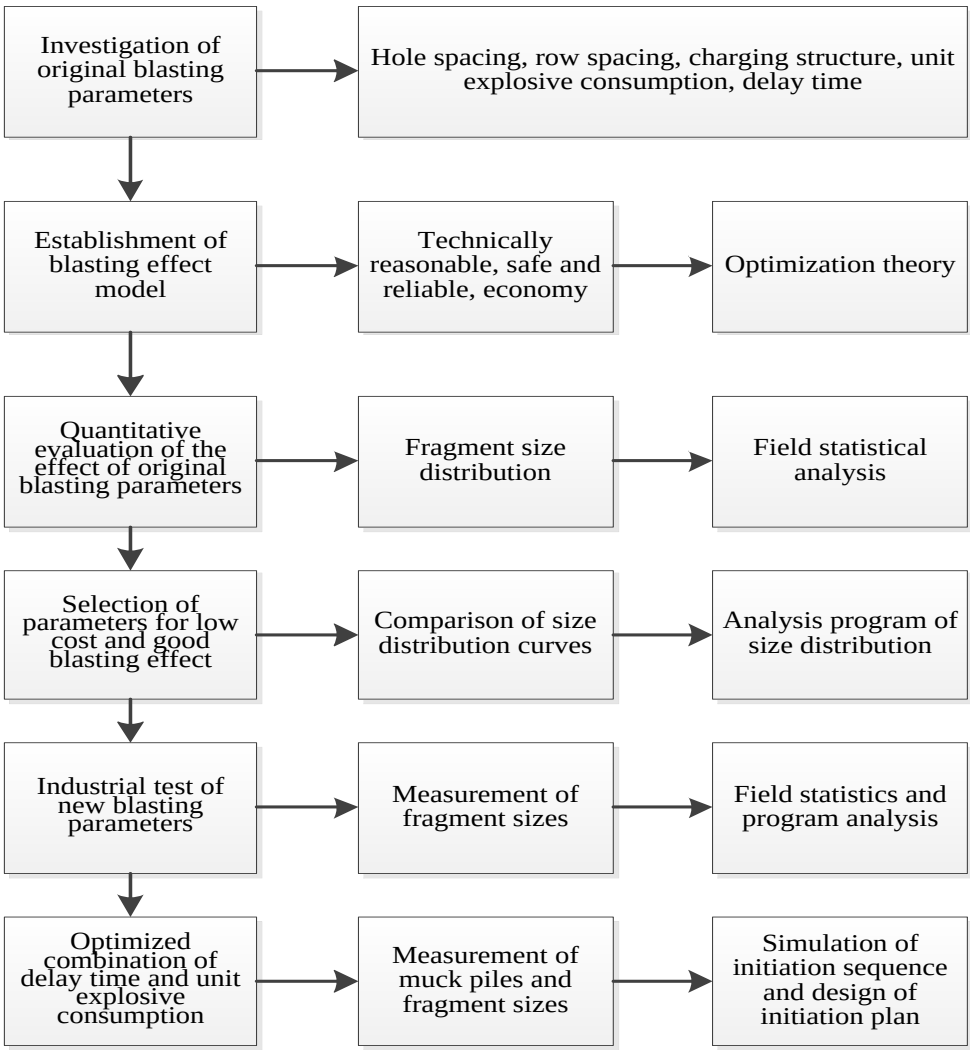

Figure 7. Optimisation flow chart of blasting parameters.

of the blasthole, the height of the step, the depth of the single blasting, and the diameter of the blasthole have been clearly determined in the actual production design, the main factors affecting the blasting effect are the blasthole pattern parameters, the initiation sequence, the delay interval, and the explosive unit consumption. The blasthole pattern parameters are determined by the program, and the field test is carried out to optimize the blasting parameters. The optimisation process is shown in Figure 7.

3 SOFTWARE INTRODUCTION

According to the requirements of digitalisation, informationisation and intelligence of blasting design, based on VC++ platform, the program code and interface integrating blasting design, optimisation and effect evaluation are developed. Based on the visualisation module of development design software of the OpenGL graphics library, the modules for the storage and output of design and evaluation results are developed. In the software development, the STL standard template library, WildMagic math function library, quaternion and other technical and theoretical methods are comprehensively applied to realize the digitisation, informationisation and intelligence of blasting design and effect evaluation.

3.1 Interface

The upper bar of the window is the menu bar, including File, Module, Edit, View, and Help. The left column of the window is the working area of the module, including the input and output of related data, parameter settings, and so on. In the middle is the effect display area of the module and at the bottom is the software status message bar. The entire interface is simple and clear, and functionally rich (see Figure 8).

Figure 8. Software interface.

3.2 Design module for bench blasting

Bench blasting design module can, based on the original data, calculate the parameters of the hole


炮孔参数列表

炮...	孔深(m)	超深(m)	孔径(m)	抵抗线(m)	抵抗线相...	坐标X(m)	坐标Y(m)	装药量(kg)	填塞高度(m)	起爆顺序	地表延期(ms)	孔内延期(ms)	起爆时间(ms)
1	14.50	2.50	0.16	5.00	0.13	29194.93	51107.59	181.46	5.00	0	0	120	120
2	14.50	2.50	0.16	6.16	0.39	29201.91	51109.27	159.34	6.16	1	12	120	132
3	14.50	2.50	0.16	3.60	0.19	29209.01	51110.39	208.13	3.60	2	24	120	144
4	14.50	2.50	0.16	3.59	0.19	29216.18	51110.90	208.37	3.59	3	36	120	156
5	14.50	2.50	0.16	3.57	0.19	29223.36	51111.18	208.85	3.57	4	48	120	168
6	14.50	2.50	0.16	3.59	0.19	29230.54	51110.74	208.34	3.59	5	60	120	180
7	14.50	2.50	0.16	3.62	0.19	29237.71	51110.30	207.90	3.62	6	72	120	192
8	14.50	2.50	0.16	3.60	0.19	29244.89	51110.50	208.28	3.60	7	84	120	204
9	14.50	2.50	0.16	3.61	0.19	29252.04	51111.29	208.03	3.61	8	96	120	216
10	14.50	2.50	0.16	3.60	0.18	29259.18	51112.08	208.17	3.60	9	108	120	228
11	14.50	2.50	0.16	3.57	0.19	29266.37	51112.25	208.82	3.57	10	120	120	240
12	14.50	2.50	0.16	3.55	0.19	29273.55	51112.25	209.09	3.55	11	132	120	252
13	14.50	2.50	0.16	3.59	0.19	29280.74	51112.25	208.39	3.59	12	144	120	264
14	14.50	2.50	0.16	3.63	0.18	29287.92	51112.49	207.71	3.63	13	156	120	276
15	14.50	2.50	0.16	3.61	0.19	29295.10	51112.82	208.08	3.61	14	168	120	288
16	14.50	2.50	0.16	3.59	0.19	29302.28	51113.15	208.45	3.59	15	180	120	300
17	14.50	2.50	0.16	3.57	0.19	29309.47	51113.01	208.82	3.57	16	192	120	312
18	14.50	2.50	0.16	3.60	0.19	29316.65	51112.76	208.15	3.60	17	204	120	324
19	14.50	2.50	0.16	6.20	0.42	29323.51	51114.91	158.53	6.20	18	216	120	336
20	14.50	2.50	0.16	3.58	0.29	29330.67	51114.28	208.60	3.58	19	228	120	348
21	14.50	2.50	0.16	3.57	0.12	29193.25	51114.58	208.80	3.57	1	24	120	144
22	14.50	2.50	0.16	4.87	0.20	29200.24	51116.26	184.01	4.87	2	36	120	156
23	14.50	2.50	0.16	3.62	0.11	29207.32	51117.47	207.91	3.62	3	48	120	168
24	14.50	2.50	0.16	3.60	0.12	29214.49	51117.98	208.27	3.60	4	60	120	180
25	14.50	2.50	0.16	3.57	0.12	29221.66	51118.49	208.85	3.57	5	72	120	192
26	14.50	2.50	0.16	3.59	0.12	29228.83	51118.05	208.45	3.59	6	84	120	204
27	14.50	2.50	0.16	3.61	0.11	29236.00	51117.61	208.01	3.61	7	96	120	216
28	14.50	2.50	0.16	3.59	0.11	29243.19	51117.54	208.37	3.59	8	108	120	228
29	14.50	2.50	0.16	3.61	0.11	29250.34	51118.33	207.99	3.61	9	120	120	240

存储到数据库 打印 导出 确定

Figure 9. Exported table of parameter list.

pattern, like the hole spacing, the row spacing, the minimum resistance line, etc., and select the appropriate value for the blasthole adaptive algorithm.

The blasting sequence diagram is determined based on Voronoi grid technology, so the blasting sequence of the holes can be clearly seen. The output of the parameter list can be exported in an Excel file (see Figure 9), and the data collection will provide an important basis for the actual blasting layout.

3.3 Blasting effect statistics module

Statistical module of blasting effect can, based on the blasting pile, carry out the statistical analysis of lumpiness distribution by using the photographic method, which provides necessary data for the combination analysis of blasting effect evaluation and optimisation. The module mainly collects the blasting effect after processing the image of the blasting stone block. The specific operation steps are as follows:

- Image reading: By analysing the image taken on site after the explosion. Select the image to be analysed for size analysis
- Select area: Hold down the left mouse button in the display area and pull the mouse to select the area to be counted
- Image processing: Threshold segmentation of the selected region image. Click the “Size Extraction” button to display the effect of image processing
- Distribution curve: Click “Size Distribution Curve” to get the distribution curve (see Figure 10).

3.4 Blasting effect evaluation module

Blasting effect evaluation module gives out comprehensive evaluations to the blasting construction based on the size distribution and other indicators from the perspectives of safety, reliability, technically reasonability and economy.

The evaluation of blasting effect is determined by weight. It can make a relatively accurate evaluation of each indicator according to the evaluation system of weight in Table 1 and constraint and target linguistic variables and their corresponding membership in Table 2, thus providing a scientific basis for the correct evaluation of the entire blasting scheme. Each item for evaluation is set through the drop-down menu. Click "ok" after setting up each item, and the evaluation output results include safety and reliability evaluation, technical rationality evaluation, economy evaluation and comprehensive evaluation. The corresponding histogram of various analyses will be generated in the middle display area, so as to see the evaluation results more intuitively.

3.5 Comparison of similar products at home and abroad

At present, the most widely used blasting software are the Shot Plus blasting design software and the

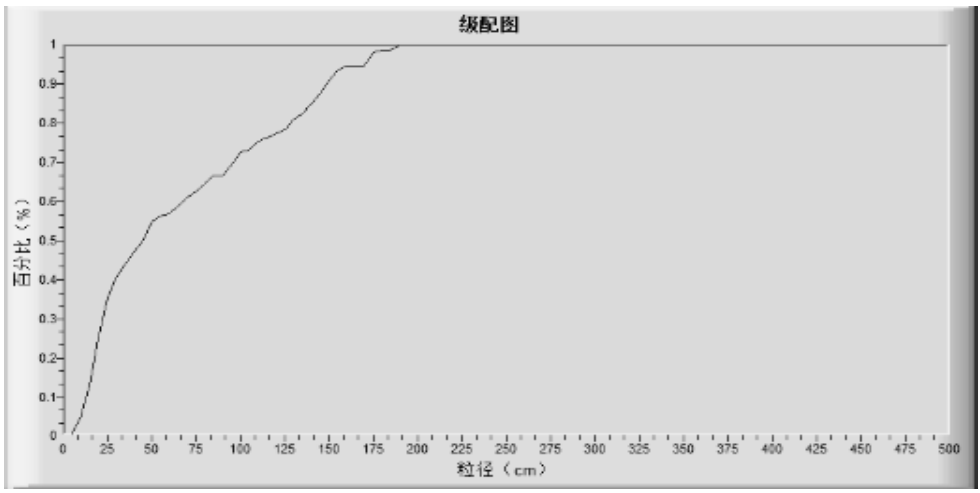

Figure 10. Distribution curve.

Table 3. Comparison of research results with similar technologies at home and abroad.

Comparison content		Research results of this project	Similar technologies at home and abroad		
			ShotPlus	Blast-Code	Huayisoft Blast
Blast design software	Analytical calculation method of hole pattern parameters	Analytical calculation method for deriving optimal hole pattern parameters based on maximum utilisation of blastholes	Determined by experience	Determined by experience	Determined by experience
	Calculation method of blasthole position	Calculation by constructing a reference line	Manual calculation	Manual calculation and comprehensive adjustment	Manual calculation
	Method for identifying charge amount and hole-by-hole blasting initiation sequence	The identification method is proposed Based on the construction of the Voronoi diagram of the blasting area	Backstepping method	Backstepping method	Backstepping method
Blast effect evaluation software	Predictive evaluation model and software for blasting vibration	Improved Anderson model and nonlinear Volterra functional series model; full-time prediction of particle vibration	Predicting PPV value	Predicting PPV value	Predicting PPV value
	Multi-dimensional muck pile size distribution algorithm and software	Automatically completing the statistics of muck pile size distribution based on the image processing technology and realising the multi-dimensional size statistics through different interface photo analysis	Image recognition and manual correction	None	None
	Comprehensive evaluation model and software for blasting effect	Conducting the refined evaluation of post-explosion blasting effect based on optimisation theory, linear programming and fuzzy mathematics	Numerical simulation	None	None
Software integrating blasting design, optimisation and effect evaluation	Visualisation	Visualization module of design software based on OpenGL graphics library	Yes	Yes	Yes
	Software operation efficiency and interface	Comprehensive application of STL standard template library, WildMagic math function library, quaternion etc. efficient and user-friendly	Low efficiency	Low efficiency	Low efficiency
	Storage and output of results	Complete storage, output and print capabilities	Yes	Yes	Yes

Blast-Code blasting design software for bench blasting, which are from Orica company, and the Huayisoft Blast. The comparative analysis is from the aspects of blast design software, blast effect evaluation software and blast system function, as shown in Table 3.

4 FIELD APPLICATION OF THE SOFTWARE FOR OPEN DEEP HOLE BLASTING DESIGN AND OPTIMISATION

4.1 Project profile

The production capacity of the Beskuduk open-pit coal mine in Xinjiang is 3 million tons/year. There are obvious stratification, developed fractures, underground rivers and large water inflow. See Figure 11 for the construction site environment.

4.2 Blast area contour lines input

The contour data is obtained by measuring the top line and the bottom line, as shown in Table 3.

The initiation sequence was determined based on the adaptive blasthole arrangement and the Voronoi grid technique, and the blasthole position map is shown in Figure 12 and the detonation sequence diagram is shown in Figure 13.

The blasthole was laid out based on the software design parameters and the blasting experiment was carried out. The blasting effect is shown in Figure 14.

Perform threshold segmentation on the selected region image, and click the ‘granularity extraction’ button to display the effect of image processing, as shown in Figure 15.

Figure 11. Site construction picture.

Table 4. The input file of blast zone profile.

Top of slope			Bottom of slope	
2			9	
12			29571.5308	51192.7225
29579.4785	51193.5682	1	29576.2669	51180.5181
29585.9648	51176.2667	1	29578.7596	51163.3325
29588.0332	51158.8203	1	29586.4870	51142.9048
29596.3203	51144.8373	1	29587.9826	51124.4779
29597.4941	51121.0298	1	29576.7655	51105.7978
29583.4922	51100.2879	1	29558.3194	51098.0767
29601.1234	51071.0468	2	29580.0047	51055.1572
29625.1155	51065.2355	2	29620.0263	51042.7166
29646.5630	51087.7544	-1		
29619.1968	51101.8081	-1		
29622.7614	51159.7639	-1		
29603.9655	51196.3505	-1		

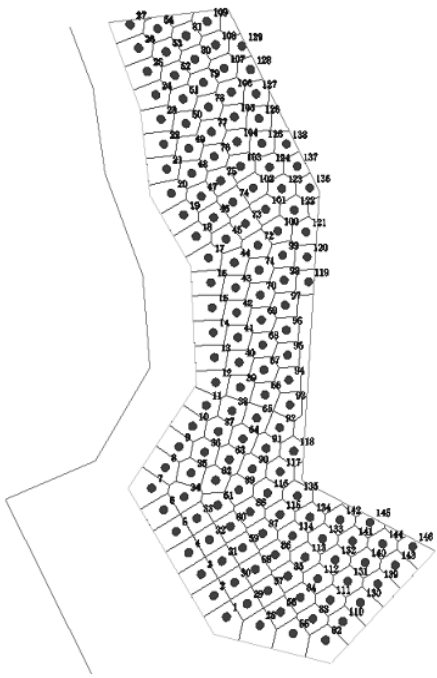

Figure 12. The diagram of Voronoi grid diagram.

4.3 Comparative analysis of application results

Through software development and engineering practice, it shows as follow:

– The software module developed by the Voronoi diagram-based charge calculation algorithm and the hole-by-hole blasting sequence determination algorithm, combined with 3D laser scanner and RTK measuring instruments, can effectively improve the precision of the blasthole layout and the efficiency of explosive energy. The engineering application shows that the explosive unit consumption is reduced by more than 10%, that the shovel loading efficiency is increased by 15%, and that the blasthole resistance line deviation is reduced from 0.056 to 0.008.
– The block rate analysis and statistics module developed based on the image processing technology, the image binarisation method and the contour recognition technology can effectively analyse the block size and collect statistics. The engineering application shows that for a given muck pile, the explosion block identification is automatically completed, and the time is shortened by more than 30%.
– The developed blasting vibration waveform prediction method based on the improved Anderson model can realise full-time prediction of blasting seismic waves, which can effectively reduce the harmful effects of blasting vibration. According to the engineering practice, the blasting vibration intensity is reduced by 20%.

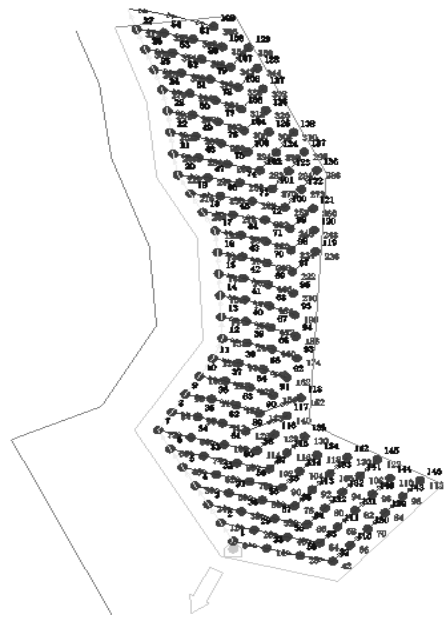

Figure 13 Initiation sequence.

Figure 14. Blasting effect.

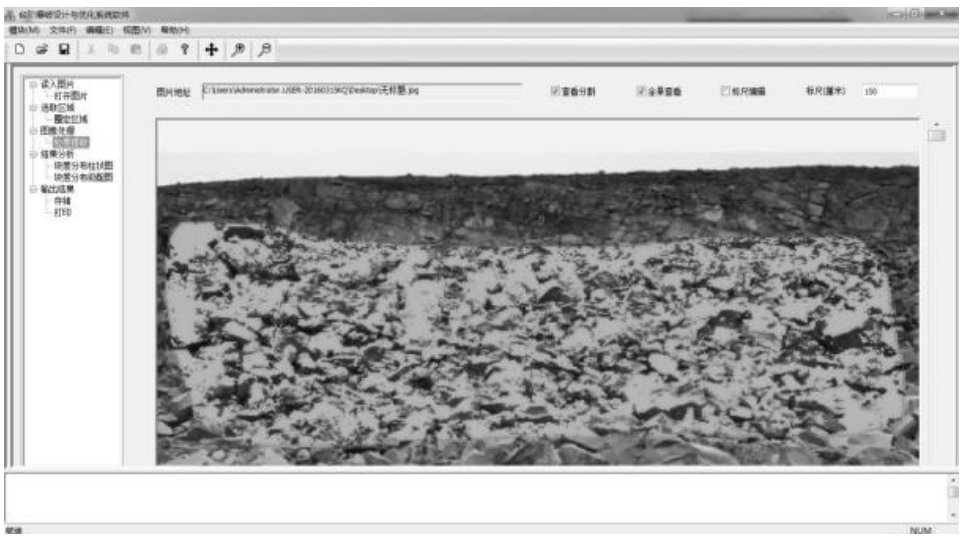

Figure 15. Diagram of granularity extraction processing effect.

5 CONCLUSIONS

This paper proposes a new method for blasthole layout and perforated blasting initiation sequence based on Voronoi theory. It realises the automotive hole layout and network design for deep hole blasting, and it develops a design and optimisation program for bench blasting.

Based on the burst size distribution algorithm and the image segmentation technique, the burst size distribution algorithm is proposed based on image processing technology, and the block rate statistical analysis program is developed.

Based on the improved Anderson model, the blasting vibration waveform prediction method realizes the full-time prediction of blasting seismic

waves, which effectively reduces the harmful effects of blasting vibration.

A comprehensive evaluation module for blasting effect is developed. It, with the combination the optimisation theory, the linear programming and the fuzzy mathematics, can accurately and effectively predict blasting effects, which can provide a decision-making basis for blasting parameter optimisation.

REFERENCES

Chen, Q.S., Zhang, Q.L., Chen, X., Xiao C.C. & Jiang Q. 2016. Prediction of blasting-vibration-peak-speed based on GRA−GEP. *Journal of central South University (Natural Science Edition)*, 47(07): 2441-2447.

Duan, Y., Xiong, D.Y. & Xu, G.Q. 2015. A new technology for digital drilling and automatic lithology identification. *Metal Mine*, (10): 125-129.

Fei, H.L. & Guo, L.J. 2015. Digitization of blasting construction. *Proceedings of the eighth annual conference of engineering and demolition Specialised Committee of China mechanics society and academic exchange conference*, Engineering blasting Specialised Committee of China mechanics Society: Chinese Society of Theoretical and Applied Mechanics,.

Guo, J.P., Wang, J. & Li, J.Q. 2017. Study on optimum design of blasting hole arrangement in medium-length hole blasting. *Blasting*, 34(03): 79-84+89.

Guo, L. *et al.* 2011. CAD secondary development of medium-depth hole blasting design system based on object/ARX. *Applied Mechanics and Materials*, Vol. 65, pp. 285-290.

Hu, X.L., Qu, S.J., Jiang, W.L., Li, H., Yang, W., Huang, H.B. & Hu, G.Q. 2017. Attenuation law of blasting induced ground vibrations based on equivalent path. *Explosion and Shock Waves*, 37(06): 966-975.

Lei, Z., Yang, R.S., & Tao, T.J. 2015. Comprehensive evaluation of bench blasting effect based on uncertainty measurement theory. *Journal of China Coal Society*, 40(02): 353-359.

Liu, B. & Wang, M.L. 2015. Overview of theory maturity and feasibility application in digital blasting. *Proceedings of the eighth annual conference of engineering and demolition Specialised Committee of China mechanics society and academic exchange conference*, Engineering blasting Specialised Committee of China mechanics Society: Chinese Society of Theoretical and Applied Mechanics.

Liu, J., Wu, M., Yun, B., Zhao, C.B. & Li, T.T. 2010. Prediction of structure vibration induced by potential ambient excitation. *Chinese Journal of Solid Mechanics*, 31(S1): 143-151.

Liu, J., Zhang, Y. & Yun, B. 2012. A new method for predicting nonlinear structural vibrations induced by ground impact loading. *Journal of Sound and Vibration*. 331: 2129-2140.

Qiu, X.Y., Shi, X.Z., Zhou, J., Huang, D. & Chen, X. 2017. On vibration reduction effect of short millisecond blasting by high-precision detonator based on HHT energy spectrum. *Explosion and Shock Waves*, 37(01): 107-113.

Shen, S.W., Xu, J.C., Dai, S.L. & Xu, Y. 2013. Extenics evaluation of joint rock tunnel blasting quality based on entropy weighting method. *China Civil Engineering Journal*, 46(12): 118-126.

Shi, J.J., Li, Q.Y., Zhang, Q., Wei, X. & Wang, H.. Forecast system for blasting vibration velocity peak based on Matlab and BP neural network. *Explosion and Shock Waves*, 37(06): 1087-1092.

Wang, M.Z., Shi, X.Z., Zhou, J. & Qiu, X.Y. 2018. Multi-planar detection optimisation algorithm for the interval charging structure of large-diameter longhole blasting design based on rock fragmentation aspects. Taylor and Francis Ltd.

Writing group of 'Coal mining design manual'. 1987. *Mining design manual* (2). Mineral exploration roll (top). Beijing: China Architecture & Building Press.

Xie, F., Han, L., Liu, D.S. & Li, C. 2018. Vibration law analysis for a tunnel's field near blasting based on waveform superposition theory. *Vibration and Shock Waves*, 37(02): 182-188.

Yu, D.X., Zhang Z.W., Zhou, X.D., Xiao, F., Tan Y. & Zhao R.Q. 2010. Software development of design and optimisation for hole-by-hole bench blasting. *Blasting*, 27(01): 37-40.

Zhang, D.B., Chen, Z.Q., Yi, L.L. & Xu, H.X. 2018. Binarisation representation of image microstructure and the application of object recognition. *Journal of Electronics and Information Technology*, (03): 633-640.

Zhou, K.P., Shi, W.C., Wang, M.Z. & Ke, B. 2017. Intelligent identification and auxiliary design for blasting parameters of large diameter deep hole. *Blasting*, 34(04): 73-79.

Helsinki Conference Proceedings 2019, R. Holmberg et al

Numerical study of the impact of joints on rock fragmentation by blasting

C.P. Yi, D. Johansson, H. Schunnesson & H. Åhlin
Division of mining and rock engineering, Luleå University of Technology, Luleå, Sweden

ABSTRACT: Rock masses consist essentially of intact rock and discontinuities such as joints. Blasting is mostly used method for the rock excavation. To investigate the effects of joints on the fragmentation by blasting, three models with different joint patterns and one model without joint were created in the LS-DYNA code. In these models, a bonded particle model was used to represent the rock to be blasted, a finite element model was adopted to model the remaining rock mass and a particle blast model was employed to describe the detonation of explosives. To validate the contact model for joints, the fragmentation pattern and the individual particle motion from two single borehole shot models with and without joints were compared. The numerical results indicated that the existence of joints has a significant effect on fragmentation and vibration. The models with joints produced finer fragmentation compared to the model without joints in the paper. Keywords: blasting, joints, fragmentation.

1 INTRODUCTION

Blasting technology is widely employed in mining in order to fragment the rock into smaller pieces to facilitate subsequent handling (mucking, haulage, crushing, etc.). Rock masses are far from being continua and consist essentially of two constituents: intact rock and discontinuities such as joints. It is a well-known fact that rock mass properties play an important role in rock fragmentation. Further, properties like rock mass strength and joint pattern have maximum influence on the rock explosive interaction.

The works of Belland (1968) and Talhi *et al.* (2003) indicated that the fragmentation improved considerably by orienting the free face parallel to and on the dip side of the principal joint planes. Singh & Sarma (1983) conducted a model-scale study of single hole blasts in constructed test specimens with different burdens and joint orientations. It was found that the degree of fragmentation at a particular point in the model was dependent on the distance to the charge and the number of joints between the point and the charge.

Yang & Rustan (1983) performed 40 one-hole blasts on model-scale specimens. Besides reference blocks, three types of models were constructed: one with weakness planes parallel to the face, one with weakness planes parallel and perpendicular to the face and one type with short weakness planes in three or more directions randomly distributed. They concluded that weakness planes can attenuate the stress wave and

grow radial cracks during blasting depending on the direction and property of the weakness planes, the weakness planes usually decrease the strength of the rock and make it difficult for cracks to pass across them. Another conclusion was that with increased jointing it became more difficult to change the median fragment size, by changing the charge concentration, compared to less jointed models. Finally, Yang & Rustan (1983) also concluded that if a weakness plane is open and filled with air it has a very strong influence on the fragmentation compared to, if the weakness plane is filled with solid material.

Lilly (1986, 1992) introduced a blastability index in which weighted rating values were used to describe the resistance of a rock mass to blasting. The structural nature of the rock is the most important factor in this index as it is heavily weighted towards the orientation and spacing of weakness planes (joints) in the rock mass.

The field tests carried out by Beyglou *et al.* (2015) indicated that there is a correlation between blast performance and initiation direction according to the dip and strike of discontinuities.

Hyldahl (2017) developed a method for representing/introducing artificial joint planes into concrete blocks and carried out a series of small-scale tests to assess the influence of jointing on fragmentation. The results indicated that all the fabricated joint sets produce a finer median fragment size (x_{50}), than the median fragment size obtained from the reference blocks without joint sets.

Investigation of the impact of joints on fragmentation by scaled or full-size experiment is very expensive and time-consuming. Numerical methods as a useful tool are becoming increasingly popular in rock blasting. Many numerical investigations have been done to investigate the effect of joints on the propagation of stress wave (Huang *et al.* 2015, Zhao *et al.* 2012, Resende 2010). In this paper, the impact of joints on the fragmentation by blasting were numerically evaluated by using the LS-DYNA code based on a small-scale test. In the numerical models, several different numerical methods were coupled to make the models more realistic. A bonded particle model (BPM) was used to model the block to be blasted. The remaining block was modelled with finite element method (FEM). The detonation of explosives in the blast hole was modelled with

Figure 1. The set-up for the tests (Johansson & Ouchterlony 2013).

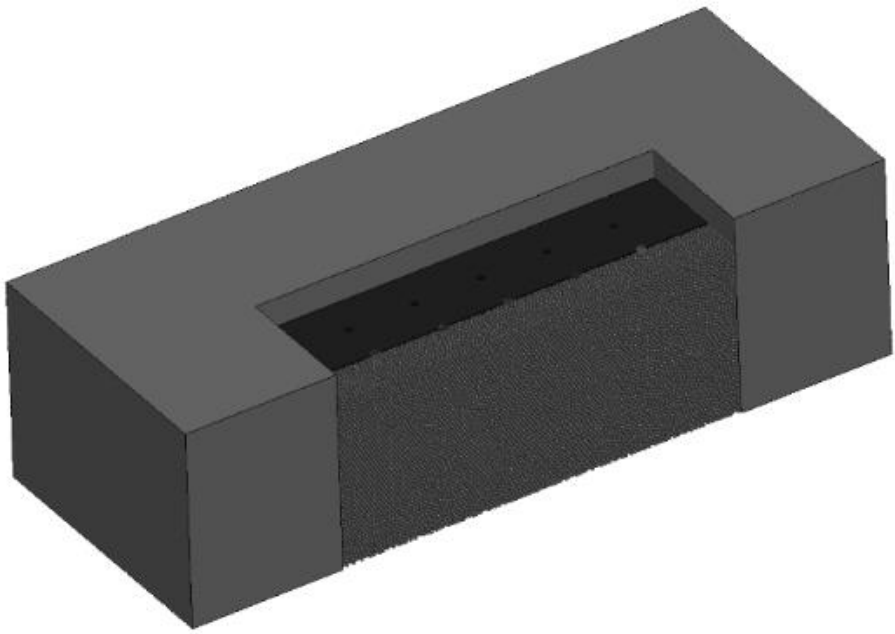

Figure 2a. Numerical model without joints.

particle blast model (PBM). The behaviour of joints was characterised with a contact model.

2 NUMERICAL MODELLING OF EFFECT OF JOINTS ON FRAGMENTATION

2.1 Numerical models with and without joints

The models are based on the small-scale tests conducted by Johansson & Ouchterlony (2013). To test the hypothesis that the short delay can improve the blasting effect, Johansson & Ouchterlony (2013) carried out a series of small-scale tests. The tests were made on magnetic mortar blocks. The blocks used had a size of 660×205×300 mm (L×W×H) with two rows with five Φ10 mm blastholes in each row. The spacing and burden was 110 mm and 70 mm respectively. To minimise reflecting waves and to emulate the full-scale geometry, the block was confined by a U-shaped yoke (Figure 1).

The explosive source was decoupled Pentaerythritol tetranitrate (PETN) cord with the strength of 20 g/m, giving a specific charge (q) of 2.6 kg/m^3 and a coupling ratio of 2.4. The delays were set by using different PETN-cord lengths to adjust the delay times between the blastholes.

Above each blasthole, a 59 mm high cylindrical initiation mounting block of plastic was positioned. After the blasting, the fragments were sieved and the fragment size distribution was taken as the evaluation indicator for the blasting performance.

To investigate the effects of joints on the fragmentation, three models for different joints patterns were created based on the set-up of the tests, see Figure 2 (Numerical models with and without joints). Figure 2a is a model without joints as a reference for jointed models and Figures 2b, 2c and 2d are models with joints. The joints were modelled with a contact model in LS-DYNA. All surfaces of the models shown in Figure 2 are free surfaces. The explosive is initiated hole-by-hole from the left to the right and the delay time is 28 μs.

2.2 Parameters of models

As mentioned early, the explosive source was decoupled PETN cord with the strength of 20 g/m with a coupling ratio of 2.4. The charge configuration in numerical models is shown in Figure 3a. The gap between the explosive and the wall of blasthole is filled with air. The initiation sequence is shown in Figure 3b.

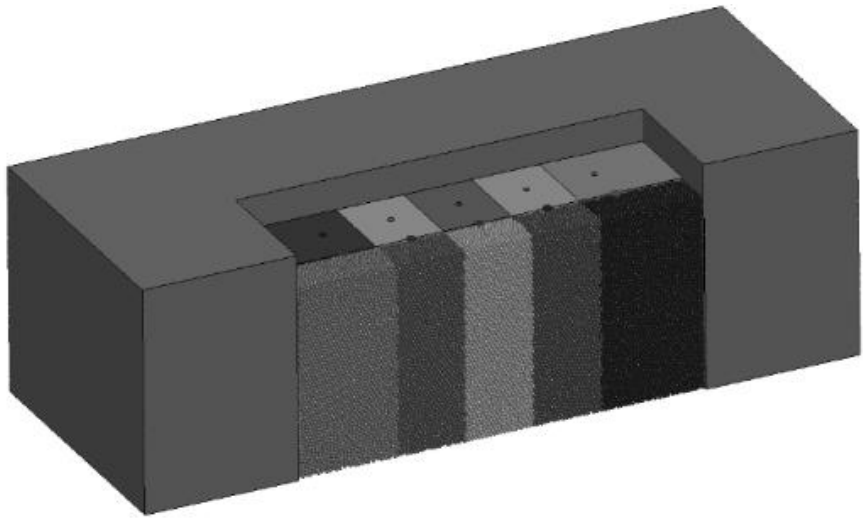

Figure 2b. Joint set I, Strike/dip = 0°/90°.

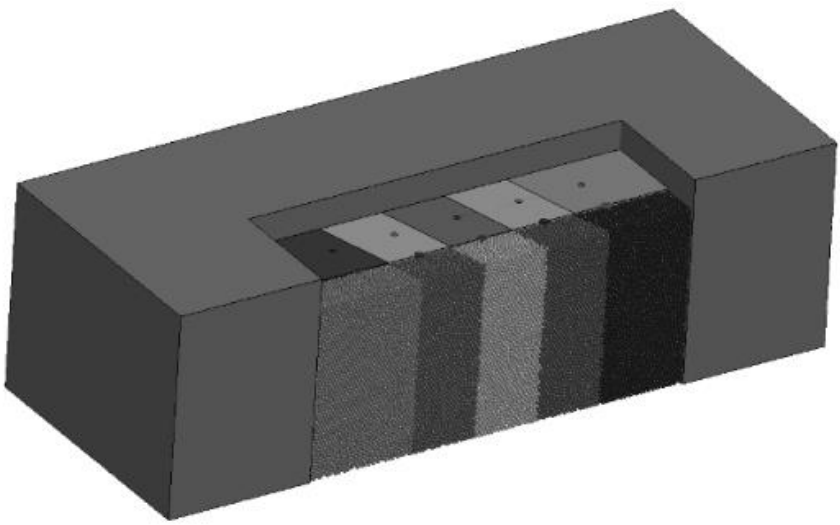

Figure 2c. Joint set II, Strike/dip = 15°/90°.

The detonation of explosives is described with the particle blast method. A co-volume effect has been introduced in this method to better represent gas behaviour at extreme pressure. For an efficient contact treatment, the particles are given a spherical shape. The particle-structure interactions are purely elastic collision. Each particle contains translational energy and spin energy. The balance between translational energy and spin energy is determined directly from the heat capacities. By grouping many molecules as one particle, the particle blast method reduces the degree of

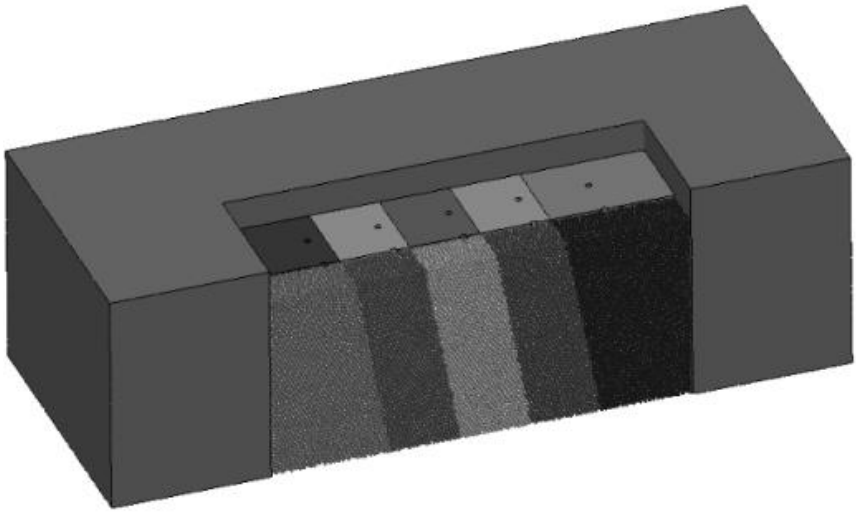

Figure 2d. Joint set III, Strike/dip = 0°/75°.

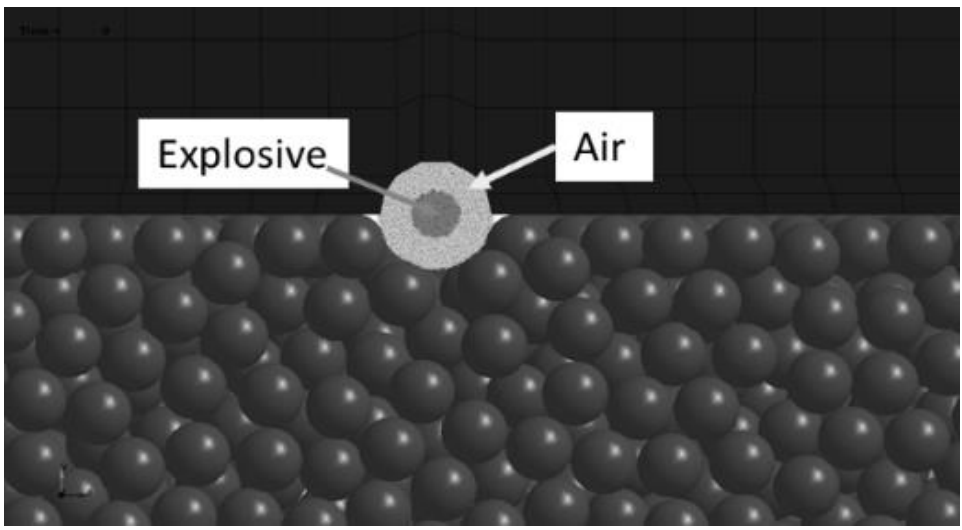

Figure 3a. Charge configuration.

freedom of the system by several orders of magnitude. The parameters used in the particle blast method of the PETN explosive are shown in Table 1.

The detonation velocity D, internal energy E, and density were taken from the Jones-Wilkins-Lee (JWL) (Lee *et al.* 1968) equation of state parameters of PETN explosive (Dobratz & Crawford 1985). The heat capacity ratio γ was also derived from the JWL equation of state parameter ω as $\gamma = 1 + \omega$. Co-volume coefficient b is from similar explosives. The built-in parameters of air in LS-DYNA is shown in Table 2.

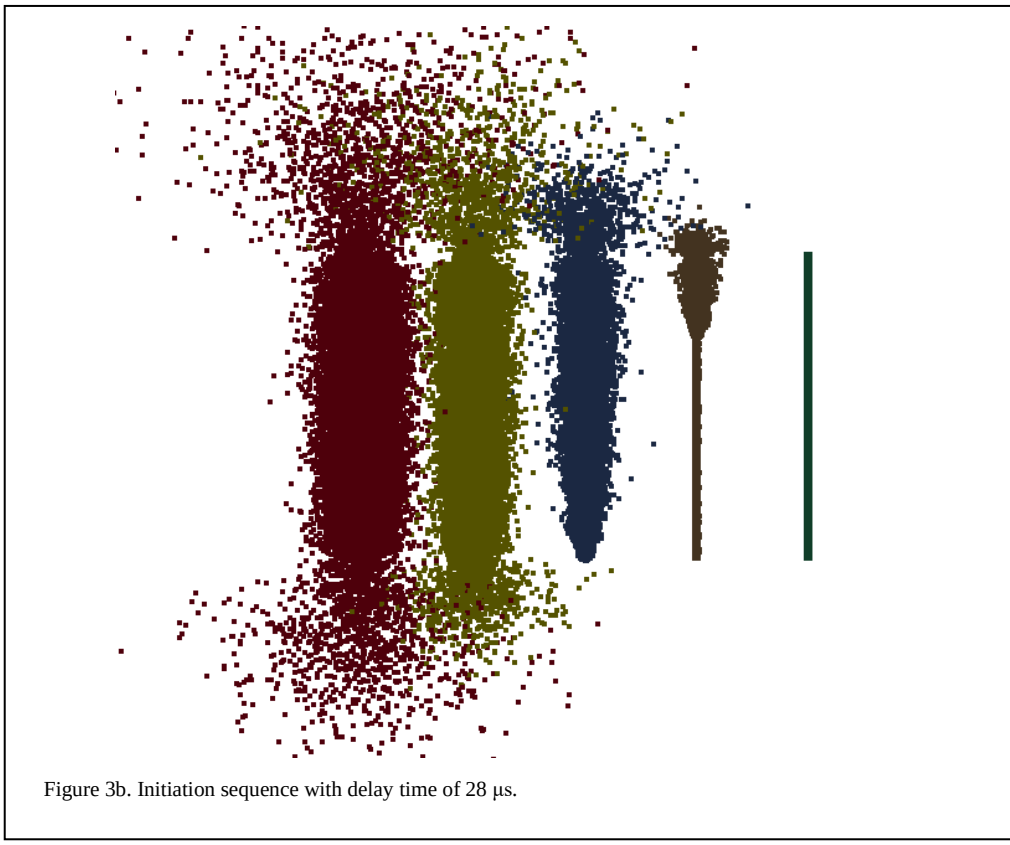

Figure 3b. Initiation sequence with delay time of 28 μs.

Bond particle models to 'bond' the particles have been developed in the LS-DYNA code, which originated the work of Potyondy & Cundall (2004). This makes modelling of a continuum possible. The bond models can be used to simulate the mechanical behaviour of an elastic solid as well as brittle fracture analysis (Karajan *et al.* 2013). Herein, all spherical particles are linked to their neighbouring particles using bonds which represent the complete mechanical behaviour of solid mechanics, see Figure 4. Bonds are independent of the DEM. Each bond is subjected to tension, bending, twisting and shearing. Bonds are calculated from the bulk and shear modulus of materials. Rock rupture is represented explicitly as broken bonds.

Table 1. Parameters of PETN.

D (m/s)	γ	ρ (Kg/m^3)	E (J/m^3)	b
7450	1.28	1500	8.56E9	0.35

In the model, there are 77,550 spherical particles with 3 mm radius. The parameters of the bonded particles are listed in Table 3.

Table 2. Parameters of air (Teng, personal communication).

ρ (Kg/m3)	E (J/m3)	Heat capacity ratio
1.27	2.53	1.4

The yoke is represented with FEM and the rigid body material is used for the yoke because the strength of yoke is much higher than that of the blasted block. The remaining part is represented with FEM and the Riedel-Hiermaier-Thoma (RHT) (Riedel *et al.* 1999) material is used to describe the dynamic response of the remaining part. The RHT material model in the LS-DYNA code is an advanced damage plasticity model for brittle materials such as concrete and rock. The material model involves three limit surfaces which

describe the strength of the material shown in Figure 5. The first surface is the yield surface which is limited by a cap surface. Beyond this surface, the material starts to deform plastically with a linear hardening description. When the material reaches the failure surface, the damage of the material starts to evolve until the damage is equal to one. When the residual surface is reached, the material is considered to be fully damaged and the strength is determined by a residual surface. The strain rate effect is also included in this model.

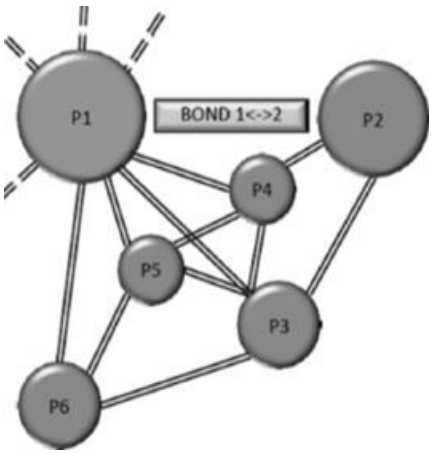

Figure 4a. Bonded particle model and possible force and moment transmission modes between two bonded particles (Karajan, *et al.* 2013).

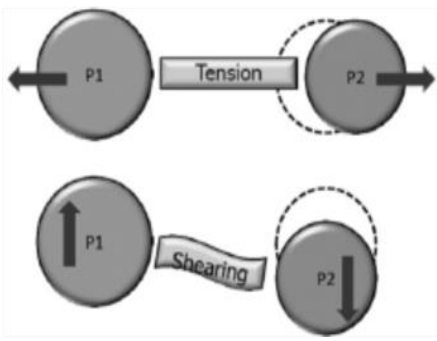

Figure 4b. Bonded particle model and possible force and moment transmission modes between two bonded particles (Karajan, *et al.* 2013).

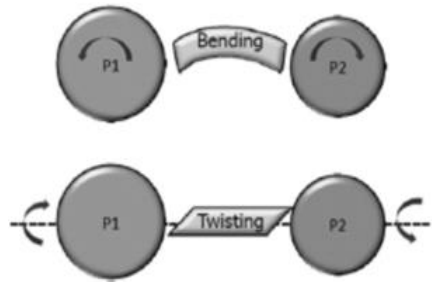

Figure 4c. Bonded particle model and possible force and moment transmission modes between two bonded particles (Karajan, *et al.* 2013).

Table 3. Parameters of bonded particles.

Particle properties:	
- Particle contact modulus (GPa)	21.9
- Scale factor of normal spring constant	0.01
- Scale factor of shear spring constant	0.00286
- Static coefficient of friction	0.51
- Rolling friction coefficient	0.1
Parallel-bond properties:	
- Shear stiffness/normal stiffness	0.5
- Parallel-bond modulus (GPa)	31.9
- Parallel-bond normal strength (MPa)	60.0
- Parallel-bond shear strength (MPa)	100.0

In this model, the damage level is defined using $= \sum \frac{\Delta \varepsilon^p}{\varepsilon^f}$, where $\Delta \varepsilon^p$ is the accumulated plastic strain and ε^f is the failure strain. D=1 means fully damaged while D=0 means undamaged. The main parameters of the RHT material model are listed in Table 4. In Table 4, ρ is the density and G is the shear modulus, σc is the uniaxial compressive strength and σt is the uniaxial tensile strength.

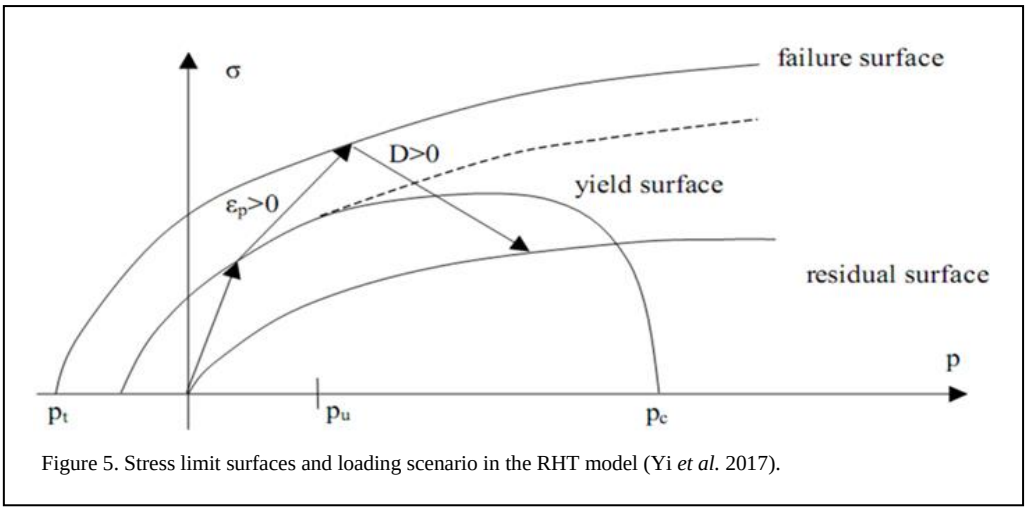

Figure 5. Stress limit surfaces and loading scenario in the RHT model (Yi *et al.* 2017).

Table 4. Parameters of mortar.

ρ (kg/m3)	G (GPa)	σc (MPa)	σt (MPa)
2511	8.98	50.7	5.22

2.3 Fragmentation analysis

The fragmentation patterns of the models with and without joints are shown in Figure 6. It can be seen from Figure 6 that many particles gather together still after blasting and form a lot of fragments which consist of different numbers of particles. In order to evaluate the fragment size distribution of each case after blasting, a code combining Fortran and Perl programming languages was developed. In the code, a collection of particles in which the distances between two adjacent particles are equal to the diameter of particles are treated as a fragment. The size of the fragments is the cube root of the volume of a fragment. The volume of a fragment is the sum of volumes of the particles that make up the fragment. It can be seen from Figure 6 that some particles at the corners do not move during the blasting. Similar phenomena can be found in small-scale tests, see Figure 6. Particles with displacement less than 2 mm are removed from the fragments in the code.

The fragment size distribution for four cases is shown in Figure 7. Figure 7 indicates that the existence of joints in the investigated cases improves the fragmentation compared to the reference case. For the fine fragment part, all cases have the similar size distribution. For the big fragment part, the models with joints give finer fragments compared to the reference case, which means the existence of joints benefits to reduce the boulder in the cases.

Table 5. Percentile sizes X30, X50 and X80 for four cases.

Size		No joint	Joint set I	Joint set II	Joint set III
Fraction (mm)	X30	10.41	8.15	9.4	10.52
	X50	43.98	38.88	34.47	35.59
	X80	69.24	49.11	54.25	51.6

Table 5 shows the percentile sizes X30, X50 and X80. The values correspond to the cumulative mass passing 30 %, 50 % and 80 %, respectively, based on linear interpolation between the two nearest fragment sizes in the size distribution graph.

If X50 is taken as the evaluation indicator for fragmentation, the improvement of X50 is 11.6%, 21.6% and 19.2% for the cases of Joint set I, Joint set II and Joint set III, respectively, which means the joint pattern can affect the fragmentation. A careful adaptation of blast design to existing discontinuities can yield significant improvement in fragmentation and therefore save the cost of production. However, the potential improvements are directly linked to the actual joint sets in the rock mass to be blasted and must be

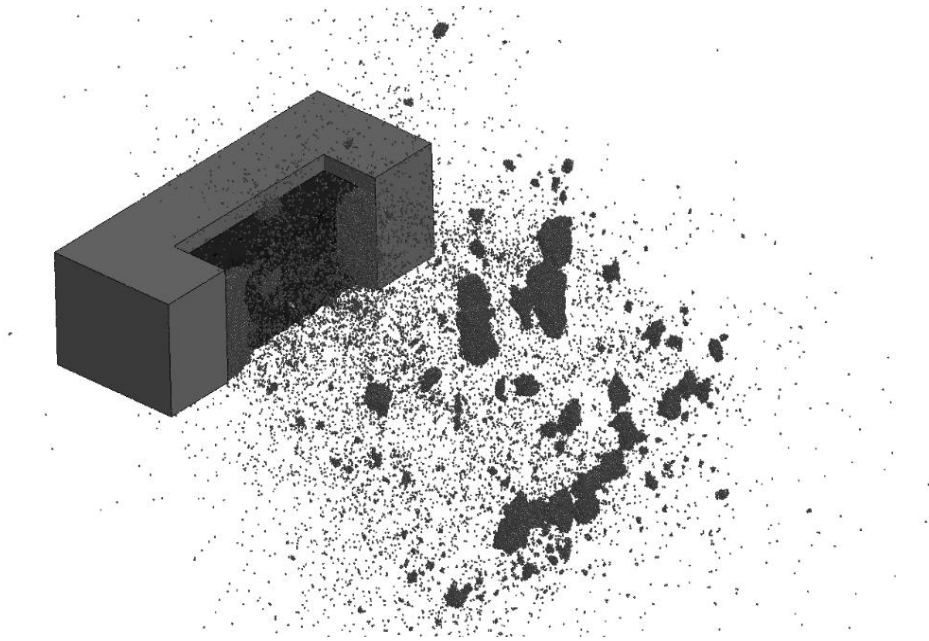

Figure 6a. Fragmentation pattern of the model without joints.

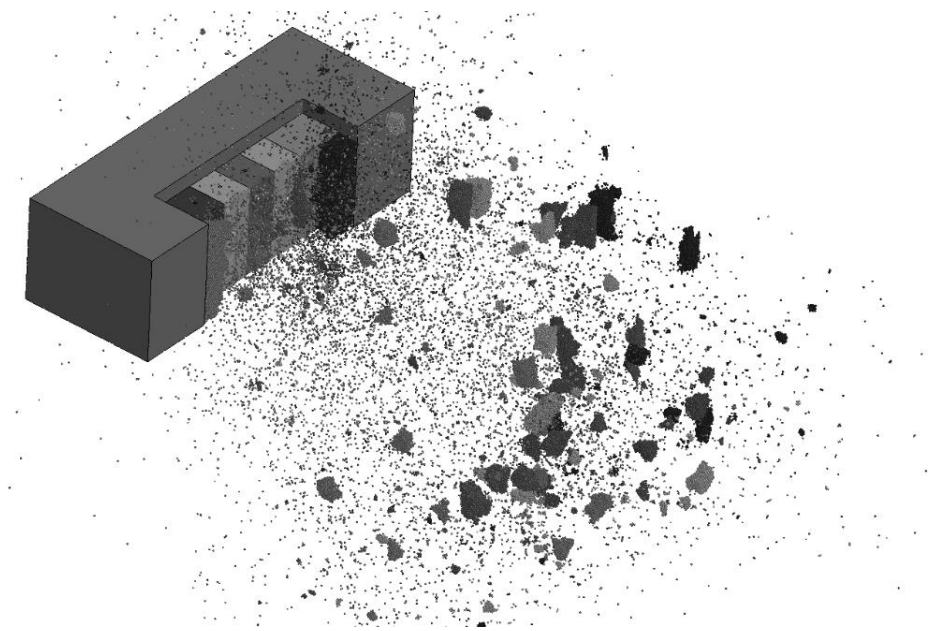

Figure 6b. Fragmentation pattern of the model with joint set I.

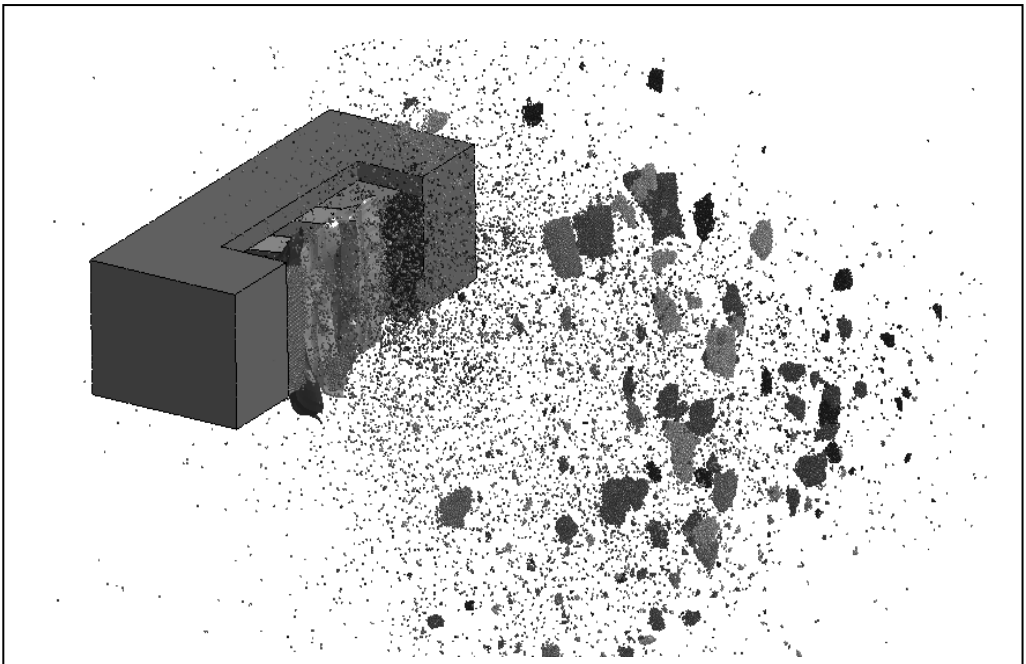

Figure 6c. Fragmentation pattern of the model with joint set II.

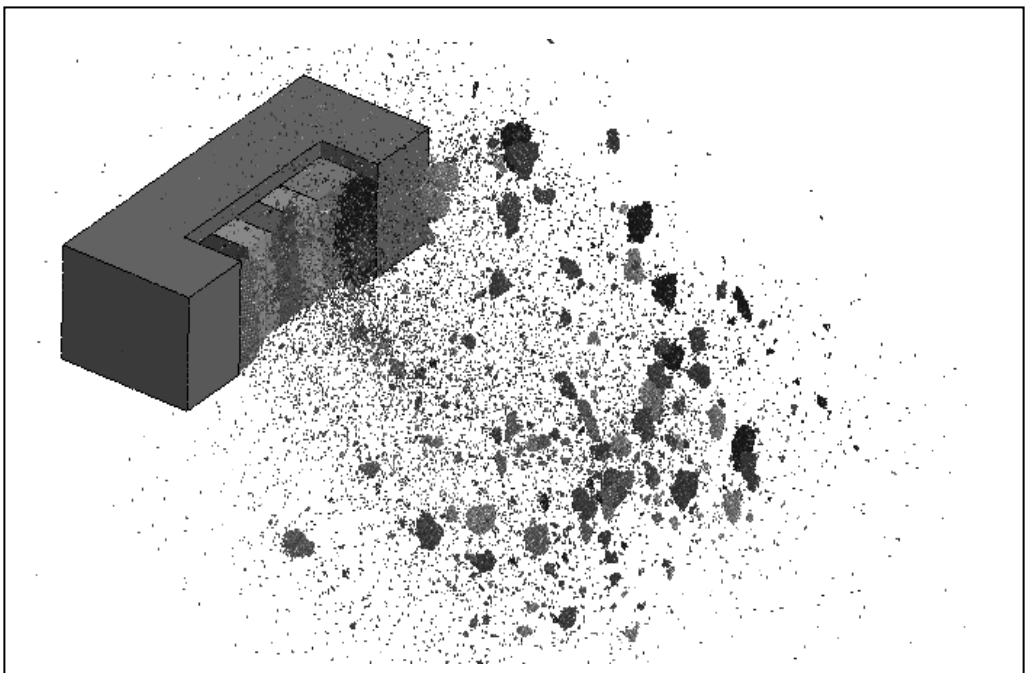

Figure 6d. Fragmentation pattern of the models with joint set III.

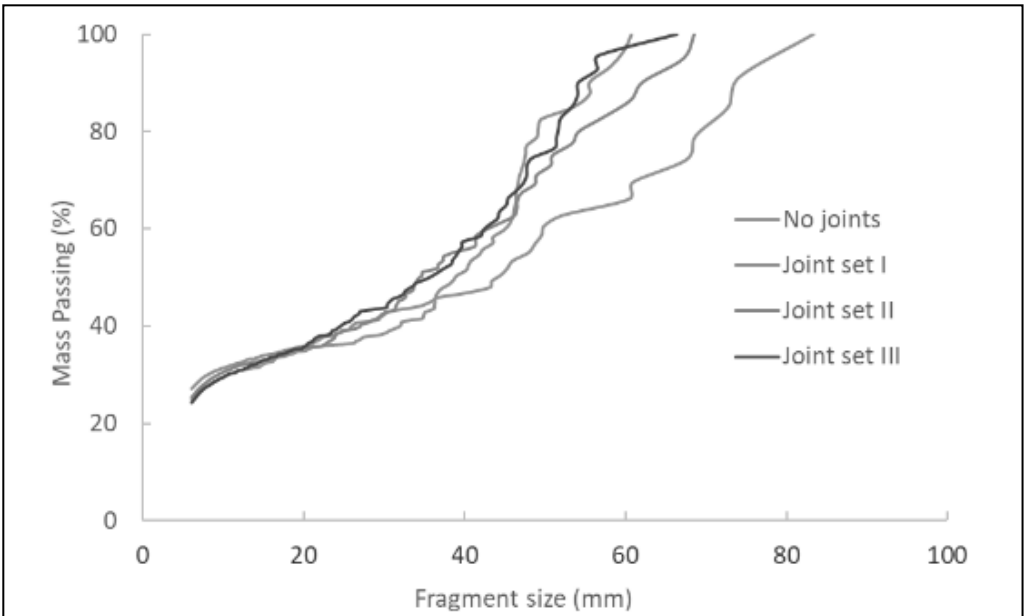

Figure 7. Fragment size distribution.

individually evaluated to give correct guidelines in which direction the blast should have. It is clearly seen in the models above, that there is good potential to adapt the rock quality (i.e. joints) and reduce the costs with maintained fragmentation results.

3 VIBRATION AND FRAGMENTATION FROM A SINGLE SHOT

To further validate the joint model used in the numerical model, two single shot models were created to investigate the effects of joints on

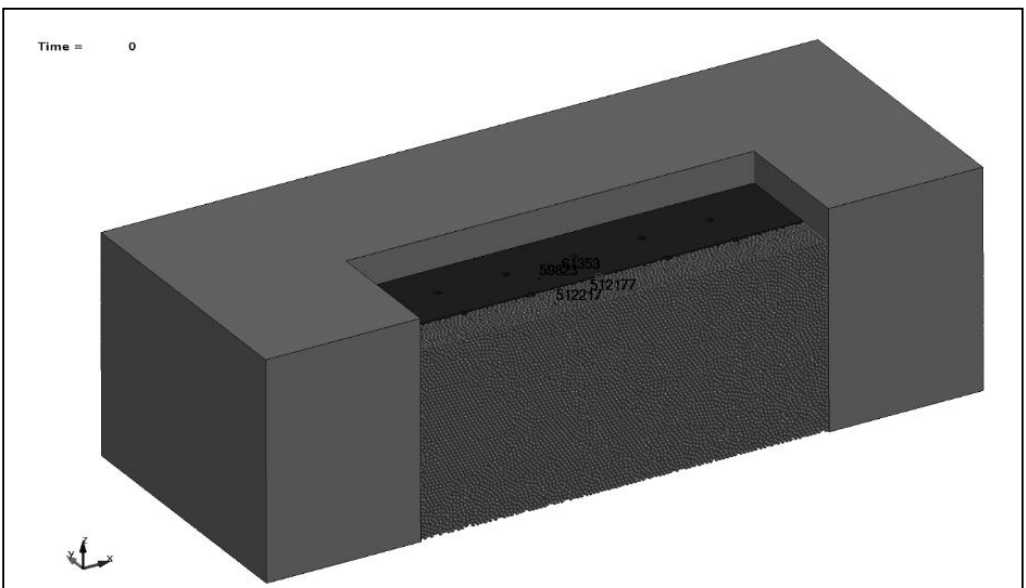

Figure 8a. Single shot model without joints.

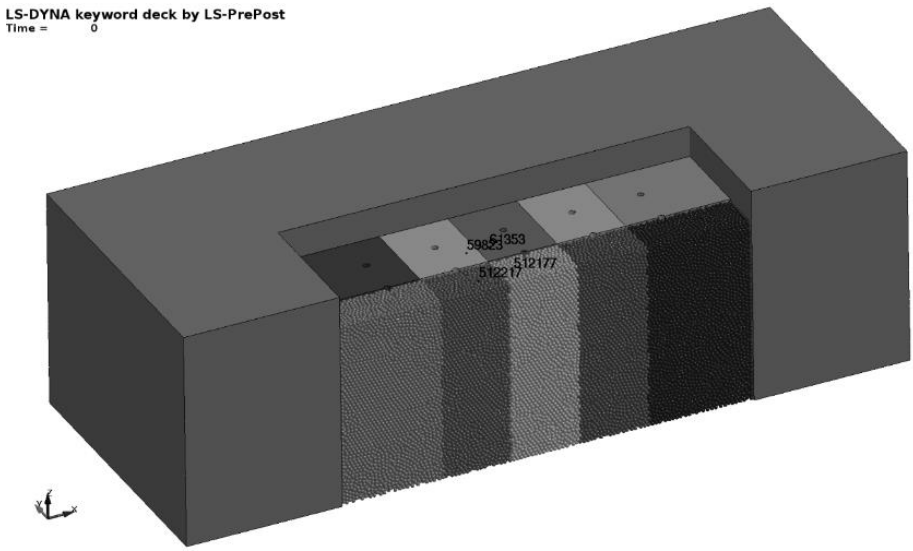

Figure 8b. Single shot model with joints.

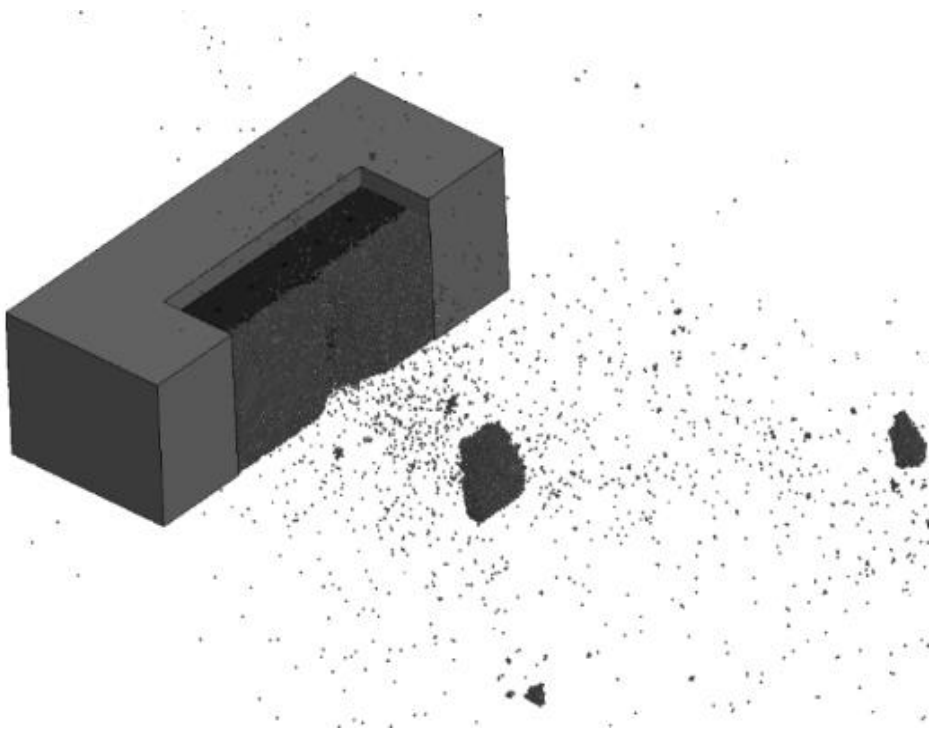

Figure 9a. Fragmentation pattern of a single shot without joints.

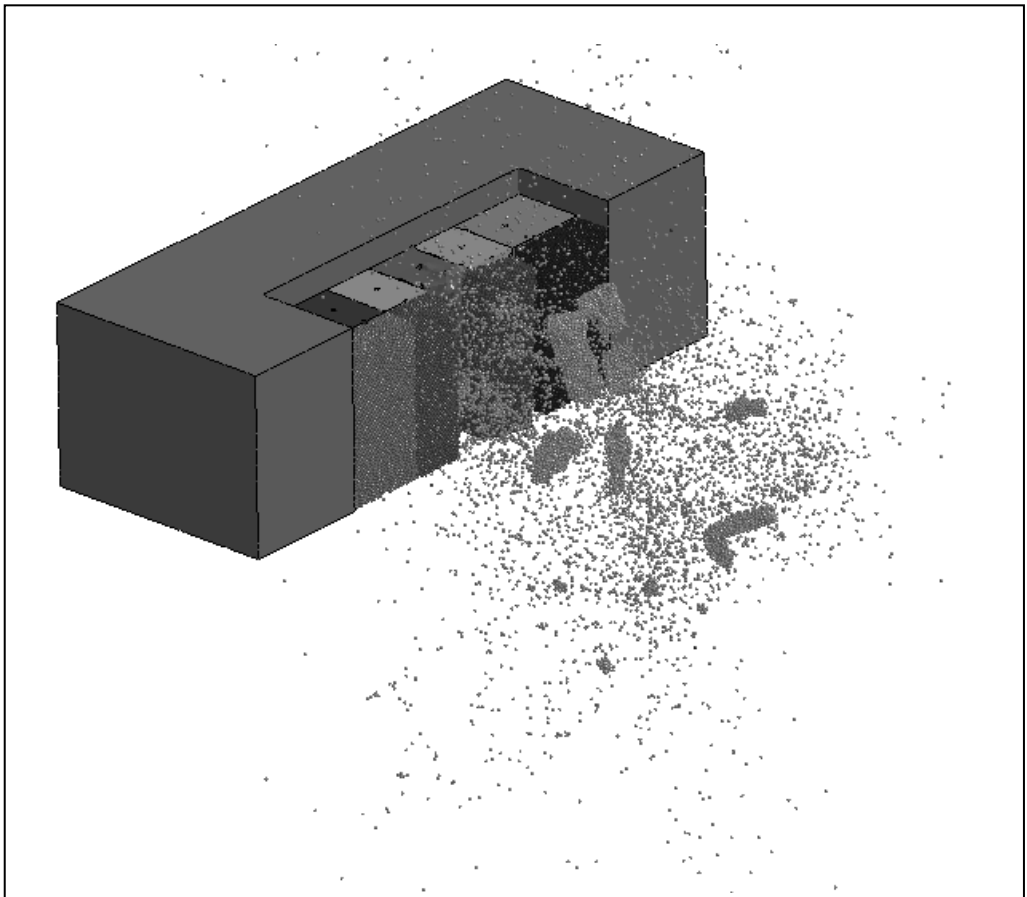

Figure 9b. Fragmentation pattern of a single shot with joints.

vibration and fragmentation. Compared to the models in Figures 2a and 2b, only the middle hole is charged in the models, see Figure 8. Two nodes, number 59823 and number 61353, were chosen to record the vibration velocity in the remaining rock mass. Figure 8b shows that there is a joint between node 59823 and node 61353. Two particles, number 512217 and number 512177, were chosen to record the displacement in the blasted rock mass. There is also a joint between two chosen particles.

Figure 9 shows that fragmentation pattern of single shot models with and without joints. It can be seen that the joints have significant influence on fragmentation. More volume of mortar is fragmented in the model with joints compared the model without joints.

The time histories of displacement in different directions of particles 512217 and 512177 are shown in Figure 10. Because particles 512217 and 512177 are close, it can be seen that they have the similar displacement-time histories in three directions for the model without joints, see Figures 10a, 10c and 10e. The displacement-time histories of these two particles also indicate that two particles did not detach from the block after the blasting because their final displacement is almost 0. In the model with joints, particles 512217 and 512177 have quite different displacement-time histories in three directions. Figures 10b, 10d, and 10f indicate that Particle 512217 detached from the block after blasting while Particle 512177 is still in the block after blasting.

The time histories of velocity in different directions of node 59823 and node 61353 are shown in Figure 11. Node 61353 is closer to the charge compared to node 59823. For the model without joints, the PPVs in X- and Y-directions of

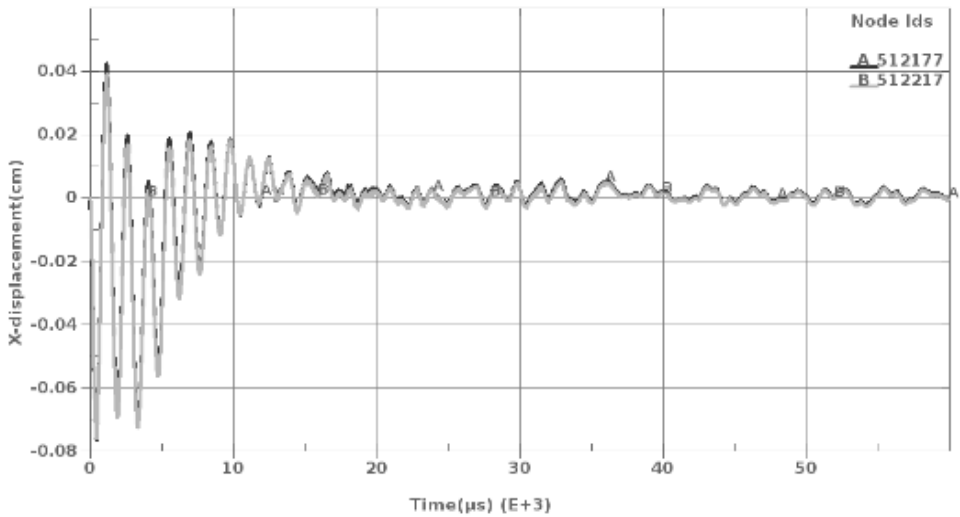

Figure 10a. Displacement in X-direction without joints.

node 61353 are higher than those of the node 59823, both nodes have the similar PPV in Z-direction. For the model with joints, the PPVs of node 61353 are higher than those of node 59823 in three directions. Comparison between of Figures 11c and 11d shows that the PPV of node 61353 in Y-direction in Figure 11d is higher that of node 61353 in Figure 11c while the PPV of node 59823 in Y-direction in Figure 11d is lower than that of node 59823 in Figure 11c. The similar phenomena can be found for PPV in Z-direction by comparing Figures 11e and 11f. The reason is that the propagation of stress waves induced by the detonation of explosives is hindered by the joints, which indicates that the contact model used in the numerical model can characterise the behaviour of joints.

Both the fragmentation pattern and the particle motion comparison show that the presence of joints has much effect on fragmentation by blasting.

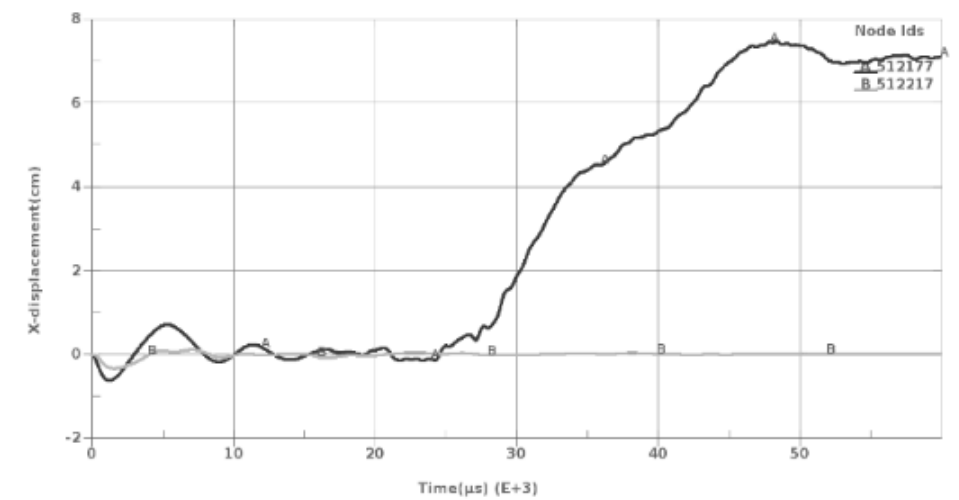

Figure 10b. Displacement in X-direction with joints.

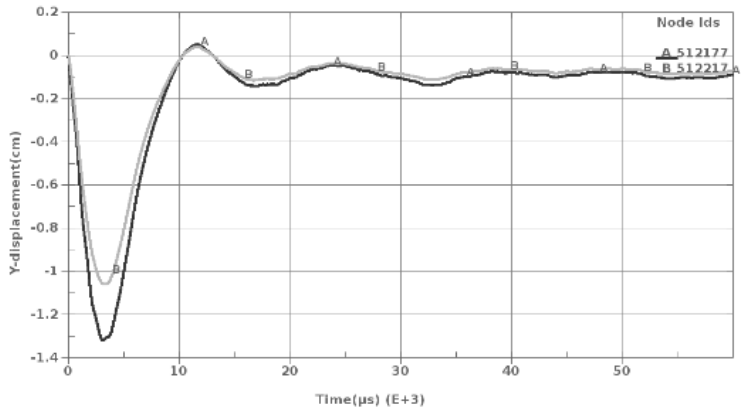

Figure 10c. Displacement in Y-direction without joints.

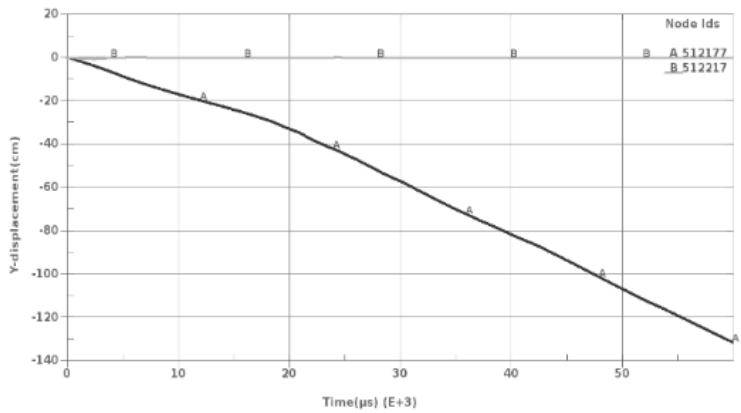

Figure 10d. Displacement in Y-direction with joints.

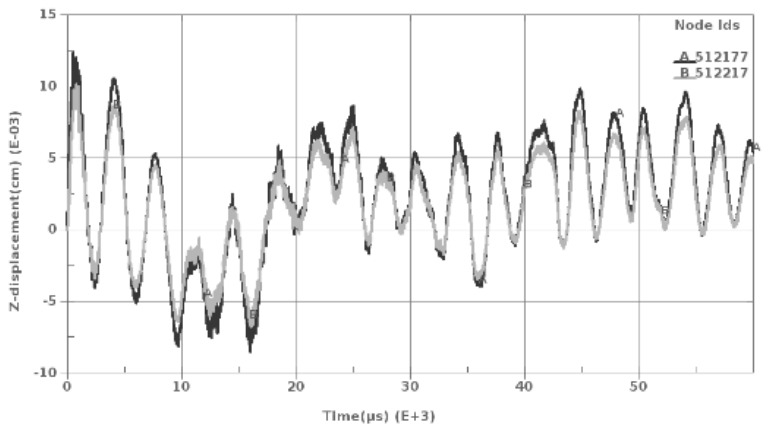

Figure 10e. Displacement in Z-direction without joints.

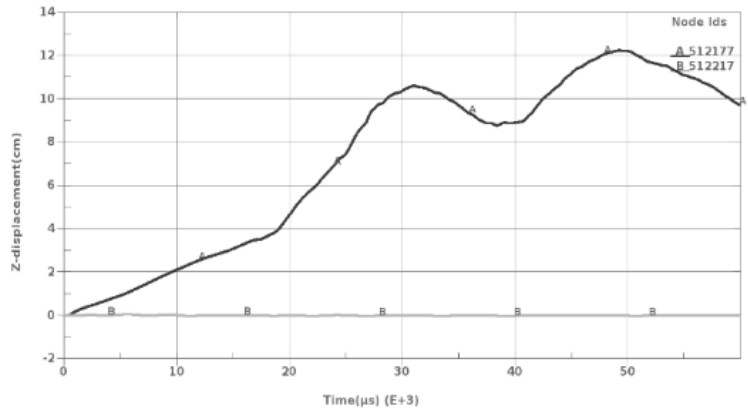

Figure 10f. Displacement in Z-direction with joints.

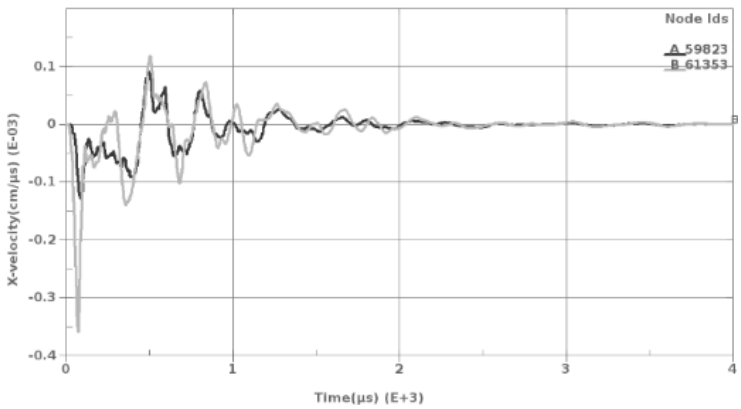

Figure 11a. Velocity in X-direction without joints.

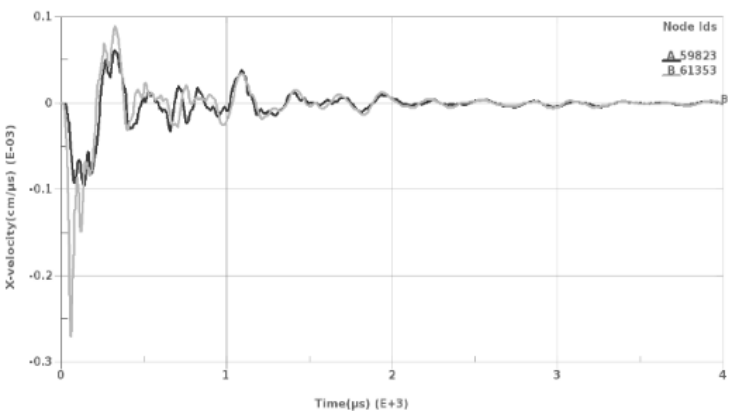

Figure 11b. Velocity in X-direction with joints.

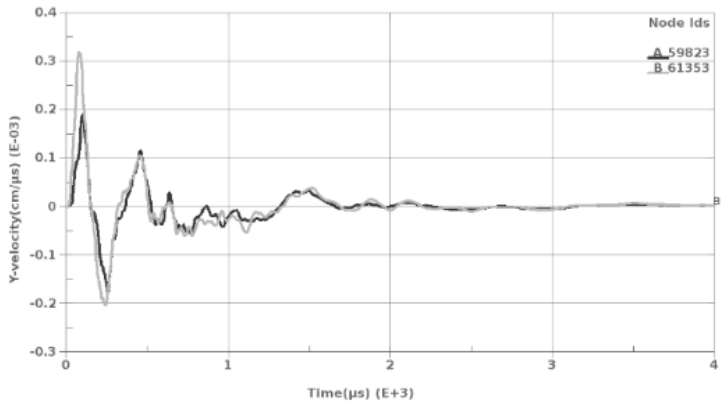

Figure 11c. Velocity in Y-direction without joints.

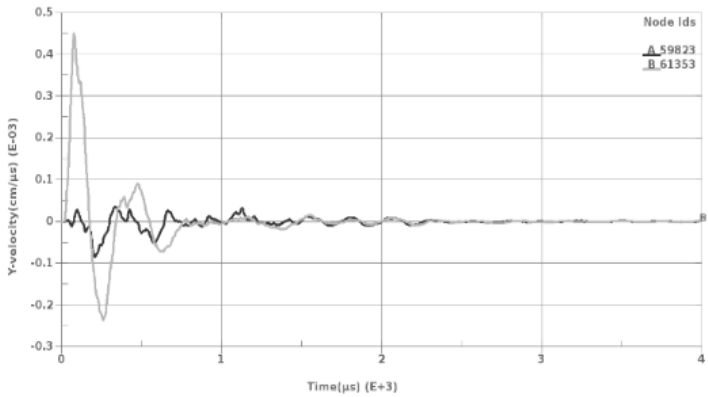

Figure 11d. Velocity in Y-direction with joints.

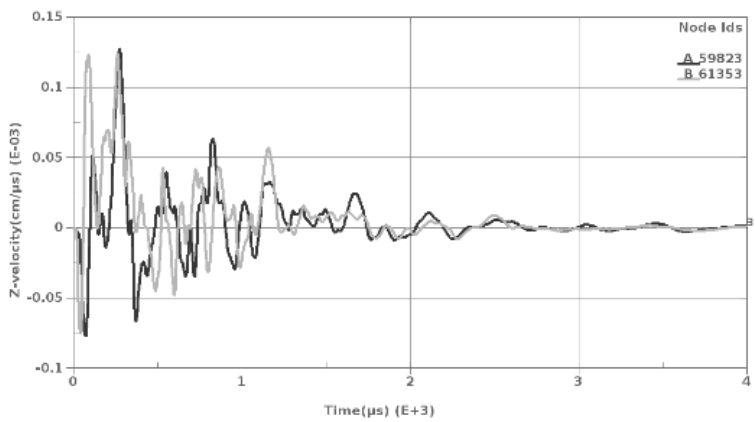

Figure 11e. Velocity in Z-direction without joints.

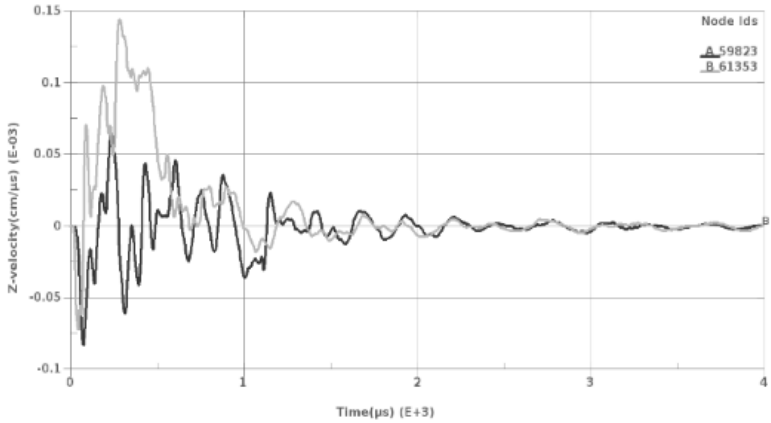

Figure 11f. Velocity in Z-direction with joints.

4 CONCLUSION

A coupled FEM-PBM-BPM model was used to investigate the effects of joints on fragmentation and vibration. The behaviour of joints was characterised with a contact model. The preliminary results indicate that the existence of joints has much effect on fragmentation and vibration. A careful adaptation of blast design to existing discontinuities could yield significant improvement in fragmentation and therefore save the cost of production.

In the research, some simple joint patterns were used. In practice, the patterns of joints in rock mass could be complicated. The orientation of the joint planes depends on two characteristic attributes of strike and dip. The effects of orientation of the joint planes, the contact stiffness of joint planes and the spacing of joints on fragmentation and vibration will be studied in the future.

5 ACKNOWLEDGEMENTS

The authors would like to thank the support from the project of SLIM funded by the European Union's Horizon 2020 research and innovation program under grant agreement nº 730294, VINNOVA and Centre of Advanced Mining & Metallurgy (CAMM2) at LTU which are gratefully acknowledged.

REFERENCES

Belland, J.M. 1968. Structure as a control in rock fragmentation Coal Lake iron ore deposit. *The Canadian Mining and Metallurgical Bulletin*, 59:323-328.

Byglou, A., Schunnesson, H., Johansson, D., Johansson N. 2015. Adjusting initiation direction to domains of rock mass discontinuities in Aitik open pit mine. *Proceedings of the 11th International symposium on rock fragmentation by blasting:* Fragblast 11, Sydney, AusIMM, pp. 385–391.

Dobratz, B.M. & Crawford, P.C, 1985. *LLNL Explosives Handbook*: Properties of chemical explosives and explosive simulants. Livermore, CA, USA.

Fourney, W.L., Barker, D.B. & Holloway, D.C. 1983. Fragmentation in jointed rock material. *Proceedings 1st International symposium on rock fragmentation by blasting*, Luleå, Sweden.

Huang, X., Qi, S., Williams, A., Zou Y. & Zheng B. 2015. Numerical simulation of stress wave propagating through filled joints by particle model. *International journal of solids and structures*, 70:23-33.

Hyldahl, J. 2018. Effects of jointing on fragmentation--design and influence of joints in small scale testing. *Master thesis*, Luleå University of Technology: Luleå.

Johansson, D. & Ouchterlony, F. 2013. Shock wave interactions in rock blasting – the use of short delays to improve frag-mentation in model-scale. *Rock mechanics and rock engineering*, 46:1-18.

Karajan, N., Han, Z., Teng, H. & Wang, J. 2013. Interaction possibilities of bonded and loose particles in LS-DYNA [online]. Available from:

<https://www.dynamore.de/en/downloads/infodays/dokumente/2013-multiphysik > [Accessed 18 July 2019].

Lee, E.L., Horning, H.C. & Kury, J.W. 1968. Adiabatic expansion of high explosives detonation products, Lawrence Livermore National Laboratory, University of California, Livermore, TID 4500-UCRL50422.

Lilly, P A, 1986. An empirical method of assessing rock mass blastability. *Proceedings large open pit mining conference*, pp 89–92.

Lilly, P A, 1992. The use of the blastability index in the design of blasts for open pit mines. *Proceedings West Australian conference on mining geomechanics*.

Nur K., Hareyani Z., Kamar A. & Mohd M.H. 2016. Effect of geological condition on degree of fragmentation in a Simpang Pulai Marble quarry. *Procedia Chemistry* 19: 694-701.

Potyondy, D.O. & Cundall, P.A. 2004. A bonded-particle model for rock. *International journal of rock mechanics and mining sciences*, 41 (8): 1329-1364.

Riedel, W., Thoma, K., Hiermaier, S. & Schmolinske, E. 1999. Penetration of reinforced concrete by BETA-B-500, numerical analysis using a new macroscopic concrete model for hydrocodes. In SKA(ed.), *Proceedings of the 9th International symposium on interaction of the effects of munitions with structures*: 315-322, Berlin.

Resende, R. 2010. An investigation of stress wave propagation through rock joints and rock masses. *Doctoral thesis*. Porto University, Portugal.

Singh, D.P. & Sarma, K.S. 1983. Influence of joints on rock blasting – a model scale study. *Proceedings 1st International symposium on rock fragmentation by blasting*, volume 2, Luleå, Sweden.

Talhi, K. & Bensaker, B. 2003. Design of a model blasting system to measure peak p-wave stress. *Soil dynamics and earthquake engineering*, 23(6): 513-519.

Yang, Z.G. & Rustan, A. 1983. The influence from primary structure on fragmentation. *Proceedings 1st International symposium on rock fragmentation by blasting*, Luleå, Sweden.

Yi, C., Sjöberg, J., Johansson, D. & Petropoulos, N. 2017. A numerical study of the impact of short delays on rock fragmentation. *International journal of rock mechanics and mining sciences*, 100: 250-254.

Zhao, J., Sun, L. & Zhu, J. 2012. Modelling P-wave transmission across rock fractures by particle manifold method (PMM). *Geomech. geoeng*. 7, 175-181.

Helsinki Conference Proceedings 2019, R. Holmberg et al

Optimising blast layouts by aerial imagery and automatic placement of boreholes

A. Gaich, M. Pötsch & P. Hergan
3GSM GmbH, Graz, Austria

ABSTRACT: The paper presents a new concept for designing surface blasts. It is a pure geometric approach relying on comprehensive and accurate 3D surface models of the entire area to blast. Photogrammetric 3D models from aerial imagery are used as for that purpose. The new approach uses the minimum burden concept and extends it with so-called minimum burden surfaces that form the basis for an automatic placement of the boreholes. The concept is especially useful at more complex or irregularly shaped blast sites as shown in the contribution.

1 INTRODUCTION

Remote-controlled camera drones have reached a level of maturity which allow their routine application in surface mining and quarrying for acquiring aerial imagery at high quality and resolution. Ongoing development in digital photogrammetry allows for a rapid and consistent processing of large sets of overlapping photos to registered 3D models. By using such 3D models several surveying and assessment tasks in surface mining are addressed such as stockpile measurements, mine planning, or stability assessments. This contribution deals with the design of surface blasts based on 3D models.

Pro-active blast design includes the adaptation of the borehole locations according the actual shape of the bench face (Moser *et al*. 2007). By doing so blasting results are improved, flyrock is omitted, and production costs may be significantly lowered (Stewart 2017).

A new approach for placing boreholes under special consideration of geometric constraints is used to provide an automatic pro-active blast design pattern. It uses the novel concept of so-called minimum burden surfaces, i.e. the sum of locations where the minimum burden constraint is fulfilled.

The presented procedure shall not replace the responsibility and the experience of the shotfirer but rather support tedious adaptation work when having complex blast sites.

2 3D MODEL GENERATION

2.1 Structure from Motion

Photogrammetry enables to generate three-dimensional models from a series of overlapping photographs. The introduction of the Structure from Motion concept (Snavely *et al.* 2014) as well the broad availability of drones brought a

Figure 1. Comprehensive 3D model of a blast site and adjacent area.

renaissance of this technology. Structure from Motion includes a series of processing steps that allows computing a comprehensive set of 3D surface points that are combined to a surface description (a mesh) in photo-realistic style. Due to high redundant information, always present geometric deviations of the used camera (lens distortion) are compensated while generating the 3D model. This auto-calibration ability makes modern photogrammetry algorithms capable to produce accurate 3D models even from low-grade cameras, so even low-priced off-the-shelf drones can be used to generate 3D models at sufficiently high accuracy (see also next section).

Several commercial software products are available (e.g. Agisoft, Pix4d, ShapeMetriX). All work in a similar way and provide comparable results. In this case the ShapeMetriX software has been used as it also includes tools for blast design.

Figure 1 shows a resultant 3D model generated from 240 photographs. The model computes in less than 1 hour on a mobile workstation (Dell Precision 7520). In this case it consists of 3 million surface points and has a ground sample distance (GSD) of 1 cm/pixel. The used drone was a consumer grade DJI Phantom 4 equipped with a 12 Mpix camera. The 3D model was referenced using surveyed ground control points.

2.2 Model accuracy

Accuracy in that context needs to be looked at in two ways: (i) *positional accuracy*, i.e. the correct location of the 3D model in a given co-ordinate grid and (ii) *shape accuracy* that reflects mainly if all the details of the rough surface are rendered by the 3D model. Both are linked to the GSD and the latter also to the spacing of the 3D surface points. For 3D models that reside in local co-ordinates the correct orientation and scale of the model is taken as quality measure instead of the positional accuracy.

Positional accuracy is best if there are some reference points (ground control points GCP) in the captured area. The GCPs are locations with surveyed co-ordinates. The referencing mechanism transforms the model to the location of the GCPs with remaining residuals in the sub-cm range if GCP bundling is used. GCP bundling refers to a method where the GCPs are included while the entire camera arrangement is computed. It may increase the positional accuracy compared to normal referencing (see Table 1). The residuals refer to the overall distance vector in 3D between GCP and according point on the 3D model.

In some cases, the installation and survey of GCPs is seen to be too time-consuming and costly.

Table 1. Typical accuracy (overall error in 3D) of geo-localisation when using ground control points; GSD: 0.5 cm/px.

Flight date	No. images	No. GCPs	Residual [cm] mean/stddev/max	Note
09.08.2018	289	11	4.8 / 2.5 / 8.9	No GCP bundling
09.08.2018	289	11	0.3 / 0.3 / 1.2	With GCP bundling
18.10.2018	302	11	3.5 / 1.9 / 6.9	No GCP bundling
18.10.2018	302	11	0.2 / 0.2 / 0.6	With GCP bundling

In such cases the 3D model might be referenced (scaled and oriented) based on GPS information that is recorded while taking the images. Such models show larger deviations from the ground truth - depending on the quality of GPS and the used flight path, the absolute localisation might be some metres off. Such pure GPS referencing is improved by using real time kinematic (RTK) or post processed kinematic (PPK) GPS. Both lead to better absolute geo-localisation of the 3D model without needing GCPs. However, final models are not guaranteed to have a certain positional accuracy.

A comparison of pure GPS-referenced 3D models with GCP-referenced ones showed that the scale of the 3D models deviated between 1 – 2 % and the angular difference (e.g. inclination of bench faces) differed by about 1°. Note that positional accuracy is not guaranteed to stay at the stated figures as the results depends

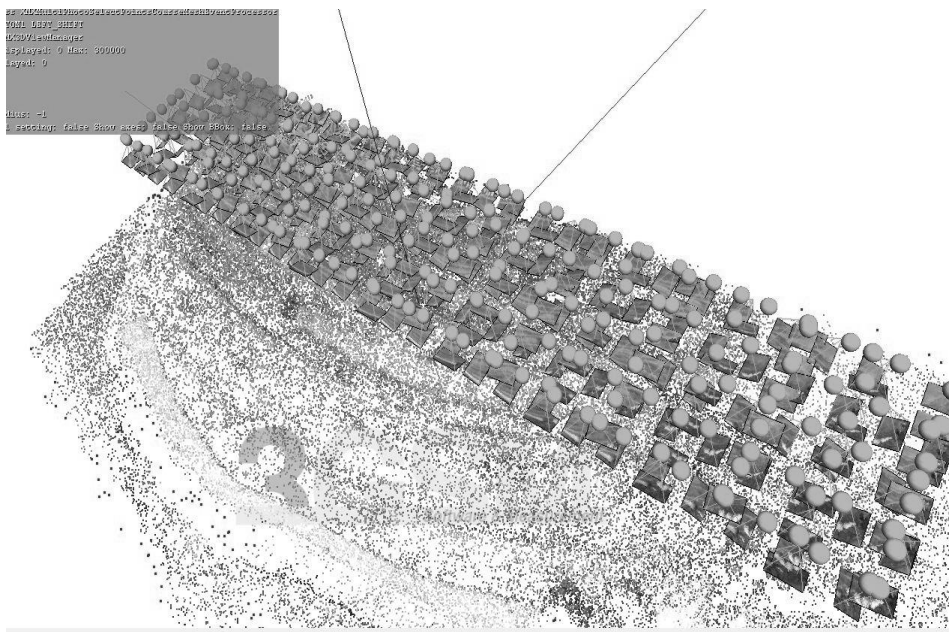

Figure 2. Analysis of deviations between camera locations from GPS recording (spheres) and photogrammetry-determined (pyramids).

on actual GPS availability and the used flight path.

3 THE MINIMUM BURDEN CONCEPT

3.1 Minimum burden diagrams

In order to describe burden as the distance from a borehole to the free surface usually the term *profile* is used. The profile provides the information what is 'in front of the hole' at a certain depth. Mathematically, the profile is the intersection of a vertical plane in front of the borehole with the surface description of the free face. This concept becomes improper if a hole is at a corner since it is not uniquely defined in which direction (azimuth) the intersection plane shall point (Figure 3a). But, for regular boreholes the intersection plane does not necessarily hit the locations where the distance between the borehole and the surface is minimal (Figure 3b). Also, in the case of an irregular bench face the resulting profile might show significantly larger values than the real shortest distance to the free face is.

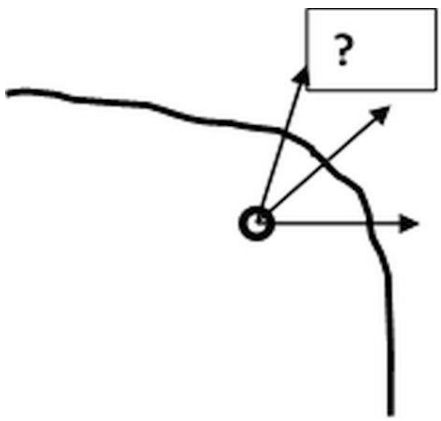

Figure 3a. In which direction shall the profile measure in case of a corner hole?

In order to overcome this, the minimum burden diagram is used. This entity provides the minimum distance at a certain depth anywhere around a borehole. For its generation, a spherical search around a certain point along the borehole is performed and the shortest distance to the surface determined. This search is repeated for all points along the borehole, typically done in small, discrete intervals. This way it is ensured that face irregularities, corner situations, or simply angular misalignments in azimuthal direction are treated correctly.

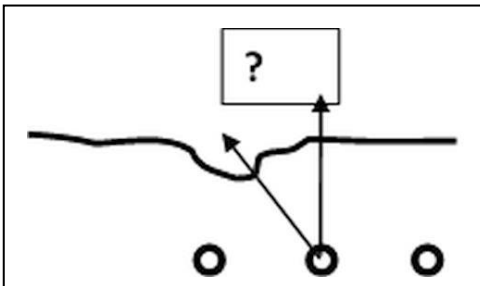

Figure 3b. In which direction shall the profile measure in case of a face irregularity?

The advantage of the minimum burden diagram becomes obvious if the burden numbers obtained by the profile and the minimum burden diagram are compared for the same borehole. In this case the face has an irregularity in front of the borehole (see Figure 4). The resulting profile shows significantly larger values than the minimum burden diagram (Figure 5). Such difference if incorrectly taken into account might be responsible for improper hole loading and all related consequences therewith.

Another characteristic is that a minimum burden search also works properly with deviated boreholes which, for example, have been surveyed by a down-the-hole-probe. Mathematically, a profile as a planar intersection is not even defined for a deviated borehole. In contrast, the minimum burden diagram computes the very same way as for straight boreholes.

3.2 Minimum burden charts

For the minimum burden diagram the shortest distance from a borehole to the free surface is looked for in a spherical search. A minimum burden chart results from searching in the opposite direction as with minimum burden diagrams, i.e. from the surface to the boreholes. Figure 6 depicts an example: for each surface location the distance to the nearest borehole is determined. The resulting coloured version of this image indicates: the surface location; design burden; light burden; and heavy burden situations. The coloured representation provides straightforward help in identifying problematic areas. The concept has been described by Gaich *et al.* (2009).

3.3 Minimum burden surfaces

An extension of the minimum burden charts leads to the computation of minimum burden surfaces.

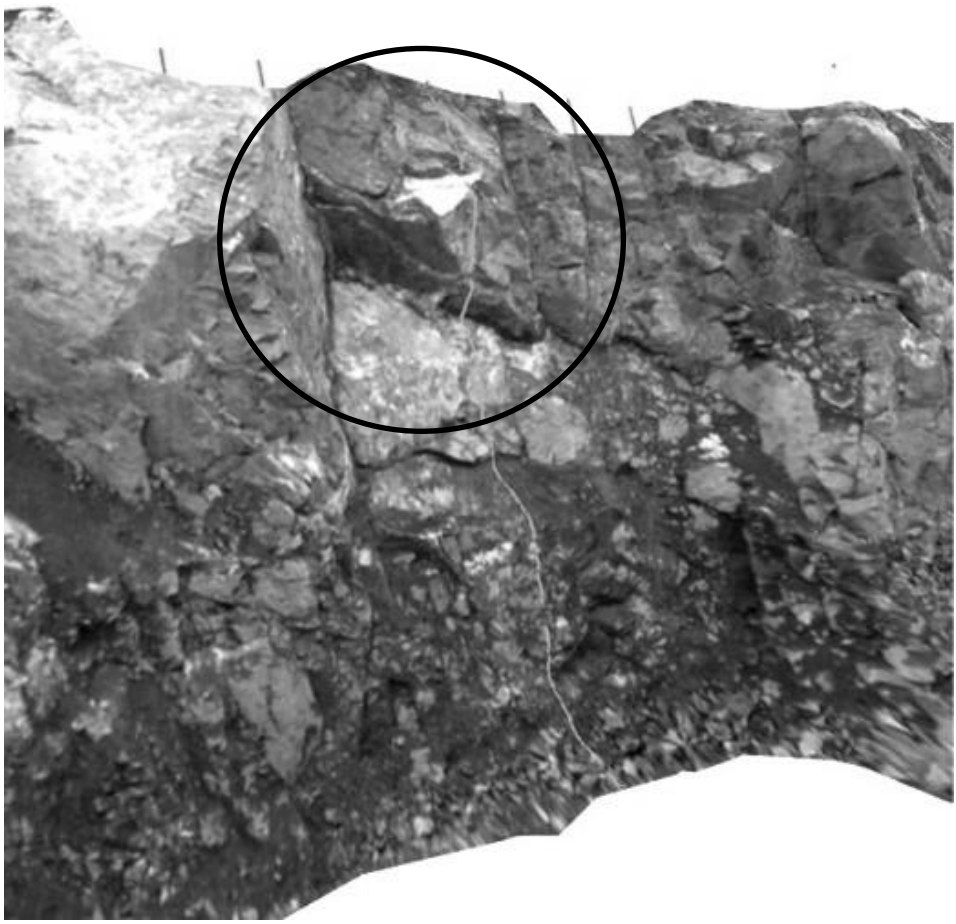

Figure 4. 3D model with a single profile; circle marks an irregularity (remainder of a detached block).

The minimum burden surface is a geometric entity that consists of those locations where a borehole *should* be in order to fulfil the minimum burden criterion. So, any borehole that is placed on the minimum burden surface therefore leads to a best possible minimum burden diagram.

The minimum burden surface is computed starting from the free face and identifying locations that are at design burden away from it. This is done for several sample point over the free face (see Figure 7). The sample points define the basis for the according minimum burden surface.

A minimum burden surface turns out to be a kind of smoothed copy of the free surface it belongs to. It is a general surface, i.e. it is not necessarily flat.

The whole process is applied repeatedly if several rows are sought. The minimum burden surface on the first row serves then as the free surface for the second row and so on.

4 AUTOMATIC BOREHOLE PLACEMENT

The components as described in the sections before, i.e. a comprehensive 3D model and minimum burden surfaces are the elements for the automatic borehole placement routine. Boreholes are arranged along the minimum burden surface for the first row. Several boundary conditions resp. degrees of freedom are possible during this process which influence the final output including:

– inclination: fixed value or variable

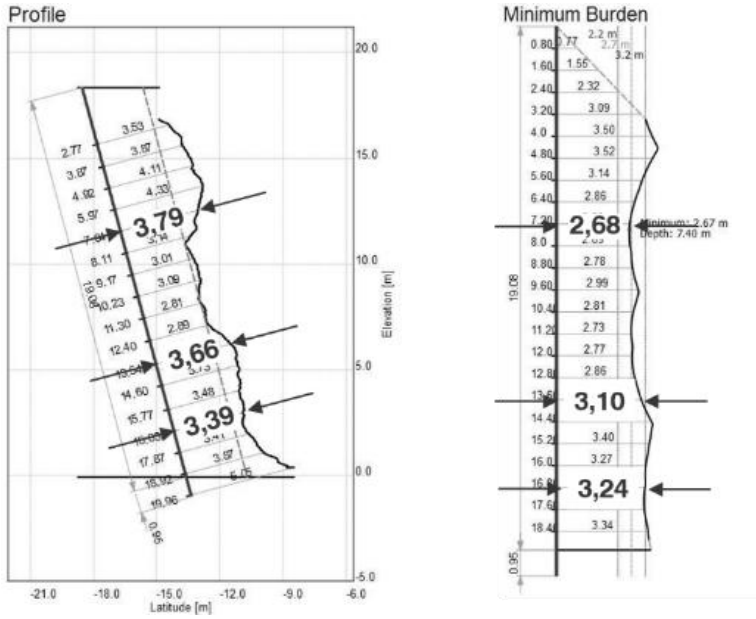

Figure 5. Profile and minimum burden diagram for the same borehole; note the significant differences at the indicated hole depths.

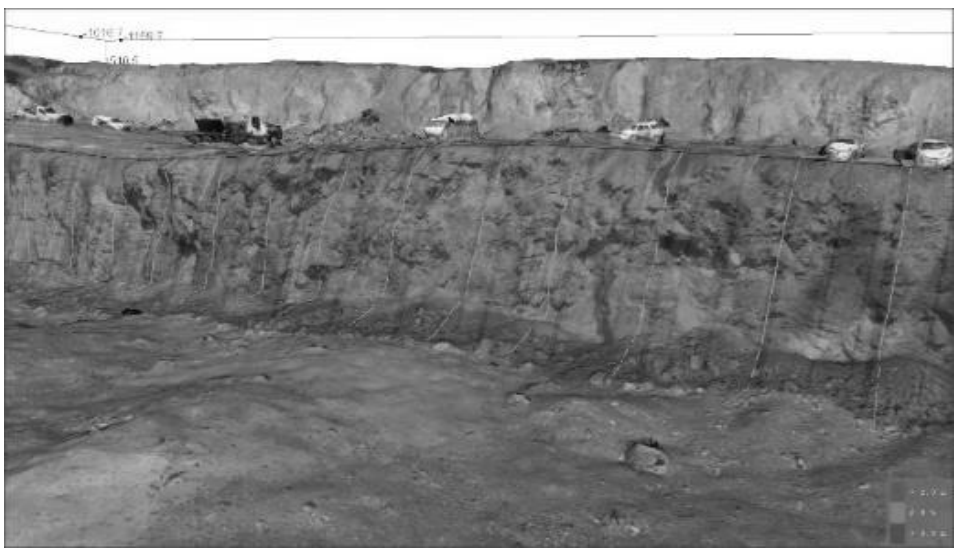

Figure 6. Minimum burden chart with indicated location of boreholes.

- azimuth: fixed value of variable
- side spacing: constant or variable
- side spacing: fixed minimum inter-hole-distance e.g. at the bottom

The algorithm is able to follow any irregularly shaped crest and places the boreholes while simultaneously trying to keep the minimum burden constraint valid. The more reduced the

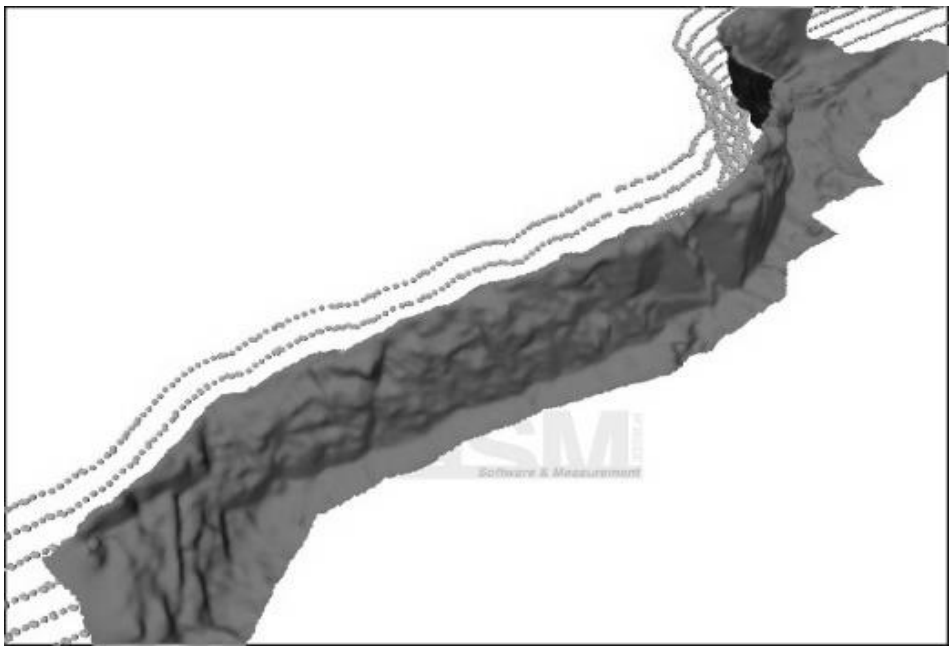

Figure 7. The computation of the minimum burden surface starts with the determination of according (dotted) sample points.

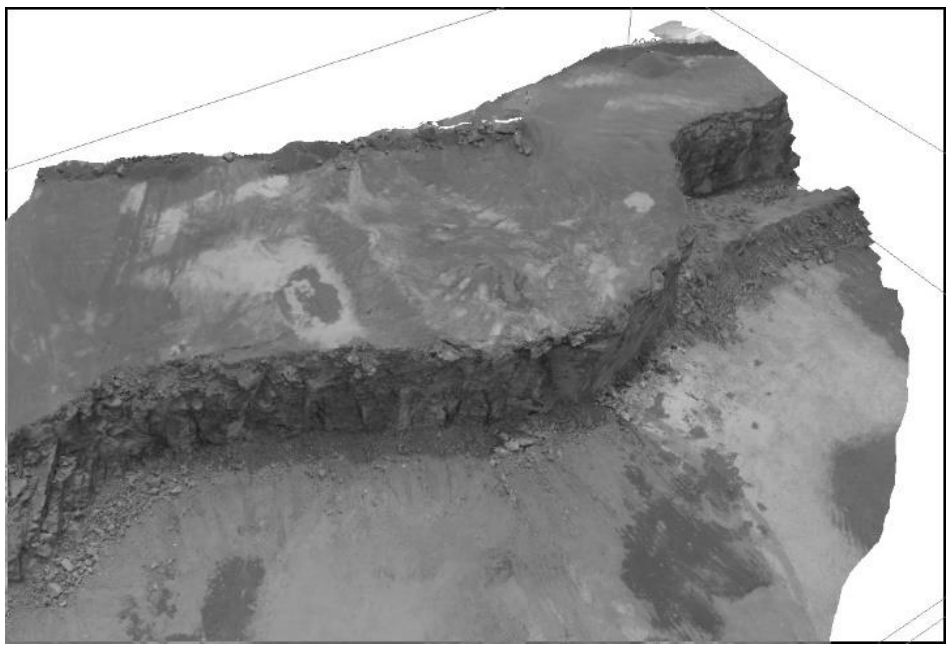

Figure 8a. 3D image of a curved blast site.

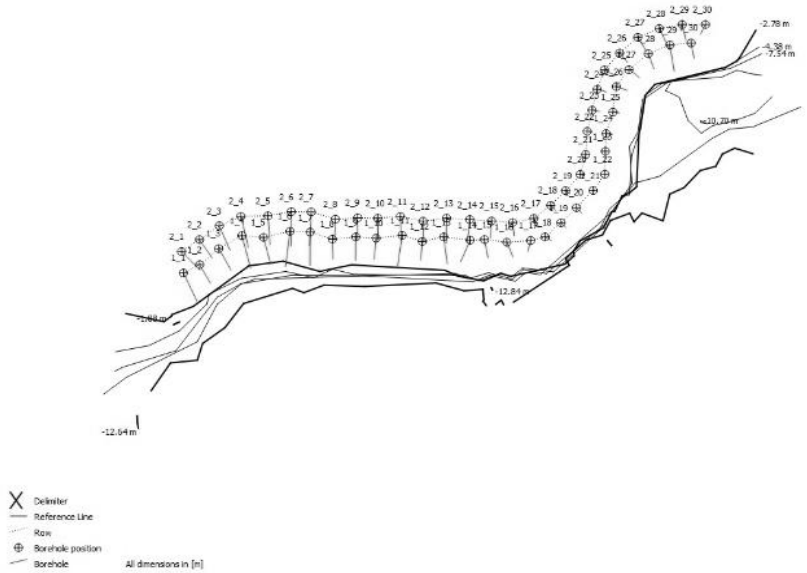

Figure 8b. Plan view of automatically placed boreholes using minimum burden surfaces; the boreholes follow the crest.

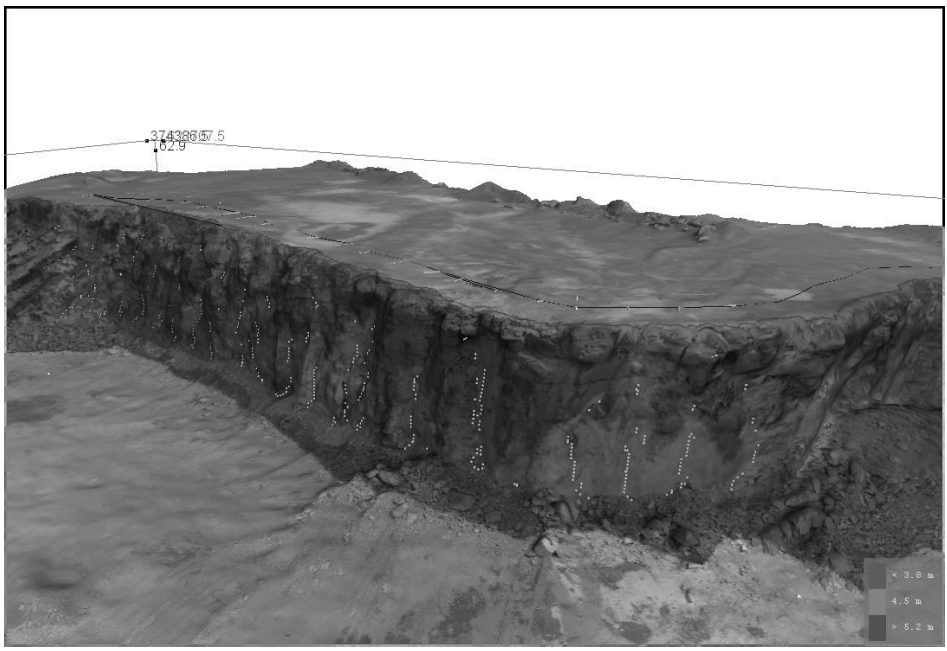

Figure 9. Minimum burden chart for automatically placed boreholes on a curved corner blast; bright dots indicate locations of minimal burden.

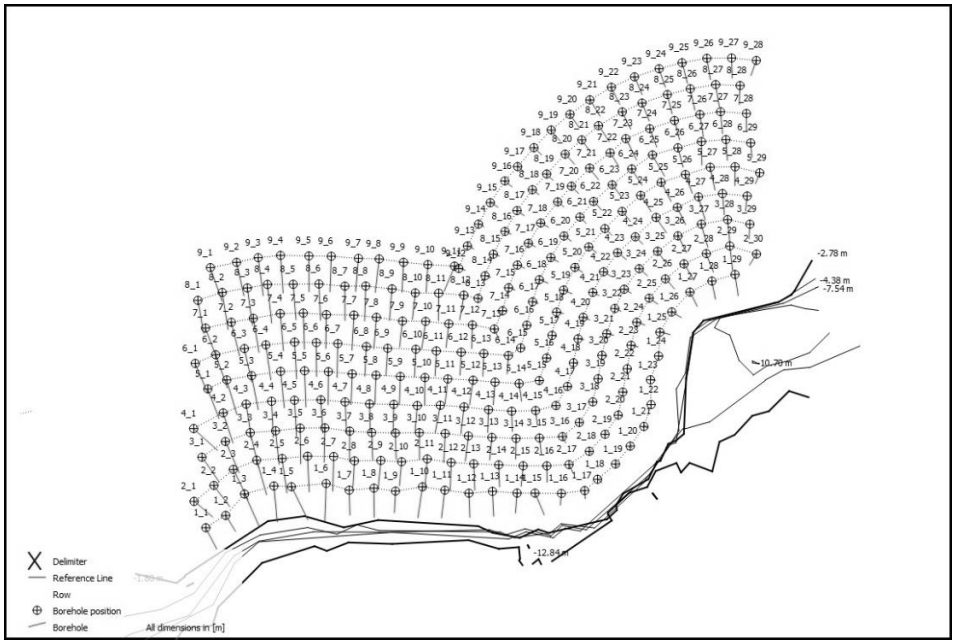

Figure 10. Automatically placed boreholes with loose constraints in azimuth and inclination.

degrees of freedom, the more the minimum burden constraint may be violated. Figure 8 shows a 3D model that includes a curved bench as well as the result of the algorithm. The layout clearly follows the crest, and in this case also inclination and azimuth were allowed to vary. The resulting minimum burden distribution is shown in Figure 9. The application of the algorithm in a multi-row design is depicted in Figure 10.

5 CONSEQUENCES AND CONCLUSIONS

3D models from photogrammetry acquire blast sites of surface blasts comprehensively and accurately (cm range). Together with the minimum burden concept real burden information instead of profiles gets associated to boreholes.

Minimum burden surfaces are an extension to existing minimum burden calculations. They reflect the sum of locations where design burden is met taking the entire blast site into account.

If boreholes are placed along minimum burden surfaces, they will follow the shape of the crest. The used algorithm is able to provide a blast pattern for highly irregular shaped blast sites.

The presented approach works purely geometric. Further work includes the automatic placement of boreholes according to associated volumes to be blasted.

6 ACKNOWLEDGEMENTS

The work has been supported by the European Union's Horizon 2020 research and innovation programme under grant agreement no. 730294.

REFERENCES

Gaich, A., Pötsch, M., Moser, P. & Schubert, W. 2009. How 3D images support bench face profiling, blast planning, and rock mass characterisation. In*: Rock Fragmentation by Blasting: Proceedings of the 9th Int. Symp. on Rock Fragmentation by Blasting - Fragblast 9*, Sept. 2009, Granada Spain, pp. 85-90.

Moser, P., Ganster, M. & Gaich, A. 2007. Experience with and benefits from the use of 3D Stereophotogrammetry for blast design and control, In: *Proc. of the 33rd annual conference on explosives and blasting technique*, Nashville, TN, Vol. I: 315-327.

Mueller, C. 2002. *The IREDES initiative*. 33. 42-43.

Snavely, N, Seitz, S.M. & Szeliski, R. 2008. Modelling the world from internet photo

collections. *International Journal of Computer Vision*: 80(2):189-210.

Stewart, D. 2017. Drill and blast improvement project using photogrammetry, GPS and drill navigation systems. In: *Proceedings of 43rd Annual Conference on Explosives and Blasting Technique*, Orlando, FL.

Website: Agisoft. https://www.agisoft.com/ Accessed 25 July 2019.

Website: Pix4D. https://www.pix4d.com/ Accessed 25 July 2019.

Website ShapeMetriX. https://3gsm.at/ Accessed 25 July 2019.

Helsinki Conference Proceedings 2019, R. Holmberg et al

SPH modelling of rock blasting: calibration from bench face movement data

M. Bermejo, J. Navarro, J.A. Sanchidrián, P. Segarra & R. Castedo
Universidad Politécnica de Madrid, Madrid, Spain

ABSTRACT: A smoothed particle hydrodynamics (SPH) model has been developed in LS-DYNA for the simulation of the movement of the rock burden. The model is validated with experimental full-scale quarry tests performed within the EU project SLIM. The explosive employed in the tests, an emulsion, has been modelled with the JWL equation of state. The rock was modelled with the RHT constitutive material model. The interaction between explosive and rock is modelled with a node-to-node penalty-based contact. The fracture in the burden and the movement of the rock were monitored by high-speed video recording, with which the initial velocity of the rock face, and the time from the detonation to the onset of the face movement were obtained. These data have been used to calibrate the SPH model. A thorough comparison of the results of tests and simulation are shown.

1 INTRODUCTION

The analysis of the rock movement with video recording is a useful tool in blast design. It can be used as a check of the explosive effect on the rock; inefficiencies in loading, stemming, geometry, timing, etc. are made apparent from the inspection of the recorded images (Chiappetta & Mammele 1987, Pérreault & Morin 2000). The videos provide the necessary data to estimate the trajectory, size and velocity of fragments framed within a specific plane with known coordinates during the movement of the blasted rock (Chiappetta *et al.* 1983). High-speed video recording has been used in this work to record the rock movement, tracking the motion of fragments coming from different height levels on the highwall. From this, the initial velocity of the fragments and the response time, i.e. time between the detonation and the first instance of movement of the bench face, are determined.

Field measurements have been compared with the results of a 2D smoothed particle hydrodynamics model of the rock bench and a blasthole. The model is able to simulate the crack propagation from a blasthole, not easy to achieve with the classical explicit finite element method. This particle method can also simulate with accuracy the detonation in the explosive, and the pressure wave transmitted to the rock.

2 HIGH SPEED VIDEO RECORDING AND DATA ANALYSIS

2.1 Field measurements

The rock movement has been analysed

through high speed video recording during the full-scale test blasts campaign in El Aljibe quarry for the EU project SLIM (Sanchidrián 2018). Blasts were recorded with a high-speed camera (HSC) 'FastCam Sa 3', model 120k C2, manufactured by Photron. It records images at a pre-set frame rate (frames per second, fps), which are saved in an internal memory. Frame rates range from 50 fps to 120,000 fps. Other setups to be considered are related with resolution of the images, shutter, shadows calibration, and type of trigger among others. Due to the limited internal memory (4Gb), it is necessary to keep a balance between the frame rate, the resolution of the images and the total recording time, which must be long enough to record the whole rock movement. In the footage used in this work, the frame rate was 2400 fps, the resolution was 768 × 448 pixels and the recording time was 3.46 s.

2.2 Definition of the reference plane

In order to transform the coordinates in the video images to actual coordinates, a plane is defined in front of the blasthole which burden will be tracked, perpendicular to the free face; for that, surveyed reference points are marked on the crest and on the bench floor, see Figure 1. Rock motion is assumed to take place in that plane.

Surveying was made with a Quarryman ALS Laser system (QLS). To define the perpendicular plane, the QLS is located over the selected blasthole and the direction of the two adjacent blastholes on each side is measured. The perpendicular orientation is obtained by pointing the QLS 90° from the mean azimuth of the previous measurements towards the grade level.

Ideally the camera should be placed so that the line of sight is parallel to the free face. However, this was difficult to achieve in practice, as can be seen in Figure 1, due to the poor visibility of the first part of the blast in the available area to locate the camera. However, using the reference points known coordinates, a transformation system can be calculated to transform coordinates from the video to the reality. Considering that U_C and U_R are local coordinates in the video and in the reality, respectively, within the reference plane defined by targets in the crest and bottom floor of the bench, the transformation is:

$$U_C = A + B \cdot U_R \quad (1)$$

where A is the translation of the reference axes and B is a transformation matrix defined as the product of three matrixes: a rotation matrix of the vertical axis, a scaling factor matrix of the image, i.e. the scaling factor between the distances in the reference plane in the screen and reality, and a skewing matrix over the vertical axis. Solving Equation 1 for U_R:

$$U_R = B^{-1} \cdot (U_C - A) \quad (2)$$

where B^{-1} is the inverse of B.

2.3 Analysis of fragment paths

The trajectory of fragments at different height of the bench and within the defined reference plane are measured at equal time intervals, until they hit the ground, or disappear within the cloud of broken rock and dust. Each fragment position tracked is associated to a time from the video images.

An approximate sample interval considered is around 0.05 s, obtaining between 10 and 30 measurements per rock, i.e., the trajectory of the rock is followed for about 0.5 to 1.5 seconds from the blasthole initiation. Figure 2 shows, as an example, the trajectory followed by a fragment. The grey cross-hairs represent the starting position of the rock, and the white cross-hairs in Figures 2

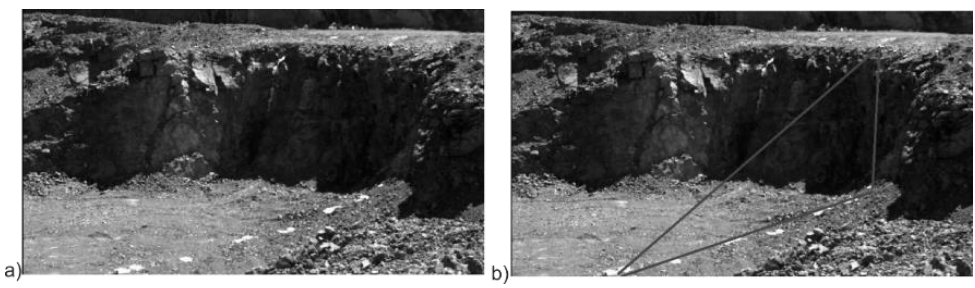

Figure 1. Reference targets.

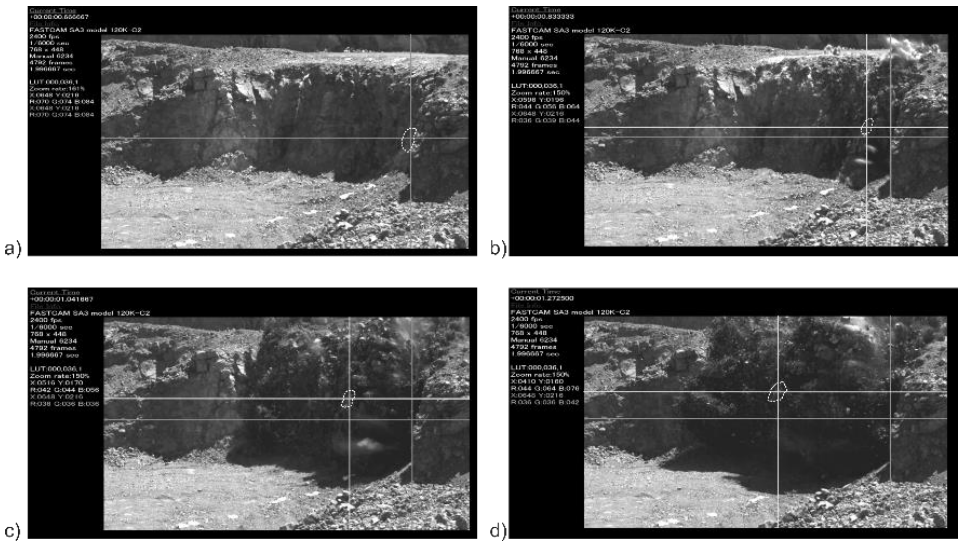

Figure 2. Analysis of the rock trajectory.

b, c and d, the position of the rock at different sample times. Coordinates of the cross position are shown in their respective shade on the left side of the screen. Using Equation 2, real coordinates are calculated.

2.4 Trajectory fitting

The trajectory of each fragment tracked is fit by point trajectory model (Segarra 2004). Figure 3 shows the forces acting on the gravity centre of the fragment; V is the velocity of the target at time t, $\dot{z}$ and $\dot{y}$ are the components of V in the Z (horizontal) and Y (vertical) axis, respectively, θ is the pitch angle, F_D is the aerodynamic drag force, m is the mass of the fragment and g is the acceleration of gravity.

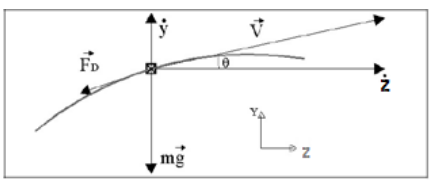

Figure 3. Forces acting on the gravity centre of the rock.

From Figure 3, the following geometrical relations apply:

$$cos\theta = \frac{\dot{z}}{V} = \frac{\dot{z}}{\sqrt{\dot{z}^2+\dot{y}^2}} \quad (3)$$

$$sin\theta = \frac{\dot{y}}{V} = \frac{\dot{y}}{\sqrt{\dot{z}^2+\dot{y}^2}} \quad (4)$$

Applying Newton's second law to the system in Figure 3, and writing the drag force as function of a drag coefficient C_D and fragment cross section S:

$$m\ddot{z} = \frac{-1}{2}\rho V^2 C_D S cos\theta \quad (5)$$

$$m\ddot{y} = -mg - \frac{1}{2}\rho V^2 C_D S sin\theta \quad (6)$$

Replacing Equations 3 and 4 in 5 and 6, respectively:

$$\ddot{z} = \frac{-1}{2}\frac{\rho C_D S}{m}\dot{z}\sqrt{\dot{z}^2+\dot{y}^2} \quad (7)$$

$$\ddot{y} = -g - \frac{1}{2}\frac{\rho C_D S}{m}\dot{y}\sqrt{\dot{z}^2+\dot{y}^2} \quad (8)$$

Equations 7 and 8 form a second order ordinary differential equation system, that can be readily solved for $z(t)$ and $y(t)$. The trajectory obtained is adjusted to the measured one by means of an iterative process in which the two components of the initial velocity are changed until the best fit is obtained. The whole trajectory tracked is used.

The paths measured (already transformed into actual coordinates) and the trajectories calculated are represented in Figure 4a. Figure 4b represents

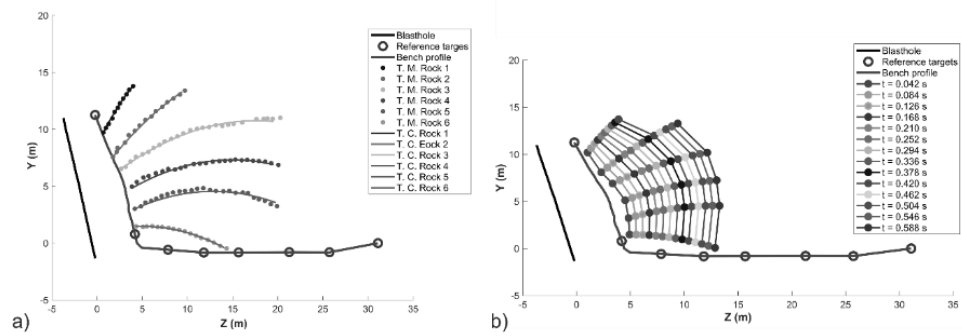

Figure 4. a) Trajectories adjustment; b) Face profiles.

the free face profiles at several times. These profiles are formed by connecting the rock trajectory points (circles) measured at the same time.

Table 1. Height and burden of fragments tracked, velocity and response time.

Fragment	Height rock m	Burden m	Initial velocity m/s	Response time ms
1	9.72	2.47	14.03	23.10
2	7.56	3.30	18.24	23.60
3	6.52	3.40	18.61	23.80
4	4.97	3.83	17.14	24.10
5	3.02	4.10	16.51	24.50

2.5 Determination of the response time

Downhole initiation with electronic detonators was employed. To measure the response time of the rock, i.e. time between the detonator firing to the first movement of the rock, it is necessary to record with the camera the precise moment at which the explosive is detonated. For that, a detonator was located outside the blasthole with the same time that the initiator, so that the initiation time was recorded by the HSC. Since the scatter of this type of detonators is minimal (around 0.1 ms as measured in the tests), both the initiator and the external detonators fire, for all purposes, at the same time.

The initiation of the detonator outside the blasthole generates a flash. Rock trajectories in Figure 4 are measured from the time of this flash or initiation of the explosive. Between the blasthole initiation flash time to the onset of movement of a given spot on the face, there is a short time interval where the rock remains still. The time at which there is a first evidence of movement is visually observed in the video recording, and the time read.

2.6. Results

The height, actual burden from the blasthole at that height, and the initial velocity and response times for five fragments are listed in Table 1.

3 NUMERICAL MODELLING WITH SMOOTHED PARTICLE HYDRODYNAMICS (SPH)

A 2D model with SPH formulation and plane-strain conditions has been used. All SPH particles have approximately equal inter-particle distance of 15 mm in both directions. In the SPH model, the repulsive contact force acting on each particle depends on the linear-spring constant or stiffness. All the SPH interpolations (density, stresses) are carried out inside the local domains of each SPH part. For the interactions between explosive and rock, a node-to-node penalty-based contact is used; this is needed especially when the materials have significantly different densities such as the detonation products and the rock. A "*DEFINE_SPH_TO_SPH_COUPLING" LS-DYNA keyword (Hallquist 2006) is used for the explosive to rock contact.

Tensile (Ganzenmüller *et al.* 2016) and rank-deficient (Dyka *et al.* 1997) instabilities, two problems related to SPH method, are solved through the hourglass control schemes. The tensile instability appears by nonphysical clumping of

particles under conditions of tensile stress. The rank-deficiency problem arises in the nodal integration when the number of integration points is too small such that the solution to the equilibrium equations becomes non-unique due to rank deficiency. Hourglass control locally linearises the deformation field to obtain stable and accurate solutions, without the need to resort to stabilisation via excessive artificial viscosity. The hourglass used within the simulation is the standard LS-DYNA viscous form with the quadratic bulk viscosity coefficient (Q_1) equal to 0.5 and the linear one (Q_2) equal to 1.5.

The model represents a borehole in the bench (Figure 5), loaded with explosive, and the upper part filled with the stemming (in the lighter shade); the rock mass is the dark grey shade. The borehole has and inclination of 11.5º, a length of 12.9 meters and a diameter of 89 mm. The bench has a height of 11.6 meters and an inclination of 32.5º. Even if there are local variations of burden due to the non-planarity of the bench face, the burden increases approximately linearly with depth (see Table 1) and its variability with respect to a theoretical plane is relatively small, so it can be represented fairly accurately with an inclined line for simulation purposes.

A 3.2 metre floor space is modelled, with 11 metres of rock downwards and 23 metres from the crest of the bench backwards. These large dimensions ensure that there are no interferences of numerical, parasitic reflected waves in the domain of interest (although a non-reflecting boundary has been used in the back and in the bottom of the model).

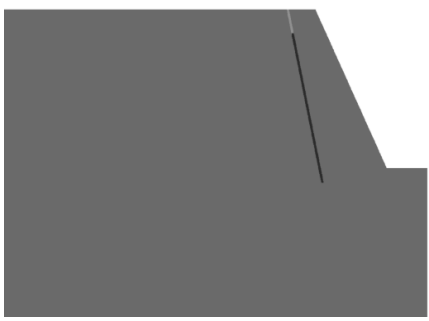

Figure 5. Particle model. Rock in green, explosive in red and stemming in blue.

The rock is described by the RHT model (Borrvall & Riedel 2011). RHT is a macro-scale material model that incorporates features required for a correct dynamic strength description of problems with high strain rates and pressures. The shear strength of the model is described by means of three limit surfaces; the inelastic yield surface, the failure surface and the residual surface, all dependent on the pressure. The post-yield and post-failure behaviours are characterised by strain hardening and damage, respectively, and strain rate effects is an important ingredient in this context. Furthermore, the pressure is governed by the Mie-Grüneisen equation of state together with a porosity-dependent pressure model to describe the pore compaction hardening effects. In our case, where the rock has a very low porosity (water absorption coefficient 0.1 % and very high P-wave velocity, 5800 m/s in lab samples and 5250 m/s in the field), the porosity is negligible and the porosity parameter (the fraction between the density of the matrix material and the rock) is taken as 1 in the initial state (i.e. fully compacted material) and the material behaviour is governed by a conventional equation of state model. The RHT strength model is expressed in terms of the three stress limit surfaces mentioned above. The model is elastic until the stress reaches the initial yield surface, beyond which plastic strains evolve. The plastic strains together with the hardening properties are used to form an effective yield surface by interpolating between the initial yield surface and the failure surface. Similarly, when the stress reaches the failure surface, a parametrised damage model applies, driven by plastic strain, which in turn represents the post-failure stress limit surface by interpolating between the failure surface and the residual friction surface. The relevant parameters of the damage model that require tailoring are D_1, D_2 and ε_p^m (Tu *el al.* 2009), see Table 2. The Hugoniot polynomial coefficients A_1, A_2, A_3 are obtained from the formulation by Xie *et al.* (2017):

$$\begin{aligned} A_1 &= \alpha\rho c^2 \\ A_2 &= \alpha\rho c^2(2s-1) \\ A_3 &= \alpha\rho c^2[(3s-1)(s-1)] \end{aligned} \quad (9)$$

where $\rho = 2714\,kg/m^3$ is the initial density of rock, and c and s are the shock Hugoniot linear expression constants:

$$U_s = c + s \cdot U_p \quad (10)$$

where c=5250 m/s has been chosen equal to the sound speed (assuming that Equation 10 holds at

Table 2. Parameters for the RHT material model.

Parameter	Value	Remarks
Density	2714 kg/m^3	Lab measured
Shear Modulus	41.6 GPa	Lab and field data; elastic relations
Pore crush (B0)	1.2	Equal to the Grüneisen coefficient(1)
Pore crush (B1)	1.2	Equal to the Grüneisen coefficient(1)
Bulk Modulus (T1)	75 GPa	Lab and field data; elastic relations
Bulk Modulus (T2)	0.0 GPa	Ding *et al.* (2013)
Hugoniot parameter (A1)	75 GPa	Eqs. 1
Hugoniot parameter (A2)	90 GPa	Eqs. 1
Hugoniot parameter (A2)	15.5 GPa	Eqs. 1
Failure surface parameter (Af)	1.6	Tu & Lu 2009
Failure surface exponent (nf)	0.61	Tu & Lu 2009
Compressive strength (fc)	182 MPa	Lab tests
Relative shear strength (fs*)	0.18 MPa	Lab(2)
Relative tensile strength (ft*)	0.1 MPa	Lab(2)
Lode Angle (Q0)	0.68	Tu & Lu 2009(3)
Lode Angle (B)	0.0105	Tu & Lu 2009(3)
Compressive reference strain rate	3×10-5 s-1	Ding *et al.* 2013
Compressive break strain rate	3×1025 s-1	Borrvall & Riedel 2011
Tensile reference strain rate	3×10-6 s-1	Ding *et al.* 2013
Yield surface parameter (gc*)	0.53	Borrvall & Riedel 2011
Yield surface parameter (gt*)	0.7	Borrvall & Riedel 2011
Damage parameter (D1)	0.015	Tu & Lu 2009
Damage parameter (D2)	1.0	Tu & Lu 2009
Residual damaged strain (ε_p^m)	8.0×10-4	Tu & Lu 2009
Crush Pressure	182 MPa	(4)
Initial porosity parameter	1.0	Non-porous material

1 The Grüneisen coefficient is approximated as $\gamma = 2s - 1$ (Ding et al. 2013).
2 Shear and tensile strengths normalised with compressive strength; the von Mises criterion for shear strength is used.
3 Strength-reduction parameters.
4 Equal to the compressive strength (fc) since the initial porosity parameter is 1.

low particle velocities). The slope *s* varies for strong rocks (e.g. granite) from about 0.6 to 1.5 depending on the shock range (Sekine *et al*. 1995); we as been chosen *s*=1.1.

Table 2 summarises the parameters used for the RHT model. The basic elastic parameters used are field-measured P-wave velocity and dynamic Poisson ratio, the latter obtained from laboratory values of P- and S-wave velocities (no S- wave velocity is available from the field tests). Other parameters such as shear modulus or bulk modulus are derived from them. Compressive and tensile strength are obtained from laboratory tests.

The stemming was modelled with material '*Mat_Soil_And_Foam'. The density, shear modulus and bulk modulus used are 1650 kg/m^3, 10 MPa and 13.6 GPa respectively.

The explosive is an emulsion with density 1177.5 kg/m^3, velocity of detonation 5448 m/s and detonation pressure calculated at 7.94 GPa. The material "*Mat_High_Explosive_Burn" is used. This material model must be used in combination

Table 3. Parameters for the JWL equation of state.

A (GPa)	B (GPa)	C (GPa)	R1	R2	ω	E0 (GPa)
35.243	4.163	0.406	5.612	1.185	0.37	2.757

with an equation of state to define the detonation products pressure-volume-energy relation. The equation of state used is the Jones-Wilkins-Lee (JWL):

$$P = A\left(1 - \frac{\omega}{R_1 V}\right)e^{-R_1 V} + B\left(1 - \frac{\omega}{R_2 V}\right)e^{-R_2 V} + \frac{\omega E}{V} \quad (11)$$

where A, B, R_1, R_2 and ω are parameters for a given explosive in a given detonation condition (e.g. density, diameter, etc.), P is pressure, E is internal energy per unit initial volume and V is relative volume. The constants have been determined from cylinder test data (Sanchidrián *et al.* 2015, López *et al.* 2018, Castedo *et al.* 2018) where explosive density and velocity of detonation were measured at the values given above. The JWL parameters are reported in Table 3. E_0 is the initial energy available. A single ignition point at the bottom of the blasthole has been used.

4 RESULTS AND DISCUSSION

Figure 6 shows the initial state of the model, together with the map of velocity 30 ms from the initiation of the detonation. No reflected waves from the back or the bottom boundaries are formed, which confirms that the dimensions of the model are sufficient. The free face reflected wave is simulated correctly. A positive velocity gradient from the blasthole to the free face is obtained, whereas velocity decreases steadily backwards and downwards.

The velocity and response time of five fragments formed in the bench face at the same height levels in Table 1 have been calculated from the model results. Clusters of particles moving together have been selected as 'fragments'. These are shown in black with its respective number in Figure 7. The histories of velocity of the particles in each cluster are obtained from the model and the average computed. Figure 8 shows an example of velocity history of a particle and the average velocity of the cluster. There is an initial phase with zero velocity until the P-wave reaches the cluster position, then the velocity ramps up until a steady value is attained; the initial velocity refers to this value. Calculated and test-measured values are given in Table 4. The agreement is quite acceptable and validates the SPH model developed.

In figure 9, the initial velocity of the target fragments is plotted against the ratio of the target height to the bench height, both measured and calculated. Lines are quadratic fits, similar to those shown by Sanchidrián *et al.* (2005).

The response time is taken as the time at which 99 % of the steady velocity (see Figure 8) of the cluster mean velocity is attained. Table 5 shows the comparison between test and model. The model results fall slightly below the measured, though no attempt has been done to tailor the model parameters to match the test data more

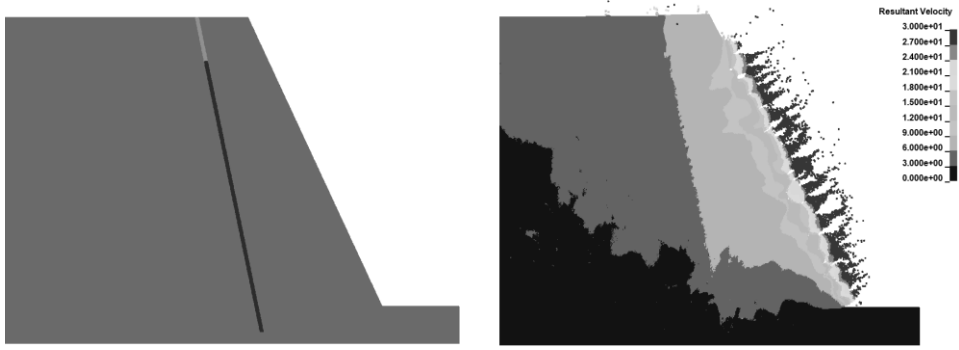

Figure 6. Initial state of the model and map of velocity at 30 ms from initiation.

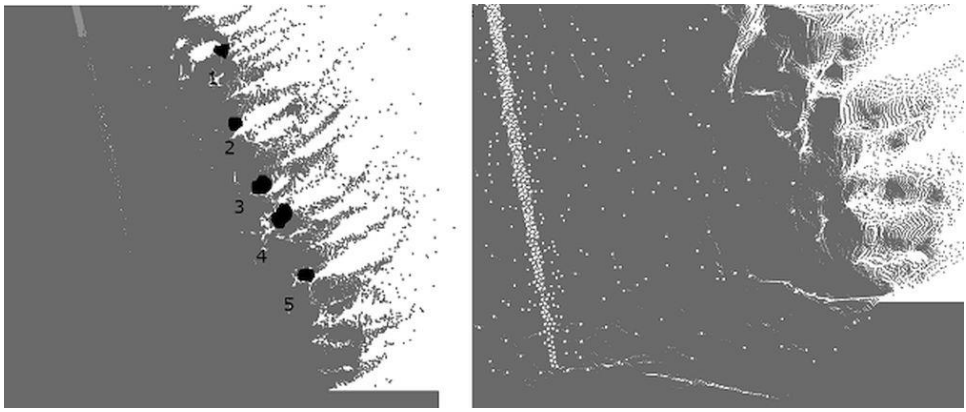

Figure 7. The model 60 ms from initiation. Left: the five fragments selected, Right: detail of the bottom of the borehole; particles ejected and patterns of fractures.

Table 4. Initial velocity. - measured and calculated values.

Fragment	Height of fragment (m)	Burden (m)	Initial velocity, test (m/s)	Initial velocity, model (m/s)	Difference between model and test (%)
1	9.72	2.47	14.03	17.50	24.7
2	7.56	3.30	18.24	18.22	0.11
3	6.52	3.40	18.61	22.00	18.2
4	4.97	3.83	17.14	17.90	4.4
5	3.02	4.10	16.51	17.23	4.3

Table 5. Response time - measured and calculated values.

Fragment	Height of fragment (m)	Burden (m)	Response time, test (ms)	Response time, model (ms)	Error between model and test (%)
1	9.72	2.47	23.1	20.7	-10.5%
2	7.56	3.30	23.6	20.9	-11.4%
3	6.52	3.40	23.8	23.1	-2.9%
4	4.97	3.83	24.1	23.1	-4.1%
5	3.02	4.10	24.5	21.3	-12.9%

accurately. The response time shows a slight direct relation with burden, see Figure 10.

5 CONCLUSIONS

Numerical results indicate that the explosive-to-rock coupled SPH-SPH model can be applied to predict the rock movement, and to calculate the initial velocity of the rock and the response time. The model is validated with data obtained from a full scale quarry test blast. Conclusions on the modelling are:

– 2D SPH models with plane-strain conditions and node-to-node penalty-based contact are useful to simulate the explosive to rock

interaction and the fragments ejection.
– The equal inter-particle distance of 15 mm is appropriate to obtain valid results.

From the analysis of the results, it follows that:

– The face velocity follows a convex function of the target height, being maximum at about mid-height, decreasing towards the top and the floor of the bench. The initial velocity values measured are in the range 15-20 m/s.
– The face response time measured is 23-25 ms from the hole initiation. The response time seems to have a slight direct dependent with burden.

Wave interactions between holes obviously require a 3D model; the 2D model shown in this work is a preparatory exercise for a full 3D SPH-SPH explosive-to-rock interaction model.

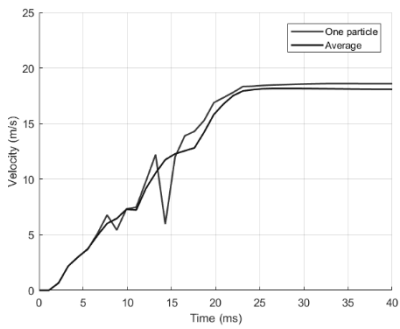

Figure 8. History of velocity, cluster no. 3 in Figure 7. Example of one particle and average of the cluster (smoothed).

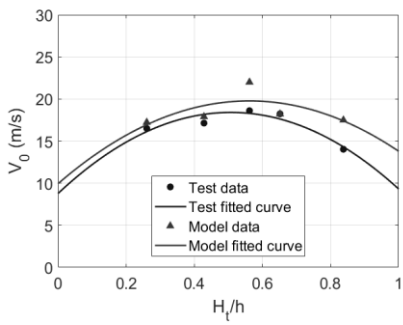

Figure 9. Fragments initial velocity as function of normalised height.

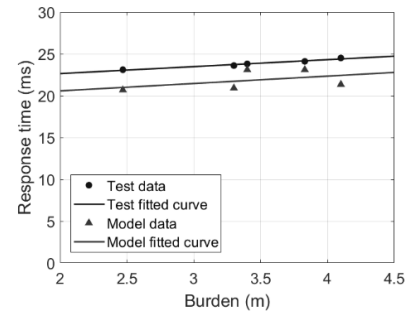

Figure 10. Response time versus burden.

6 ACKNOWLEDGEMENTS

This work is part of the SLIM project, funded by the European Union's Horizon 2020 research and innovation program under Grant agreement no. 730294.

REFERENCES

Borrvall, T. & Riedel, W. 2011. The RHT concrete model in LS-DYNA. In *Proceedings of the 8th European LS-DYNA users conference*, May, Strasbourg - May 2011.

Castedo, R., Natale, M., López, L.M., Sanchidrián, J.A., Santos, A.P., Navarro, J. & Segarra, P. 2018. Estimation of Jones-Wilkins-Lee parameters of emulsion explosives using cylinder tests and their numerical validation. *International Journal of Rock Mechanics and Mining Sciences, 112*: 290-301.

Chiappetta, R.F., Bauer, A., Dailey, P.J. & Burchell, S.L. 1983. The use of high speed motion picture photography in blast evaluation and design. In *Proceedings of the Ninth Conference on explosives and blasting technique*, January 31-February 4, Dallas, Texas. Society of Explosives Engineers.

Chiappetta, R.F. & Mammele, M.E. 1987. Analytical high-speed photography to evaluate air decks, stemming retention and gas confinement in presplitting, reclamation and gross motion applications. In W.L. Fourney & R.D. Dick, *Proc. 2nd Int. Symp. on rock fragmentation by blasting*, Keystone, CO, 23–26 August. Bethel, CT: Society for Experimental Mechanics.

Ding, Y.Q., Tang, W.H., Zhang, R.Q. & Ran, X.W. 2013. Determination and validation of parameters

for Riedel-Hiermaier-Thoma concrete model. *Defence Science Journal* 63(5): 524-530.

Dyka, C.T., Randles, P.W. & Ingel, R.P. 1997. Stress points for tension instability in SPH. *International Journal for Numerical Methods in Engineering* 40(13): 2325-2341.

Ganzenmüller, G.C., Sauer, M., May, M. & Hiermaier, S. 2016. Hourglass control for smooth particle hydrodynamics removes tensile and rank-deficiency instabilities. *The European Physical Journal Special Topics* 225(2): 385-395.

Hallquist, J.O. 2006. *LS-DYNA theory manual*. Livermore Software Technology Corporation, Livermore, CA.

López, L.M., Castedo, R., Sanchidrián, J.A., Natale, M., Santos, A.P., Navarro, J. & Chiquito, M. 2018. Emulsion characterisation with cylinder test and JWL parameters determination. In H. Schunnesson & D. Johansson (eds.) *Proc. 12th Int. Symp. on Rock Fragmentation by Blasting (Fragblast 12)*, 11-13 June, Luleå, Sweden, pp. 431-439.

Pérreault, J.F. & Morin, A. 2000. Optimisation des paramètres de sautage à la Compagnie Minière Québac Cartier. In *23e Session détude sur les techniques de sautage*, Département de mines et métallurgie, 2-3 November 2000, Québec, Canada. Université Laval.

Sanchidrián, J.A. 2018. SLIM: Technology for blasting to improve mining. In H. Schunnesson & D. Johansson (eds.) *Proc. 12th Int. Symp. on Rock Fragmentation by Blasting (Fragblast 12)*, 11-13 June, Luleå, Sweden, pp. 783-793.

Sanchidrián, J.A., Castedo, R., López, L.M., Segarra, P. & Santos, A.P. 2015. Determination of the JWL constants for ANFO and emulsion explosives from cylinder test data. *Central European Journal of Energetic Materials* 12(2): 177-194.

Sanchidrián, J.A., Segarra, P. & López, L.M. 2005. On the relation of rock face response time and initial velocity with blasting parameters. In *Proc. 3rd World Conf. on Explosives and Blasting*, September, Brighton, UK, European Federation of Explosives Engineers, pp. 375-389.

Segarra, P. 2004. Experimental analysis of fragmentation, vibration and rock movement in open pit blasting. *Doctoral Thesis*, Universidad Politécnica de Madrid.

Sekine, T., Duffy, T.S., Rubin, A.M., Anderson, W.W. & Ahrens, T.J. 1995. Shock compression and isentropic release of granite, *Geophys. J. Int.* 120: 247-261.

Tu, Z. & Lu, Y. 2009. Evaluation of typical concrete material models used in hydrocodes for high dynamic response simulations. *International Journal of Impact Engineering* 36(1): 132-146.

Xie, L.X., Lu, W.B., Zhang, Q.B., Jiang, Q.H., Chen, M. & Zhao, J. 2017. Analysis of damage mechanisms and optimisation of cut blasting design under high in-situ stresses. *Tunnelling and Underground Space Technology* 66: 19-33.

Helsinki Conference Proceedings 2019, R. Holmberg et al

The complete diagnostic program for underground stope blasting to optimise dilution

D. Roy
Drill and Blast Expert, BBA Inc., Montreal, Quebec, Canada

ABSTRACT: In May 2017, Goldcorp Eleonore mandated BBA to design a specific stope and install the instrumentation necessary to analyse in detail the effects of vibrations on the walls. All modelling was done using the Aegis and Deswik software. Since the mine does not have a primary crusher underground, the fragmentation of the site had to be less than 16 inches, the size of their Grizzly. Knowing the desired particle size, with the goal of maximising recovery and minimising overbreak and dilution, a break envelope could be generated by the Aegis Breaker module. Calculated using thermodynamic equations, the break envelope is created according to the following parameters: powder factor, explosive energy factors, tonnage, explosive's velocity of detonation and distribution along borehole diameter, orientation of mineralised block according to a specific explosive, waste / ore properties and P and S wave velocity. Following the analysis, the optimised burden and spacing are 2.5 m x 2.8 m, respectively. Following the hearsay of the mine, the fragmentation from the stope has been impeccable throughout the scoop tram mucking with the whole process having taken place without being interrupted by oversized blocks. The CMS showed that no collapsing occurred in the stope even with a dip varying between 68º and 61º. The dilution in the stope was of 5.3% according to the thermodynamic envelope created by Aegis and 9.3% according to the standard envelope used by the mine. The #650-5050-251 stope was therefore under the bar of the 10% coveted dilution.

1 PARAMETERS OF THE STOPE

The stope #650-5050-251 was a secondary stope while the primary one was already completely backfilled. The mineralised zone of this sector is crossed by a highly and vertically jointed zone. The stope had a dip varying between 68º and 61º and a length of 24 m, a width of 13 m and a height of 25 m.

2 DESIGN PARAMETERS

The drift on the upper level has been developed using an arc of a circle shape. In addition, one of the main design constraints was to finish the stope perpendicular to the gallery in order to avoid damaging the next stope in the mining sequence. Taking into account these constraints, three zones were designed using fanned drilling. Using the

Breaker module of the Aegis software made it possible to establish the optimal blast pattern while taking into account the geomechanical parameters of the rock as well as the types of explosives present on site. The software calculated a burden of 2.5 m, a spacing of 2.8 m and a break radius of 1.3 m for the Subtek product and 0.7 m for the Senatel Powersplit product. The three fan zones, i.e. Section 2, Section 7 and Section 10, were drawn as a stagger pattern to respect as much as possible the calculated burden. In the widest part of the fans, i.e. at the hanging wall, holes have been added to compensate for the staggered zone and thus trimming the wall as straight as possible. These three extra boreholes were loaded with Senatel Powersplit.

3 DIFFERENT TESTS PERFORMED

3.1 Flexit

A survey with a Flexit probe, from the company Reflex, was performed to demonstrate the effectiveness of the product and to validate the deviation of the boreholes. The hanging wall holes were prioritised over the short holes of the foot wall. Some boreholes could not be surveyed with the probe due to areas restricted by a metal barricade and the Simba drill. The Flexit survey result versus the CMS results can be found in Appendix A. In these sections and in the plan view, it is possible to see the extent of the deviation of the boreholes surveyed by the Flexit probe as well as the surveying of the BT holes at the total station. Furthermore, the collars of the holes were surveyed to position the Flexit probe in space. In the section views, it is obvious that the collars of some holes have been moved. The drill probably did not have enough space to drill and had to be moved. It is possible to see that this displacement caused a loss in the hanging wall ore recovery, see the final CMS. Thereby, the spacing between the holes has been drastically reduced. These changes may cause damages to adjacent holes and create charges deconfinement. With the theoretical VOD of the Subtek Intense, being of 5 800 m/s, it will take 2.6 m/s for a 15 m column of charge to detonate and 4.3 m/s for a 25 m column. In this case, the delay between the hanging wall holes and their neighbour was of 34 m/s, leaving about 30 m/s between the two blastholes to create damage and deconfinement. It must be understood that deviation plays a very important role both in the fragmentation and in the control of the walls. After analysing the seismographs, it seems that all the hanging wall blastholes have detonated properly with respect to the number of kilograms of explosives present in each of them.

3.2 High frequency geophones

3.2.1 Primary blasting

During the loading of the primary blast, two boreholes were cancelled. The first, because it intercepted an adjacent borehole and the second one because it was blocked at 9 m. A good practice from the drillers would be to take note of all situations where they intercept any cavities or irregularities while drilling. No drill log mentioned such details. During the final blast, the blasthole containing 3 electronic detonators programmed at the delay of 6063 m/s did not respond when all personnel had evacuated the mine. Different causes may be involved; the most likely one is related to the working method used by some blasters. When the loading of a borehole is completed the operator twists the detonators' wires with the 'carry strap' preventing them from being free and/or in the way. In the event that the emulsion column descends due to a non-effective wooden borehole plug at the bottom or other reasons, the detonator wires will stretch and could possibly break at some point.

Figure 1 and Figure 2 show the readings from the high frequency geophones G-03 and HF 02, installed near the primary blast. These two figures show a plan view of the blasthole collars with their respective theoretical delay. The different shaded pellets show the amplitude ranges of vibration, in mm/sec, developed for the Eleonore Mine in a previous study. The dark shade, ranging from 0 to 300 mm/sec, indicates that the associated blasthole did not force excessively to break and move the ore tonnage proportional to its burden. Therefore, the charge's level of confinement, its delay and the angle of attack were all appropriate. The medium shade, ranging from 300 to 500 mm/sec, indicates that the associated blasthole has forced more to break and move its burden, without creating too much damage to its surrounding. The lighter shade, ranging from 500 to 1000 mm/sec, indicates that the blasthole has created damage to nearby walls. In such case, most probably, the level of confinement of the charge has been altered prior to its detonation. The blasthole either had an excessive burden to push or the explosive could not produce enough detonation pressure due to lack of confinement (reduced burden). It could also be explained by a non-adequate burden relief

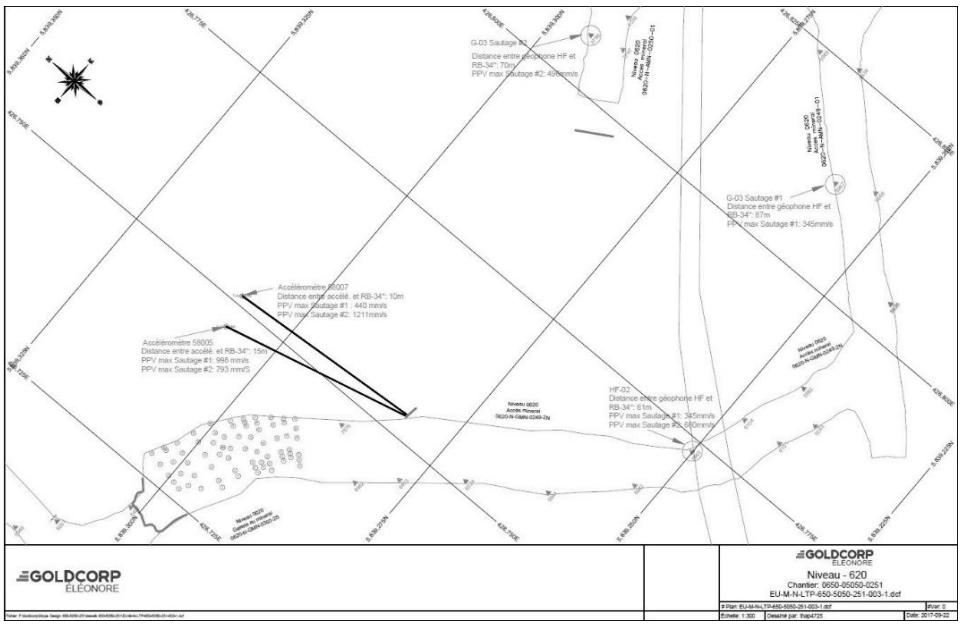

Figure 1. Location of geophones and accelerometers with distances and maximum PPV obtained.

or by the fact that the previously programmed firing sequence was no longer adequate for these conditions. The darkest shade, being greater or equal to 1000 mm/sec, defined irreversible damages to adjacent rock. These damages are characterised by additional fracturing and the opening of cracks in the host rock pillar.

Following the analysis of the first two figures,

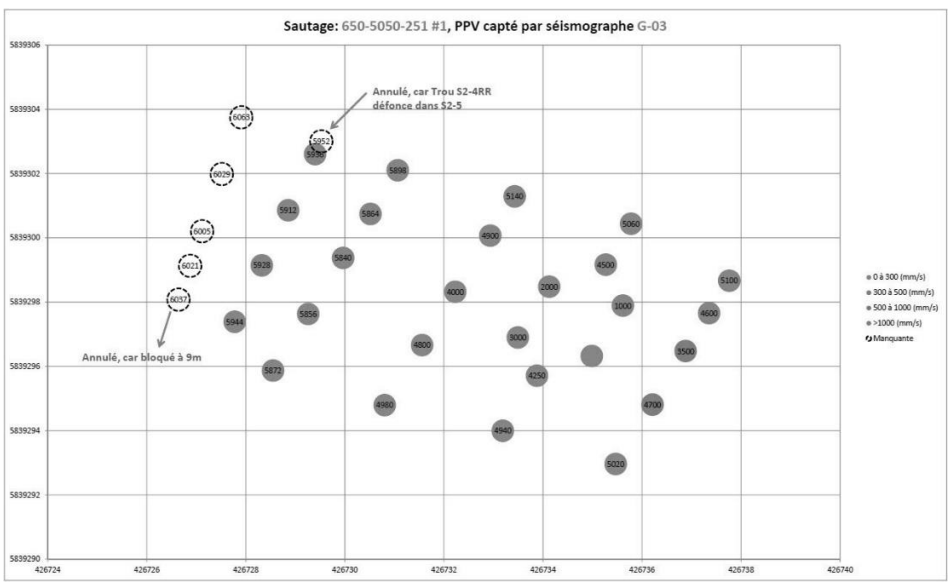

Figure 2. Plan view of Blast #1 with PVS value for each blasthole according to seismograph G-03.

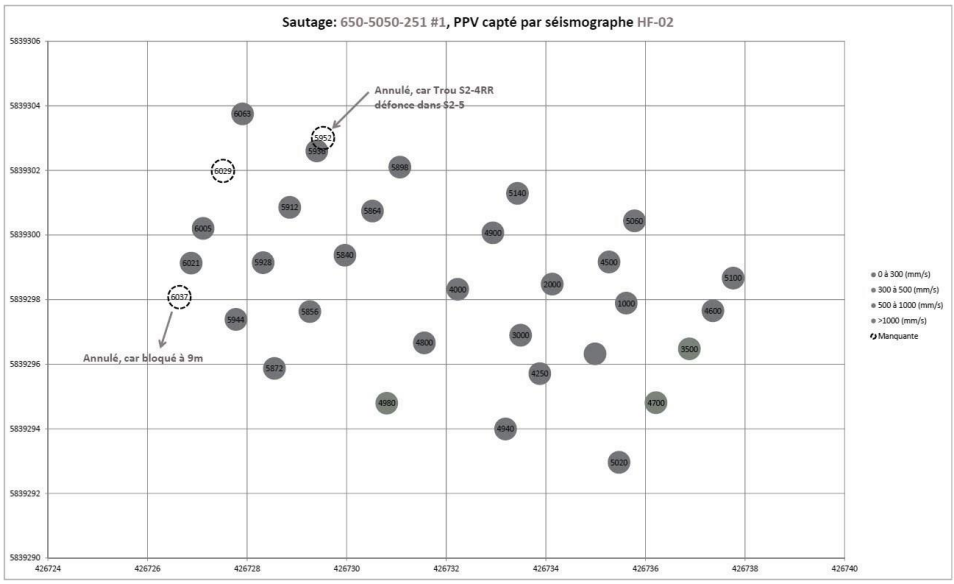

Figure 3. Plan view of Blast #1 with PVS value for each blasthole according to seismograph HF-02.

it is possible to say that the primary blast remained in a fairly low vibration range. The blastholes in the 0 m/s – 3000 m/s interval show no excessive vibration suggesting adequate relief of the mass in the void of the 34" primary slot borehole. Towards the end of the blast, some seismic data is missing. The reason is that when delays are so close to each other it becomes very difficult to isolate the pulse of each blasthole on the entire seismic trace.

Figures 3 and 4, in relation with the final blast,

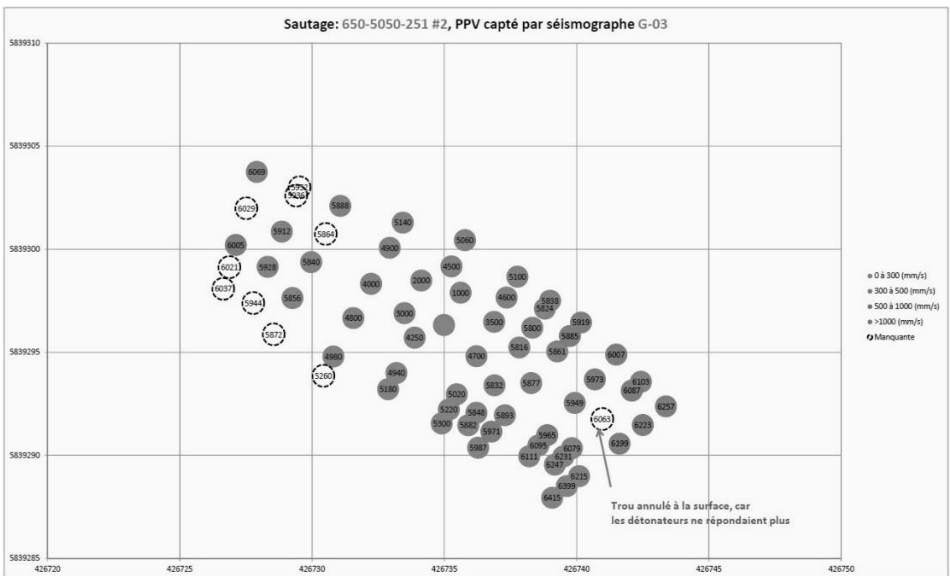

Figure 4. Plan view of Blast #2 with PVS value for each blasthole according to seismograph G-03.

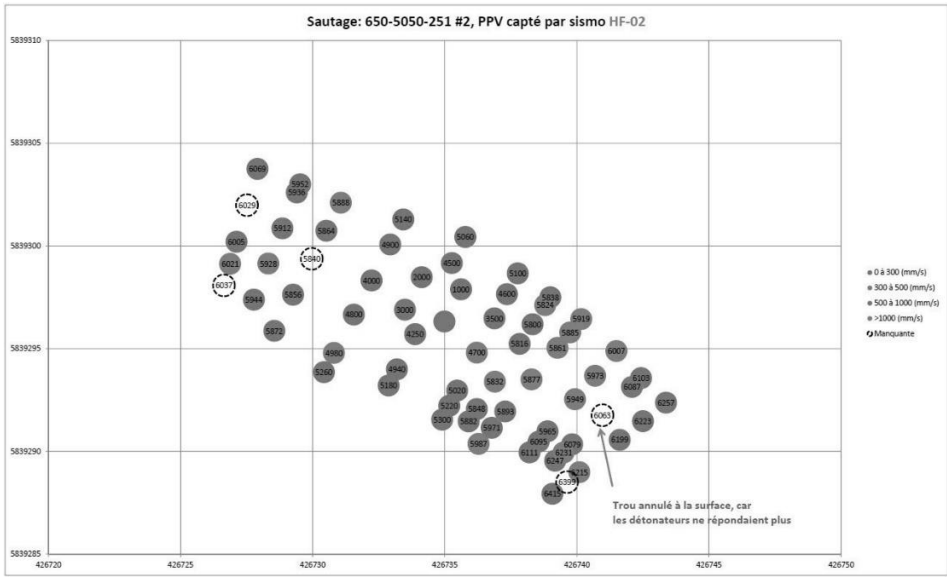

Figure 5. Plan view of Blast #2 with PVS value for each blasthole according to seismograph HF-02.

show more intense vibrations between Sections 7 to 11. Again, the blastholes around the 'open cut' did not show any issues. Some higher peaks can be explained by the 6063 m/s blasthole that didn't detonate and so over-confining the following blastholes behind.

In general, both blasts went well without going out of the spectra previously established.

3.3 Velocity of Detonation (VOD)

A Velocity of Detonation (VOD) test was also performed in the series of tests. The data collection device, the DataTrapII, contains 8 channels on which data can be stored. Since the two accelerometers took a total of 6 channels, the seventh was used for the VOD test and the eighth

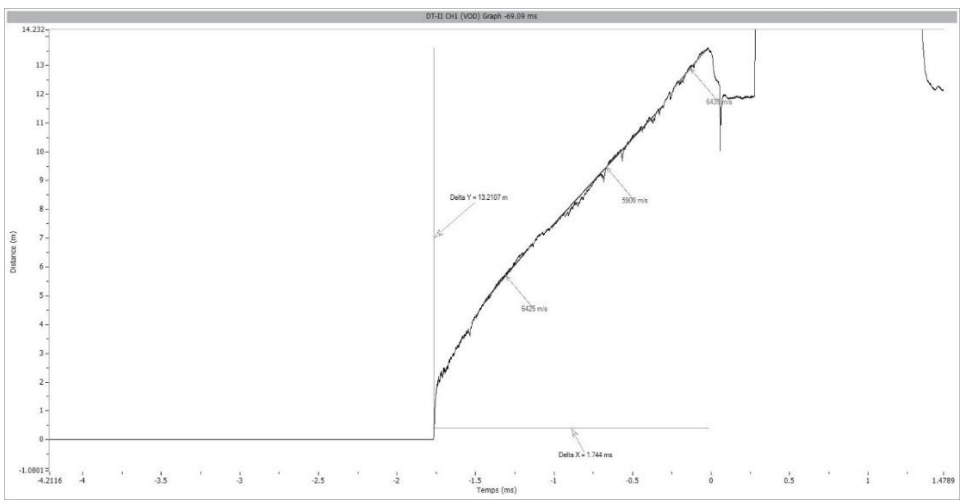

Figure 6. VOD result for the blasthole detonated at 0 m/s for Blast #2.

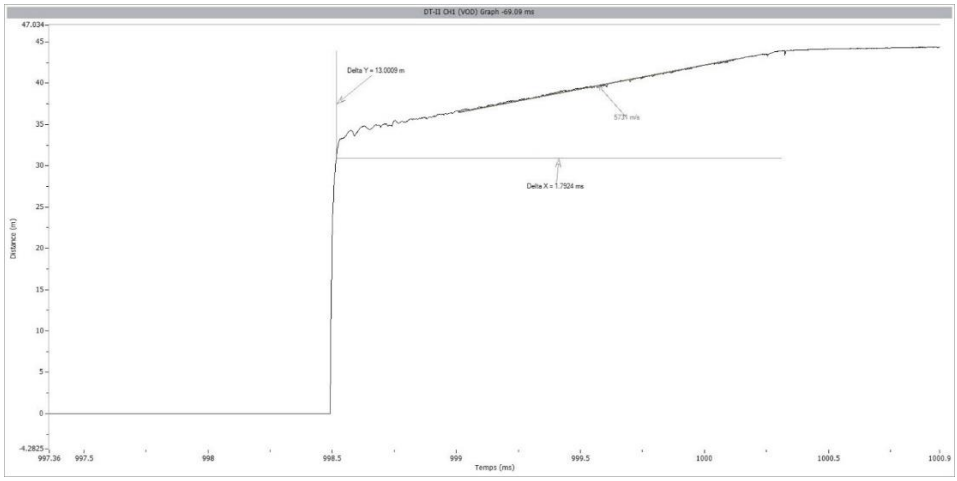

Figure 7. VOD result for the blasthole detonated at 1000 m/s for Blast #2.

as a trigger to give the starting point to the DataTrapII.

The only conclusive results were captured during the second shot. For the two blastholes where the instrumentation was installed, the delay was modified (i.e. +5 m/s) for the detonator located in the upper section of the column to be able to analyse the results. If the two detonators had detonated on the same delay, it would have been impossible to see the detonation velocity along the total length of the explosives column.

According to the specifications found in the Explosive supplier's technical data sheet, the Subtek Intense is expected to have a velocity of detonation of around 5800 m/s under ideal conditions.

The instrumentation was installed in the 0 m/s and 1000 m/s blastholes, i.e. the first two blastholes to be initiated on the perimeter line of the RB-34" primary slot. The VOD results are shown in Figure 6 and Figure 7. The first figure shows blasthole 5C-1, which was detonating at 0 m/s and the second figure shows blasthole 5C-2, which was detonating at 1000 m/s. Both figures show a charge of about 13 m in length and a detonation duration ranging from 1.7 m/s to 1.8 m/s. Both figures show detonation velocities falling within the technical specifications, therefore being compliant according to the supplier's technical specifications.

Since all the channels of the DataTrapII were used and the majority of the memory was used for data collection of the accelerometers, it was impossible to put too many VOD instruments in this particular stope. It would be, however, relevant to push the VOD analysis a little further, i.e. gathering information elsewhere than in the first blastholes firing, by placing instrumentation in adjacent blastholes of a single ring, as well as on parallel rings of a 'Dice 5' drill pattern and 'fanned pattern' ones. It will then be possible to assess the impact of adjacent blastholes timing, or between sections of drilling. This future test would be used as an additional validation on the efficiency of the actual burden and spacing used during the test in stope #650-5050-251.

3.4 Buffer row loading

Three holes were initially planned to be loaded with the Senatel PowerSplit 32 mm. This type and diameter of explosive was previously specified for 4" boreholes in a previous report for Goldcorp: Technical Support for the design of narrow stopes (3 metres). A visit to the 410 and 650 level magazines was made to confirm that the product was as requested. The Senatel PowerSplit 22 mm was the only one of its kind to have been found in the magazines. So, during the loading, the product was doubled in each blasthole following our request. A borehole plug was then placed at the proper final loading height and the rest of the collar was filled with crushed stone (stemming material).

It became obvious that such type of decoupled loading, or with a variable density emulsion, will

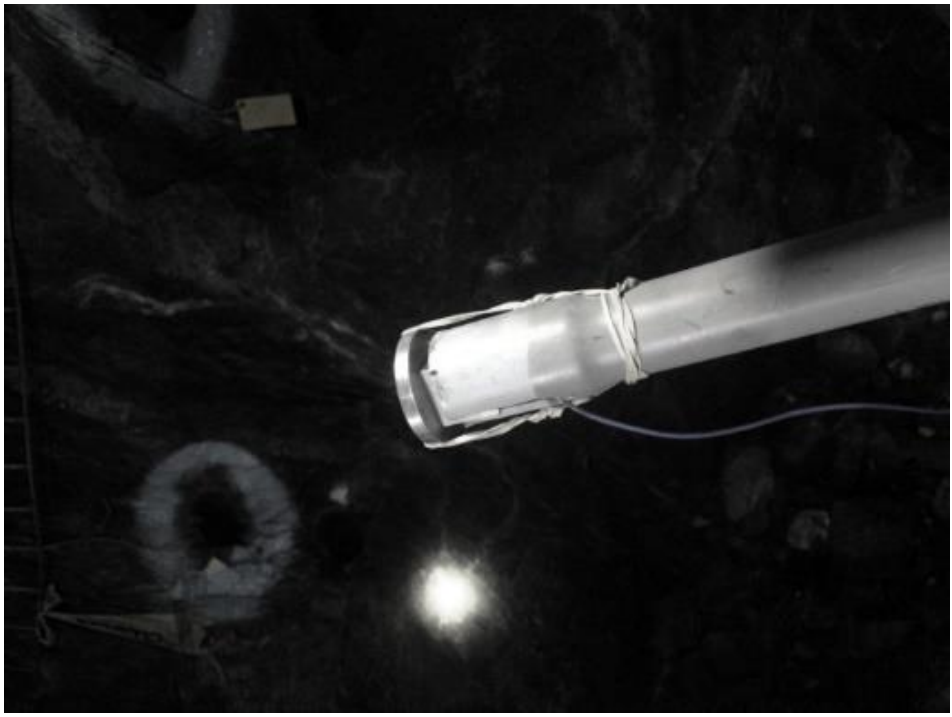

Figure 8. Assembly of the first PVC pipe with the accelerometer inside the flared part with its cable. The accelerometer is attached to the aluminium washer with rubber bands.

be part of the future of the Eleonore Mine. The most recent information obtained from the mine's definition drilling programs indicates that stopes widths will mostly be below 5.0 m. Furthermore, the results from the geomechanical compilations conducted by the site's engineers have provided valuable information regarding the damages to the hanging wall caused by stopes orientations and the different types of drill patterns they used.

Underground field testing should be considered with the Orica people to develop a program to implement the technology already available on their bulk emulsion loading units. Specific training for the blasters, engineers or anyone involved in the blast designs could ensure the mastery of the characteristics of these new types of loading.

3.5 Accelerometers on the hanging wall

Two NQ diameter diamond drill boreholes were made to install the instruments at specific locations and distances from the hanging wall. Each accelerometer has three (3) axes (i.e. X, Y and Z). Depending on the configuration of the instrument, the X axis was positioned towards the centre of the stope's mass. Since the instruments could not simply be lowered into 28 m deep boreholes, a PVC pipe fitting was used to place each instrument at the bottom of each borehole. The accelerometers were previously mounted to a thick aluminium washer and simply attached with elastics. The assembly can be seen in Figure 8. Once the PVC pipe assembly was positioned at the bottom of the borehole, the cement crew then began to inject the liquid grout. After having poured the equivalent of 3 m in length of grout, the pipes were removed. The aluminium washer thus created a larger surface area and allowed PVC tubes to be removed by pulling on them to break the rubber bands. Once removed, the rest of the boreholes were cemented.

Figure 9 and Figure 10 show in section view the bottom of the DDH boreholes where the accelerometers were installed and the distance from the stope's hanging wall.

The data retrieved on the DataTrapII was in millivolt, some formulas had to be used to transform the results in g and mm/s^2 taking into account the calibration of each of the X, Y and Z axes for both devices. In order to have data

Trou	Angle (deg)	Dist. Ref. (m)	Long. (m)	Long. foré	Long. mésuré	BT	For. dist.	Commentaires
1	-87.1	L3.0	11.0			N		
2	-82.8	L2.1	13.5			N		
3	-74.8	L1.1	27.8			Y		
4	-72.6	R0.7	26.5			Y		
5	-70.2	R2.5	27.4			Y		
6	-66.0	R3.4	28.1			Y		
7	-61.7	R4.2	26.9			N		
			161.2					

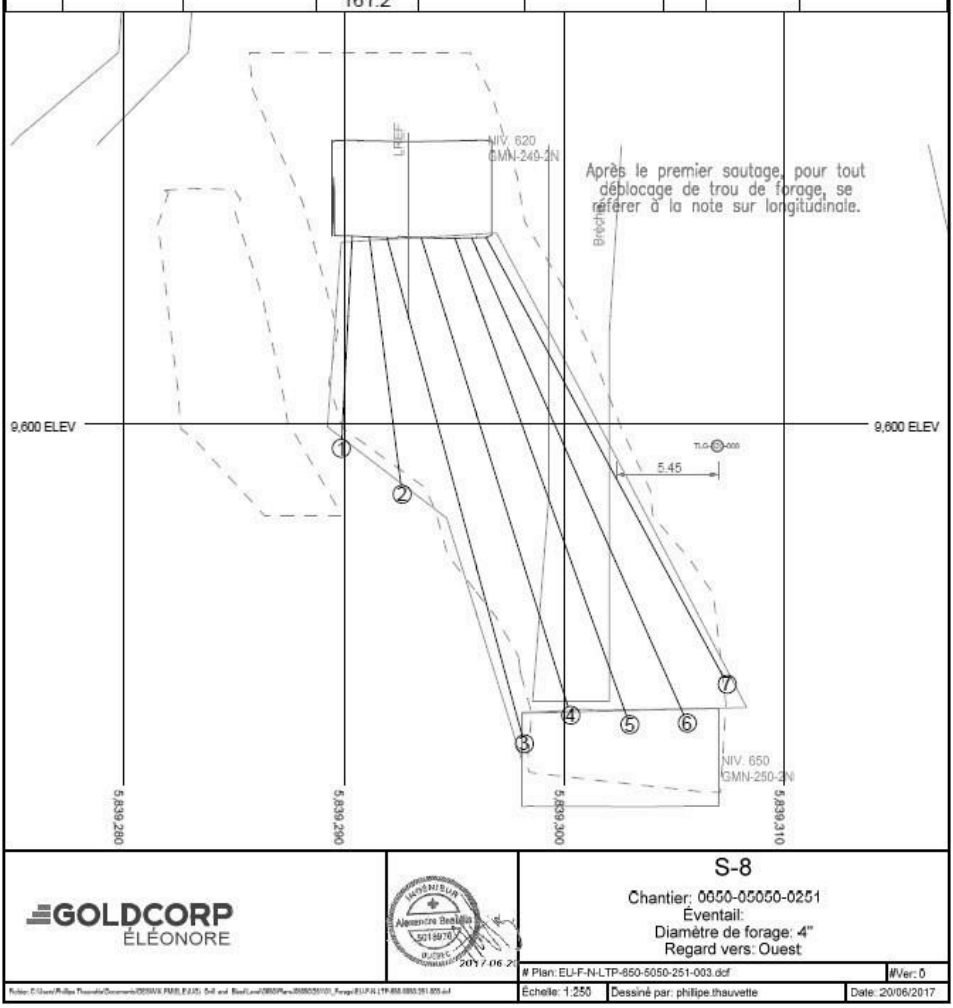

Figure 9. Distance between the accelerometer #58005 and the hanging wall.

comparable to the high frequency geophone results, all the results in mm/s^2 were integrated 'peak by peak' where each one represents a different delay. This way, it was possible to add the PPVs (in mm/sec) as well as the scaled distances to the regression formula already established for the Eleonore site. Appendix B graphically shows the results on a Log/Log graph for the field-installed instruments for stope #650-5050-251, i.e. high-frequency geophones and accelerometers compared to other data collected in 2015, 2016 and 2017. The data in blue, representing the accelerometers, show a regression curve with faster attenuation and results

Trou	Angle (deg)	Dist. Ref. (m)	Long. (m)	Long. foré	Long. mésuré	BT	For. dist.	Commentaires
1	-87.7	L2.0	11.6			N		
2	-80.0	L1.4	14.6			N		
3	-70.4	L0.8	27.0			Y		
4	-67.5	R1.1	27.5			Y		
5	-63.9	R2.5	28.6			Y		
6	-60.5	R3.9	27.8			N		
			137.1					

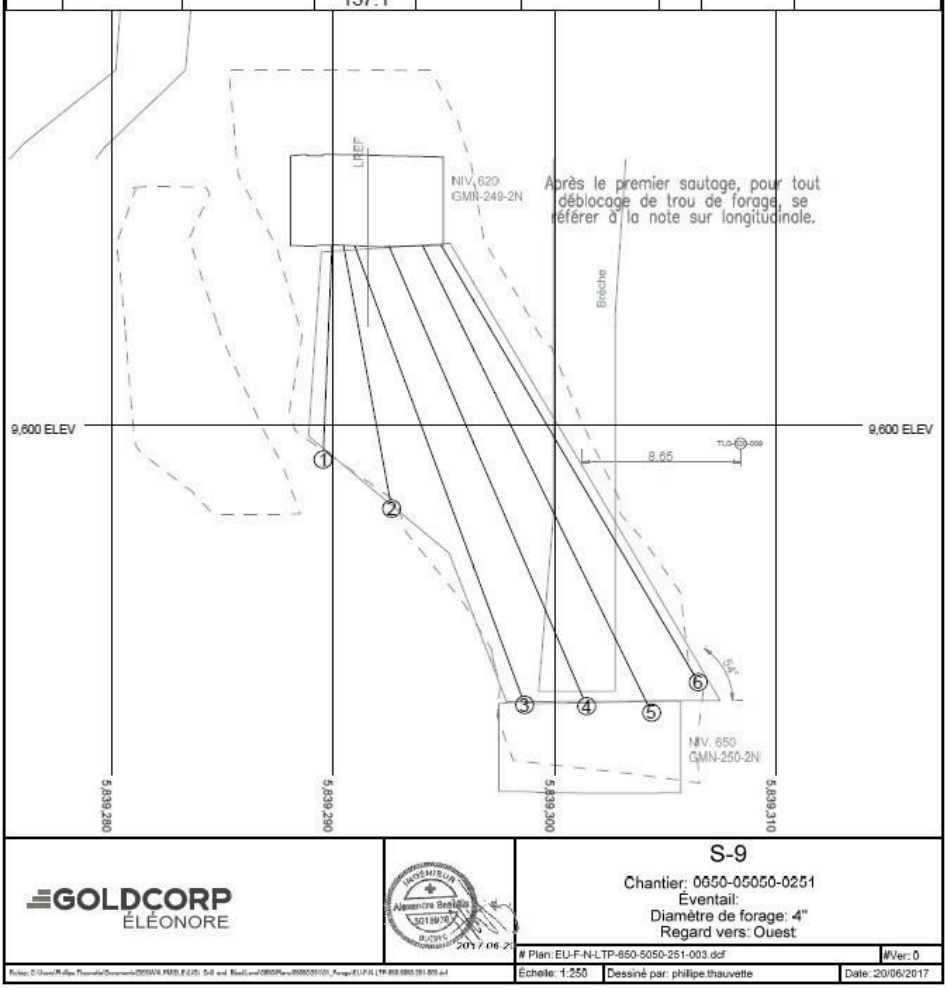

Figure 10. Distance between the accelerometer #58007 and the hanging wall.

below 1000 mm/s. All these collected data results are originating from the hanging wall of the stope and they reveal that in this case, a larger and better suited drilling pattern was less damaging to the host rock. This was the main reason why there was not any important wall collapse during the stope excavation process.

Historically, when a stope of such geometry was excavated with a tighter pattern, the seismic results were generally above the levels recorded in the recent study. Readings over 1000 mm/sec at distances of the order of 30 m were measured at that time. Such high energy impulses tend to create major damages to the walls that won't

remain stable for a long enough time to allow a complete stope mucking operation, even when it was done with urgency by mine operation people. Hazardous situations are then created, with scoops being exposed, production delays being observed, and, in the worst-case scenario, the tensile failure plans created will even extend to higher levels, thus jeopardising future stopes located above.

All observations from this study have already been the subject of many discussions in the past. Our findings and recommendations are based on precise measurements obtained by ultra-sophisticated acceleration sensors. These confirm what was previously believed. Changes to the drilling pattern, the energy distribution of the explosives, and the firing sequence led to the definition of the right recipe for the breakage mechanism sought by Eleonore.

3.6 Inter-hole and inter-row delays

Assuming that the crack opening velocity approaches the velocity of the S wave as a worst case, an empirical formula can be used:

$$T_d = \frac{C_L}{D} + \frac{S}{P_w} + \frac{S}{S_w} + \frac{S}{C_v} + N\left(\frac{B_m}{G_v}\right)$$

$T_d = Delay\ time\ (\text{sec})$

$C_L = Charge\ length\ (m)$

$D = Detonation\ velocity\ \left(\frac{m}{sec}\right)$

$S = Spacing\ (m)$

$P_w = P-wave\ velocity\ \left(\frac{m}{sec}\right)$

$S_w = S-wave\ velocity\ \left(\frac{m}{sec}\right)$

$C_v = Crack\ velocity\ \left(\frac{m}{sec}\right)$

$N = Percent\ of\ burden\ moved\ (decimal)$

$B_m = Burden\ (m)$

$G_v = Gas\ expansion\ velocity\ \left(\frac{m}{sec}\right)$

Equation 1. Formula used to calculate the delays.

Depending on the percentage of displaced burden and the gas expansion velocity, an inter-hole and inter-row delay can be found. By keeping a constant burden, spacing and explosive type, a typical delay could be established for the different types of stopes. For the stope #650-5050-251, the delays were based on this formula and modified a little bit later to protect the hanging wall. As shown in Table 2, the Gv parameter goes from 300 ft/sec to 50 ft/sec. A high Gv represents the first holes or sections to fire, those that are closer to the stope primary RB-34". The lower Gv values, represent the farthest sections progressing towards the end of the shot. In addition, by varying the percentage of burden moved (n), it is possible to find inter-hole and inter-row delays as the blast progresses. Appendix C shows the plan of delays that were applied for the final blast of the test stope.

Table 1. Parameters used, with GV and N modifiable.

Parameter	Definition	Value	Units
C_L	Charge length	25	m
D	Detonation velocity	5488	m/sec
S	Spacing	2.8	m
P_w	P-wave velocity	6414	m/sec
S_w	S-wave velocity	2608	m/sec
C_v	Crack velocity	1206	m/sec
N	Percent of burden moved	30	%
B_m	Burden	2.5	m
G_v	Gas Expansion velocity	91.46341463	m/sec
T_d	Recommended IHD	0.016587283	sec
T_d	Recommended IHD	16.58728299	ms

3.7 Modification burden – Spacing

Two of the major aspects that were modified during the design of this test stope were the burden and the spacing. The Eleonore Mine currently uses a 2.2 m x 2.5 m burden and spacing. By relying on the site-specific rock mass properties as well as the properties of the explosive they use, a constraints profile could thus be established using the Breaker module of the Aegis software. By taking the established stress profile and the energy entanglement profiles created by each of the blastholes, an optimal pattern could be defined (i.e. a burden and spacing of 2.5 m x 2.8 m). Figure 11 and Figure 12 show the constraints profiles for both types of drill patterns. An additional study was carried out for a narrow vein stope #590-5010-506, and Appendix D represents the correction results that should be applied following the calibration of the initial stope data. Therefore, a pattern of 2.2 m x 2.5 m would be optimised at 2.5 m x 2.8 m. Appendix E, for its part, represents a proposal done in 2018 where a 'Dice 5' type stope could be tested, i.e. using a lower density emulsion for blastholes located along the walls and the current version of

Table 2. Table of delays calculated according to the percentage of burden moved.

		n			
		0.3	0.6	0.8	1
Gv (pi./sec)	Gv (m/sec)	ms/trou	ms/trou	ms/trou	ms/trou
300	91.5	16.59	24.79	30.25	35.72
275	83.8	17.33	26.28	32.24	38.21
250	76.2	18.23	28.07	34.63	41.19
225	68.6	19.32	30.25	37.54	44.83
200	61.0	20.69	32.99	41.19	49.39
180	54.9	22.05	35.72	44.83	53.94
150	45.7	24.79	41.19	52.12	63.05
125	38.1	28.07	47.75	60.87	73.99
100	30.5	32.99	57.59	73.99	90.39
75	22.9	41.19	73.99	95.85	117.72
50	15.2	57.59	106.79	139.59	172.39

emulsion for the centre holes. The sketch presented in Appendix E, represents the difference between the current 'Dice 5' and the modified one.

4 NOTES TAKEN REGARDING THE DRILLING AND LOADING

4.1 Drilling

Since the gallery at the upper level was large enough, the drilling has been done using two Simba drills and only one operator. Memos about the re-drills were sent three times for different boreholes. There was a total of sixteen re-drills due to deviation. This amount of re-drills can be explained by the boreholes dip, combined to a highly jointed zone crossing the ore vein from top to bottom. Also, note that the remotely operated Simba 6 are all 'Top Hammer' type.

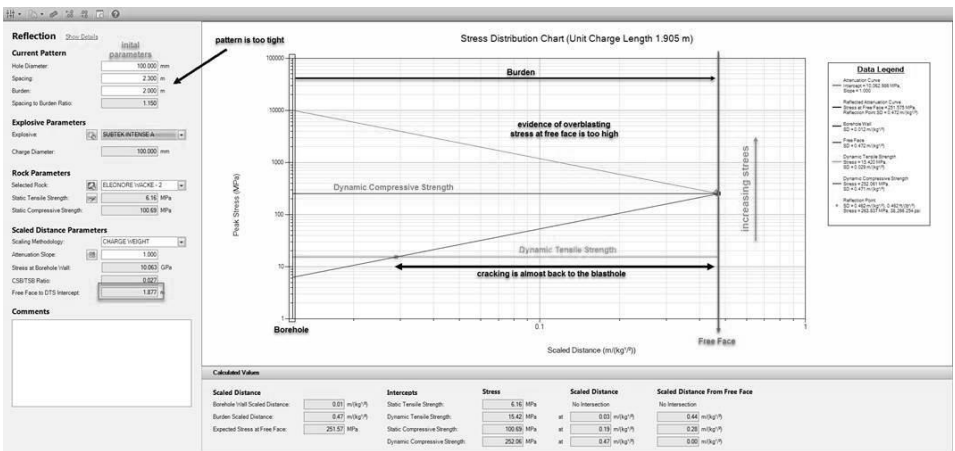

Figure 11. Constraints profile for a pattern of 2.0 m x 2.3 m.

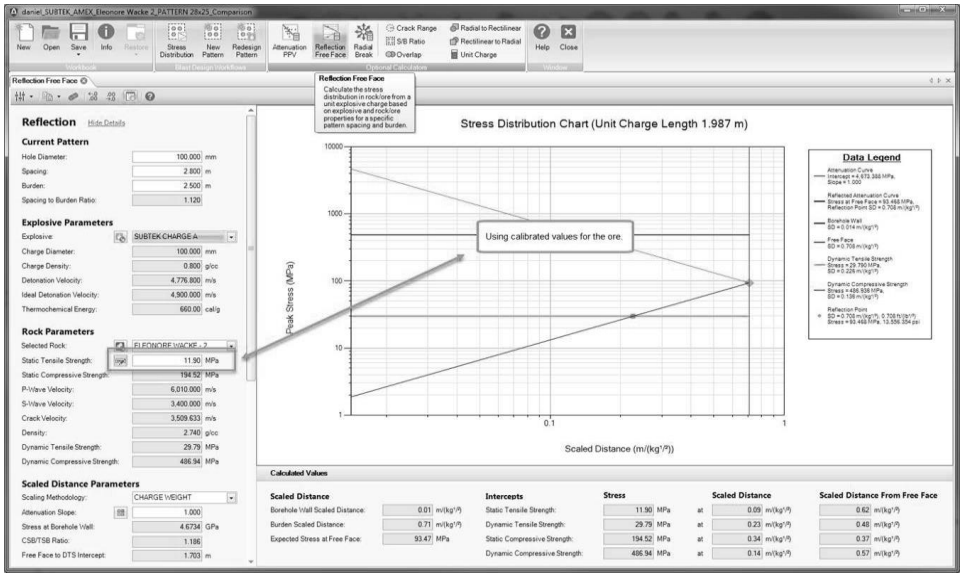

Figure 12. Constraints profile for a pattern of 2.5 m x 2.8 m.

4.2 Loading

When loading the first blast, borehole S1-1 was reported as blocked and was not loaded. During the process of plugging the break through boreholes at the lower level, the blasters realised that borehole S2-4RR and borehole S2-5 intersected each other. It was therefore decided to cancel the S2-5 and only load the S2-4RR.

Also, it is interesting to mention that even with all the precautions taken to protect the integrity of the measuring instruments, i.e. concrete blocks and yellow ribbon 'Caution', a miner found a way to get in the cross cut by passing between the concrete blocks and the yellow ribbons. He ended up cutting off the accelerometer wires. Not being ordinary wires, lucky enough we got assistance from one of the mine electricians who was able to repair them in time.

When loading the second blast, no problem was found while everybody was underground. However, once returned to surface, when the blasters used the safety key to access the firing system and the blasting machine, blast hole S10-4 containing three boosters was not responding. The problem was reported to the field control supervisor and the decision was made to overwrite the error and blast regardless of it. The most probable explanation for the three detonators of the same blast hole to fail to communicate was that they had been cut at the same time in one way or another.

5 RESULTS

As for the results that were communicated to BBA, the mucking of the stope has been done relatively quickly without any issue, which was a sign that the fragmentation was really good. It should also be mentioned that the dumping point of the haul trucks being on the same level than the draw points, this helped to speed up the stope mucking. Still not having an automatic fragmentation particle size measurement system in operation at that time, we mostly relied on the qualitative chart we had implemented with the scoop tram operators to qualify the general fragmentation produced. This stope was given an optimal fragmentation score, meaning that the broken rocks were always smaller than the grizzly opening size of 16" x 16", reason why it did not cause any delay when using the mechanical rock breaker in place.

According to the CMS results taken from the upper and lower levels after the stope mucking was complete, no major collapse occurred from the walls. These measurements and observations were made by one of Goldcorp's rock mechanics engineers. Such rapid stope blasting and mucking helped to reduce the final walls exposure time and played a key role in maintaining their stability.

The same expectations should be applied toward other test with new drill patterns.

After reconciliation, the dilution of the stope was 5.3% according to the Aegis software predicted break envelope and 9.3% according to the standard dilution calculation methodology used by the mine. Stope #650-5050-251 was therefore able to remain under the barrier of the 10% coveted dilution.

6 RECOMMENDATIONS

- maintain drilling patterns of 2.5 m of burden by 2.8 m of spacing for stopes of similar width and geometry
- avoid recreating situations where the explosive charges are too close to the free faces, which have the effect of generating a series of adverse propagation of the waves towards the back of the blast or to the adjacent blast holes
- adjust the delays between the rows according to the burdens displacement velocities established during different field studies
- always take Flexit measurements in boreholes that do not break through on the lower level; the options offered by the device's software make it possible to identify and reject the magnetically affected values; this tool, when combined with the simple and practical use of an inverted flashlight down into the bore-holes, will minimise the impacts of boreholes having deviated too much
- conduct velocity of detonation measurements periodically (every three months) in order to validate the quality of the loading methods
- introduce the concept of loading with variable density emulsions to mitigate the effects of 100 mm diameter boreholes for stopes of narrower geometry
- thoroughly proceed with seismic measurement and data collections in near field from the stopes to validate and comply with the pre-established damage limits
- complete the search for the best suited fragmentation measuring system for underground mine operation

7 CONCLUSIONS

Increasing the 100 mm borehole drilling pattern to 2.5 m by 2.8 m significantly contributed to the success of this project. The energy distributions of the bulk emulsion explosive charges with a density of 1.25 gr/cc were also optimised. This element, combined with appropriate confinement levels, allowed for better control of the effective burden of each charge, maximising their performance in terms of breakage instead of vibration generation toward the walls. Moreover, the electronic detonators sequence used was derived from estimated broken rock mass displacement velocities applicable to underground mines blasting's powder factors.

All of these factors helped producing vibration levels that were well below what the mine used to measure. Maximum amplitudes of 1,000 mm/sec were detected by the accelerometer located at 5.0 m in the hanging wall (see Appendix B). Historically, the high frequency geophone's readings were taken at distances of about 30.0 m from the stope. This is a significant reduction and it explains why no oversize block was reported during mucking operations. In addition, no major rock fall occurred from the walls during the same period. The measurements taken by the CMS confirmed that both the hanging wall and foot wall were able to withstand the impacts of multiple charges detonating in very short delays.

The dilution ratio, less than 10%, is a milestone for a gold mine producing a high daily tonnage of more than 5,000 metric tons. The knowledge gains made during this project must be transposed to the future stopes. Additional improvements could even be considered by introducing variable density emulsions in the blast holes located close along the hanging wall of narrower veins (< 5.0 m).

Pre-established vibration control limit and criteria remain a key performance indicator (KPI) of underground production blasting and the data collection activities still have to be supported and reinforced. The challenges associated to conducting frequent underground vibration measurements should be resolved by the implementation of telemetry allowing a much easier communication with the instruments located underground.

The different programming options of electronic detonator systems offer a multitude of possibilities, but it is imperative that they always be determined according to surveyed borehole locations (not just theoretical) and the resulting effective burdens displacement velocities, as it was systematically done during this exercise. Thus, new borehole deviation survey instrumentations and burden velocity measurements tools are being developed in order to validate the values that were used during this project.

APPENDICES

Appendix A: Flexit VS CMS 650-5050-251 (9 images).
Appendix B: 650-5050-251 – GoldcorpÉléonore_Vibration Analysis (1 image).
Appendix C: Blasting delay plan (1 image).
Appendix D: Calibration correction results (1 image).
Appendix E: Difference between the current dice 5 and the modified (2 images).

Trou	Angle (deg)	Dist. ref. (m)	Long. (m)	Long. mésuré	For. dist.	Charge de	Collet	Expl. type	Expl. Kg	Chargé	Commentaires
1	-86.6	L2.4	10.1			10.1	1.6	Emulsion	86		
2	-75.0	L1.6	17.5			17.5	1.6	Emulsion	161		
3	-73.1	R0.3	15.9			15.9	1.6	Emulsion	145		
4	-68.7	R4.0	14.8			14.8	1.6	Emulsion	134		
5	-64.8	R5.4	15.6			15.6	1.6	Emulsion	142		
			73.9						668		

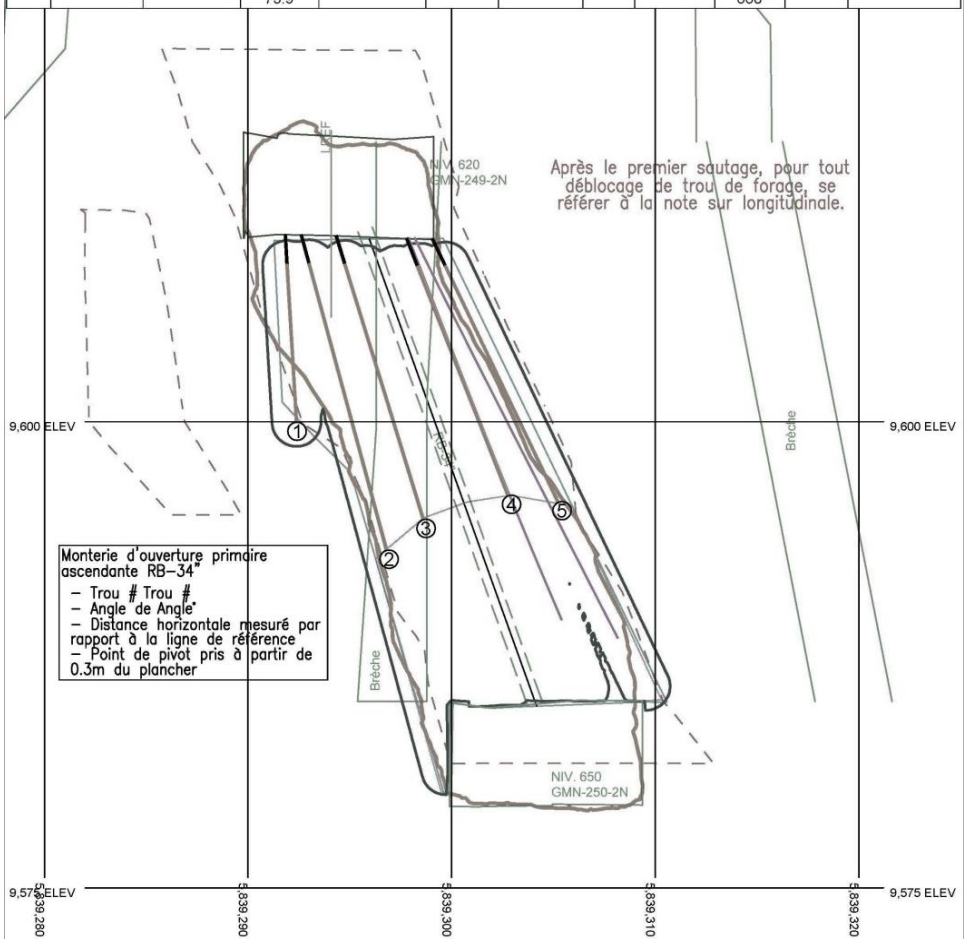

Appendix A: First image. Flexit VS CMS 650-5050-251.

Trou	Angle (deg)	Dist. ref. (m)	Long. (m)	Long. mésuré	For. dist.	Charge de	Collet	Expl. type	Expl. Kg	Chargé	Commentaires
1	-87.1	L3.0	11.0			11.0	1.6	Emulsion	95		
2	-82.8	L2.1	13.5			13.5	2.3	Emulsion	113		
3	-74.8	L1.1	27.8			27.8	1.6	Emulsion	265		
4	-72.6	R0.7	26.5			26.5	1.6	Emulsion	252		
5	-70.2	R2.5	27.4			27.4	1.6	Emulsion	261		
6RR	-66.0	R3.4	28.1			28.1	7.3	Emulsion	211		
7	-61.7	R4.2	26.9			26.9	1.6	Emulsion	256		
			161.2						1454		

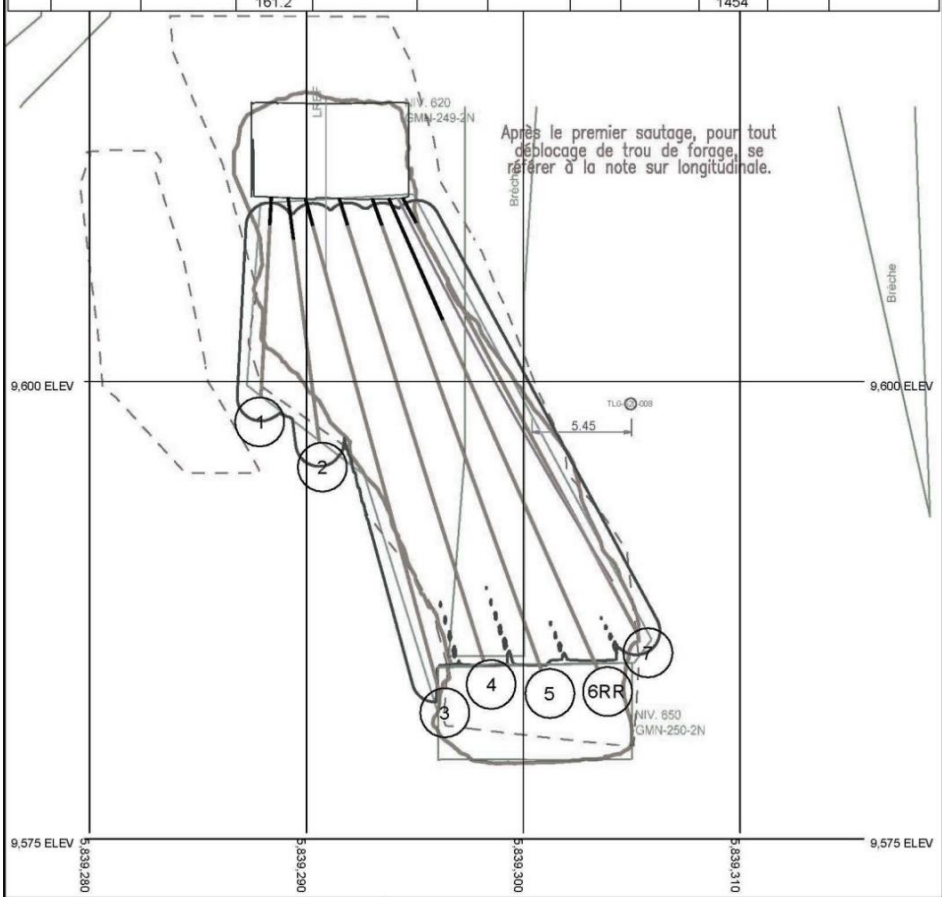

GOLDCORP
ÉLÉONORE

S-8

Chantier: 0650-05050-0251
Éventail: 90.0°
Diamètre de forage: 4"
Regard vers: Ouest

# Plan: EU-M-N-LTP-650-5050-251-003-1.dcf	#Ver: 0
Échelle: 1:250 — Dessiné par: Phillipe.Thauvette	Date: 25/08/2017

Appendix A: Second image. Flexit VS CMS 650-5050-251.

Trou	Angle (deg)	Dist. ref. (m)	Long. (m)	Long. mésuré	For. dist.	Charge de	Collet	Expl. type	Expl. Kg	Chargé	Commentaires
1	-88.2	L2.5	11.1			11.1	6.2	Emulsion	50		
2	-76.9	L1.8	18.3			18.3	5.7	Emulsion	127		
3	-73.9	L0.3	26.2			26.2	1.6	Emulsion	249		
4	-72.2	R1.7	26.4			26.4	1.6	Emulsion	252		
5R	-68.4	R2.8	27.0			27.0	5.5	Emulsion	218		
6	-64.2	R3.9	27.8			27.8	1.6	Emulsion	266		
7	-62.4	R4.3	26.8			26.8	7.0	Pre-Split	161		
			163.6						1322		

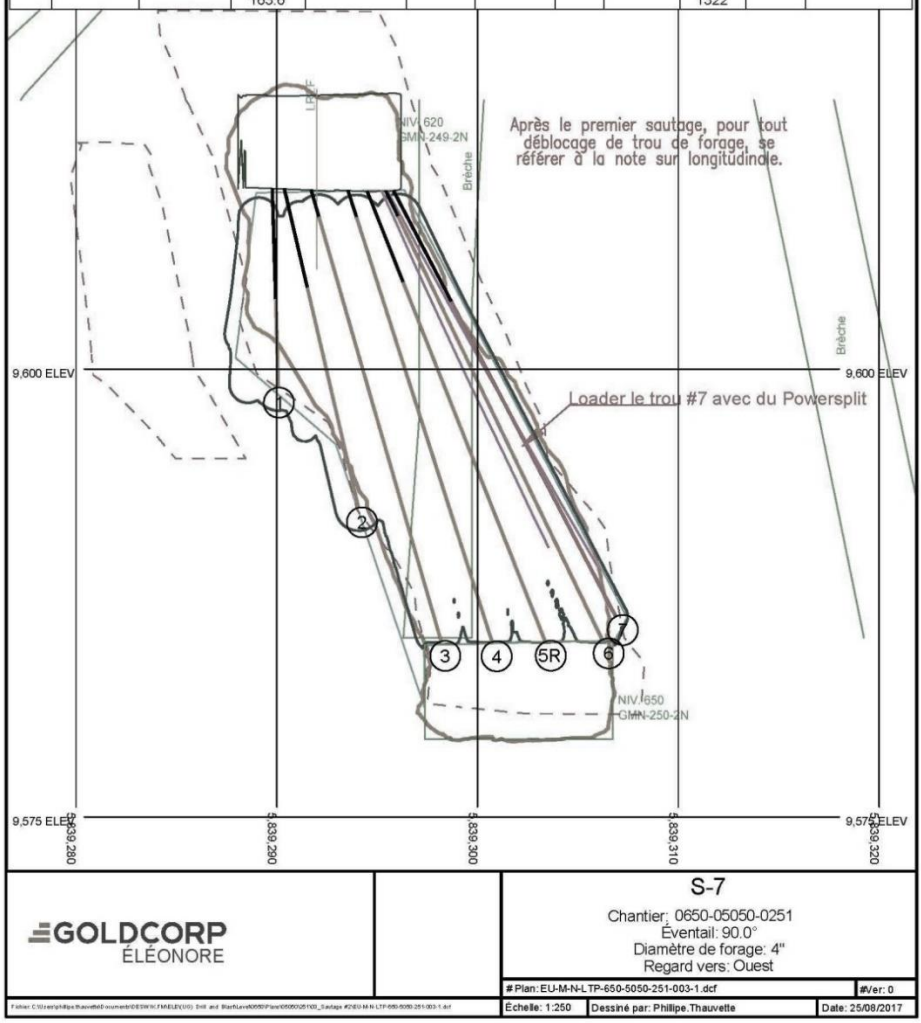

GOLDCORP
ÉLÉONORE

S-7

Chantier: 0650-05050-0251
Éventail: 90.0°
Diamètre de forage: 4"
Regard vers: Ouest

Plan: EU-M-N-LTP-650-5050-251-003-1.dcf | #Ver: 0

Échelle: 1:250 | Dessiné par: Philipe.Thauvette | Date: 25/08/2017

Appendix A: Third image. Flexit VS CMS 650-5050-251.

Trou	Angle (deg)	Dist. ref. (m)	Long. (m)	Long. mésuré	For. dist.	Charge de	Collet	Expl. type	Expl. Kg	Chargé	Commentaires
1	-90.0	L2.7	4.8			4.8	1.6	Emulsion	32		
2	-74.3	L1.7	17.4			17.4	1.6	Emulsion	160		
3	-72.6	R0.3	15.7			15.7	1.6	Emulsion	143		
4	-70.1	R2.1	15.0			15.0	1.6	Emulsion	136		
5	-67.9	R4.0	14.9			14.9	1.6	Emulsion	135		
6	-64.7	R5.3	15.6			15.6	1.6	Emulsion	142		
			83.4						748		

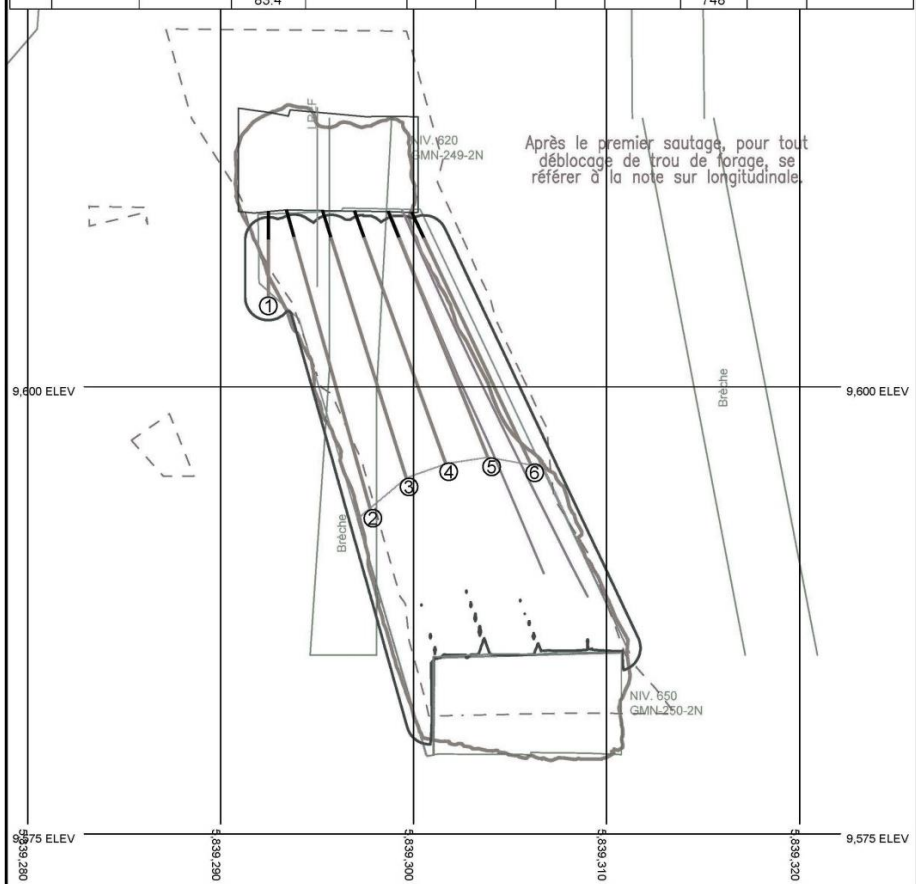

GOLDCORP
ÉLÉONORE

S-4

Chantier: 0650-05050-0251
Éventail: 90.0°
Diamètre de forage: 4"
Regard vers: Ouest

Plan: EU-M-N-LTP-650-5050-251-003-1.dcf | #Ver: 0

Échelle: 1:250 | Dessiné par: Phillipe.Thauvette | Date: 25/08/2017

Appendix A: Fourth image. Flexit VS CMS 650-5050-251.

Trou	Angle (deg)	Dist. ref. (m)	Long. (m)	Long. mésuré	For. dist.	Charge de	Collet	Expl. type	Expl. Kg	Chargé	Commentaires
1	-81.1	L3.2	8.2			8.2	1.6	Emulsion	67		
2	-84.2	L2.5	12.2			12.2	2.7	Emulsion	96		
3	-75.0	L1.7	18.1			18.1	1.6	Emulsion	167		
4	-73.1	R0.3	16.3			16.3	1.6	Emulsion	149		
5	-70.5	R2.1	15.6			15.6	1.6	Emulsion	142		
6	-66.9	R3.4	15.5			15.5	3.2	Emulsion	125		
7	-62.8	R4.5	16.0			16.0	1.6	Emulsion	146		
			101.9						892		

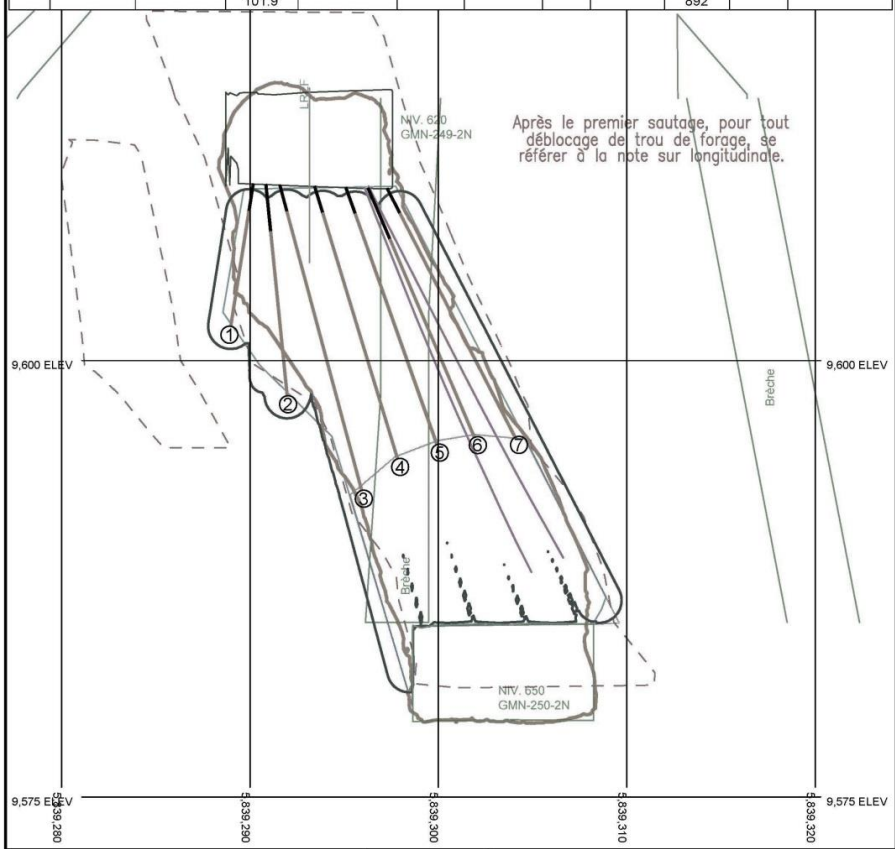

GOLDCORP
ÉLÉONORE

S-6

Chantier: 0650-05050-0251
Éventail: 90.0°
Diamètre de forage: 4"
Regard vers: Ouest

Plan: EU-M-N-LTP-650-5050-251-003-1.dcf | #Ver: 0

Échelle: 1:250 | Dessiné par: Philipe.Thauvette | Date: 25/08/2017

Appendix A: Fifth image. Flexit VS CMS 650-5050-251.

Trou	Angle (deg)	Dist. ref. (m)	Long. (m)	Long. mésuré	For. dist.	Charge de	Collet	Expl. type	Expl. Kg	Chargé	Commentaires
1	-74.3	L1.6	17.4			17.4	1.6	Emulsion	160		
2R	-72.4	R0.3	16.6			16.6	1.6	Emulsion	152		
3RR	-70.0	R2.2	16.0			16.0	1.6	Emulsion	146		
4R	-66.9	R3.7	15.9			15.9	1.6	Emulsion	145		
5	-64.2	R5.2	16.0			16.0	1.6	Emulsion	146		
			81.9						749		

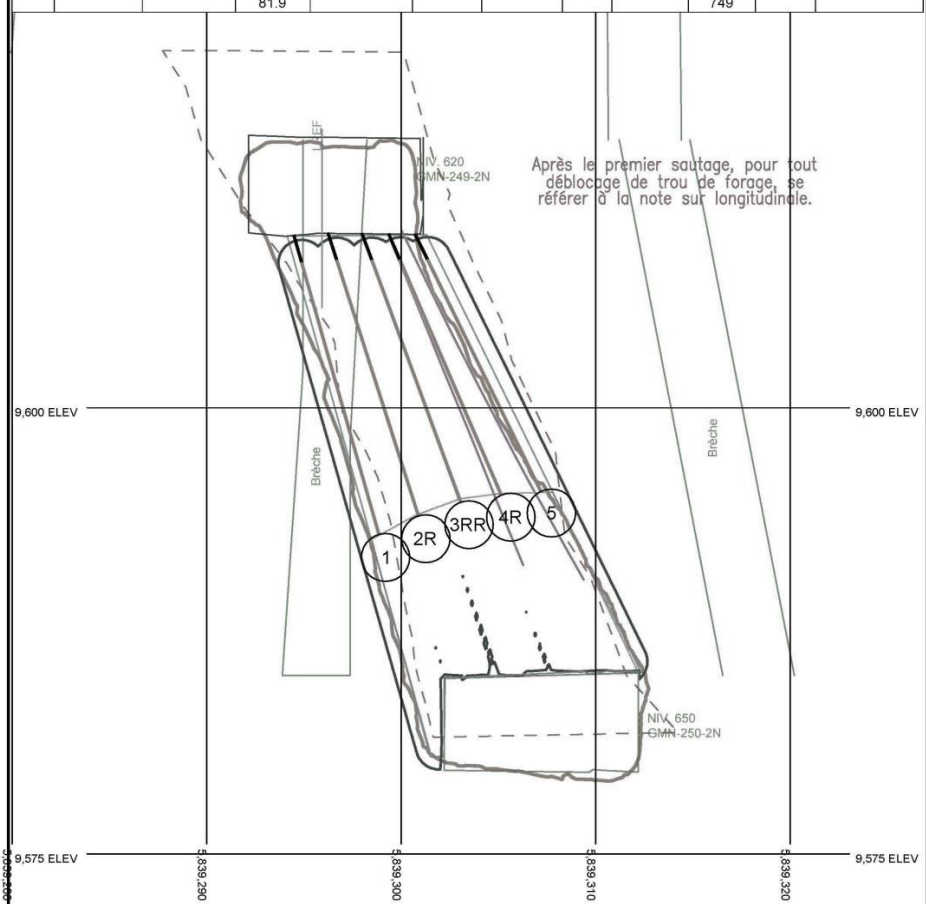

GOLDCORP
ÉLÉONORE

S-3

Chantier: 0650-05050-0251
Éventail: 90.0°
Diamètre de forage: 4"
Regard vers: Ouest

Plan: EU-M-N-LTP-650-5050-251-003-1.dcf | #Ver: 0

Échelle: 1:250 | Dessiné par: Phillipe.Thauvette | Date: 25/08/2017

Appendix A: Sixth image. Flexit VS CMS 650-5050-251.

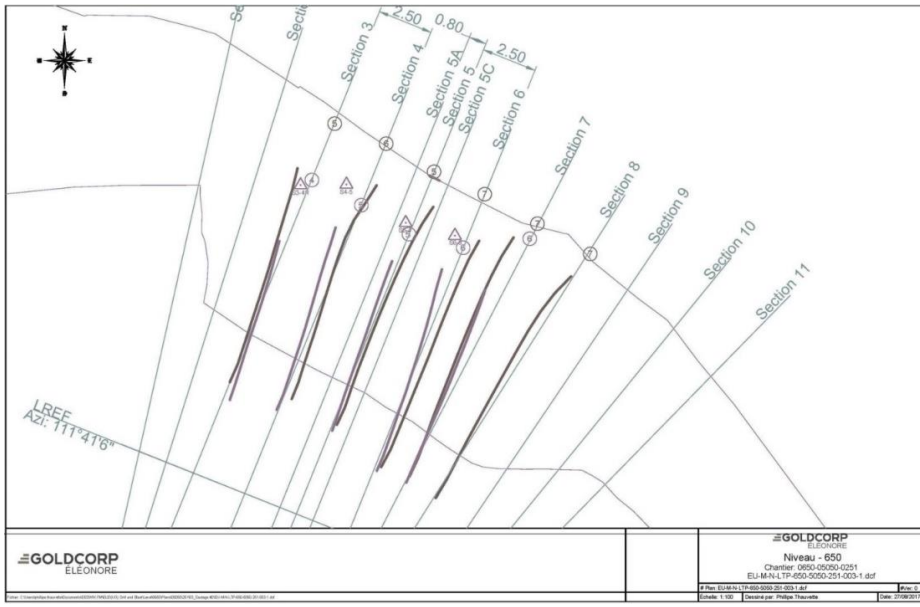

Appendix A: Seventh image. Flexit VS CMS 650-5050-251.

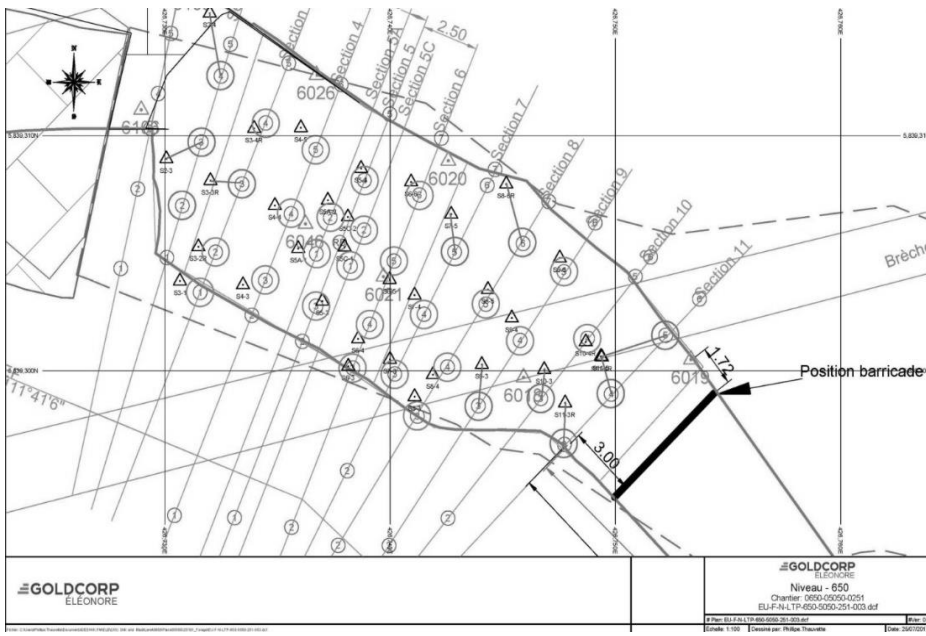

Appendix A: Eighth image. Flexit VS CMS 650-5050-251.

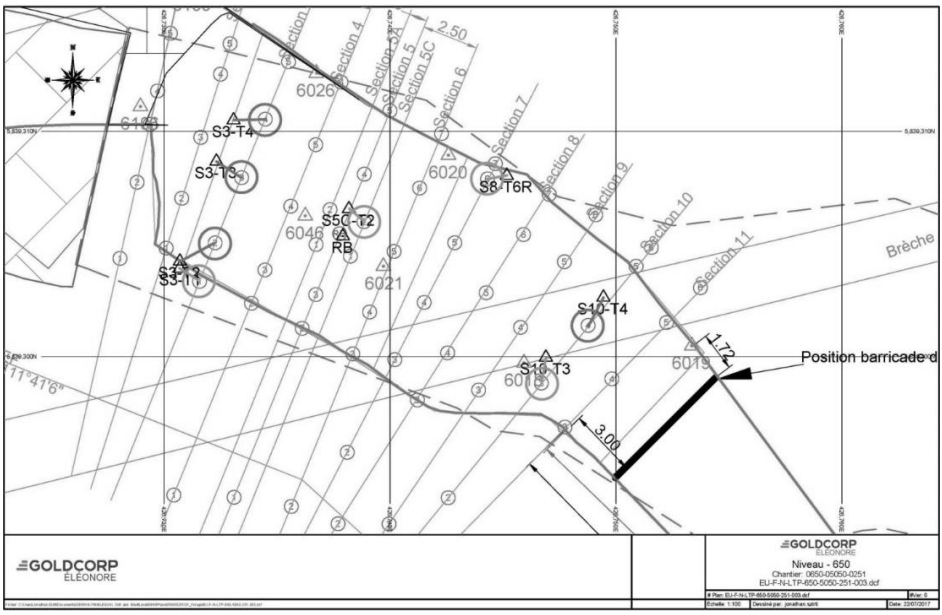

Appendix A: Ninth image. Flexit VS CMS 650-5050-251.

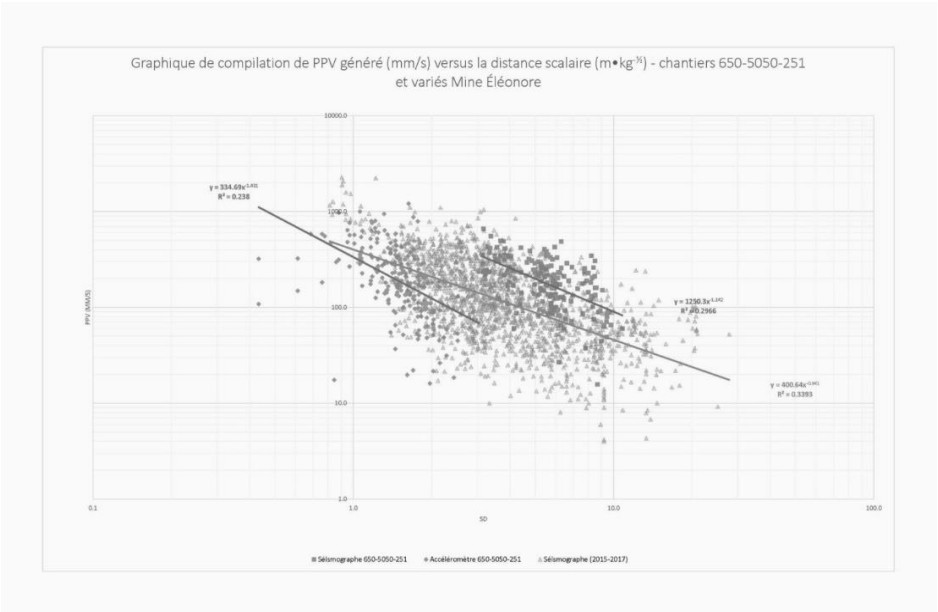

Appendix B: 650-5050-251 - GoldcorpÉléonore_Vibration Analysis.

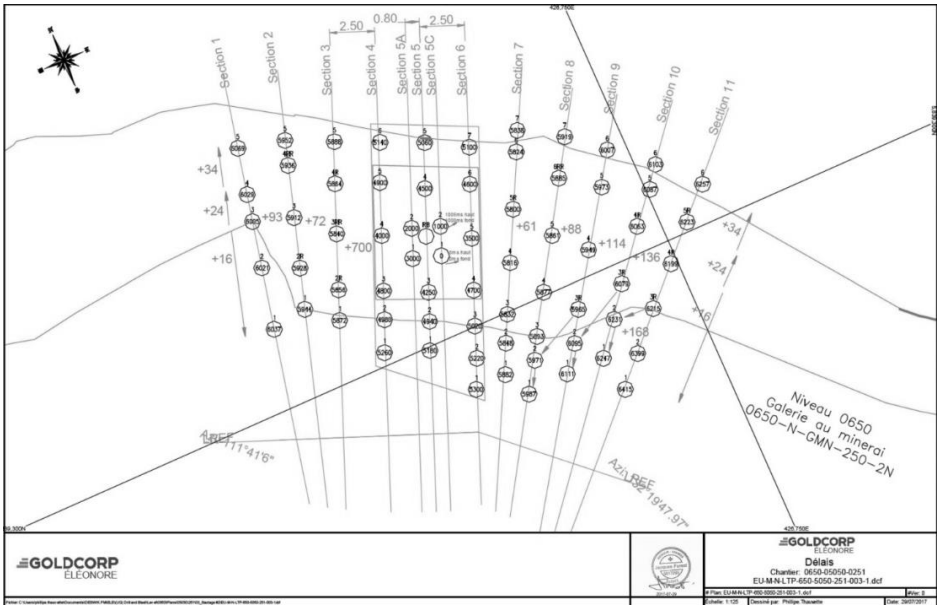

Appendix C: Blasting delay plan.

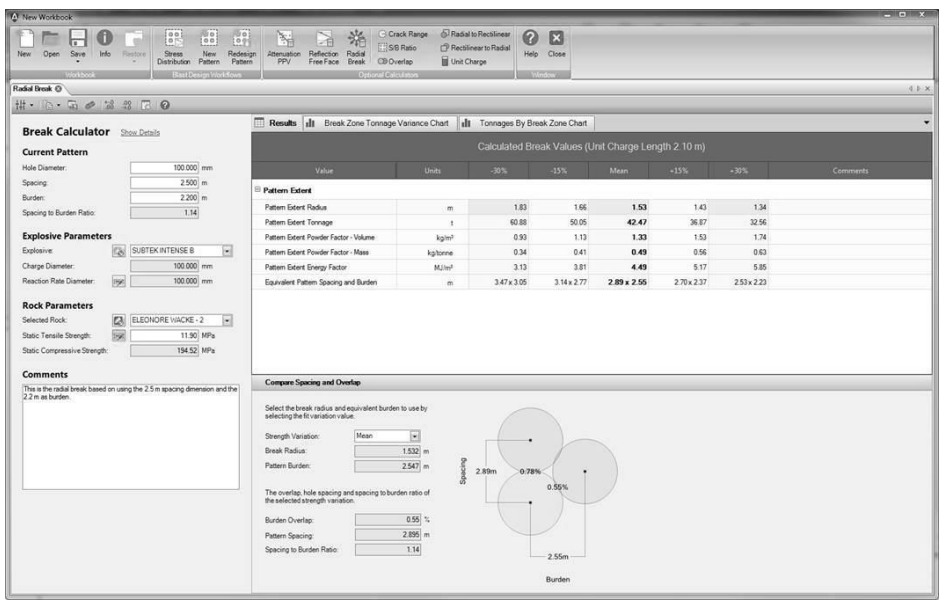

Appendix D: Calibration correction results.

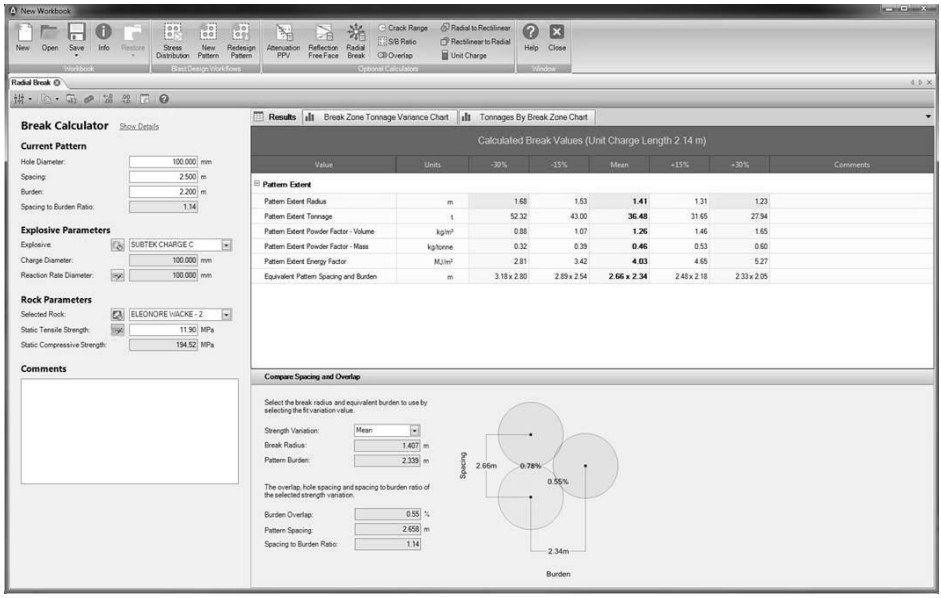

Appendix E: First image. Difference between the current dice 5 and the modified.

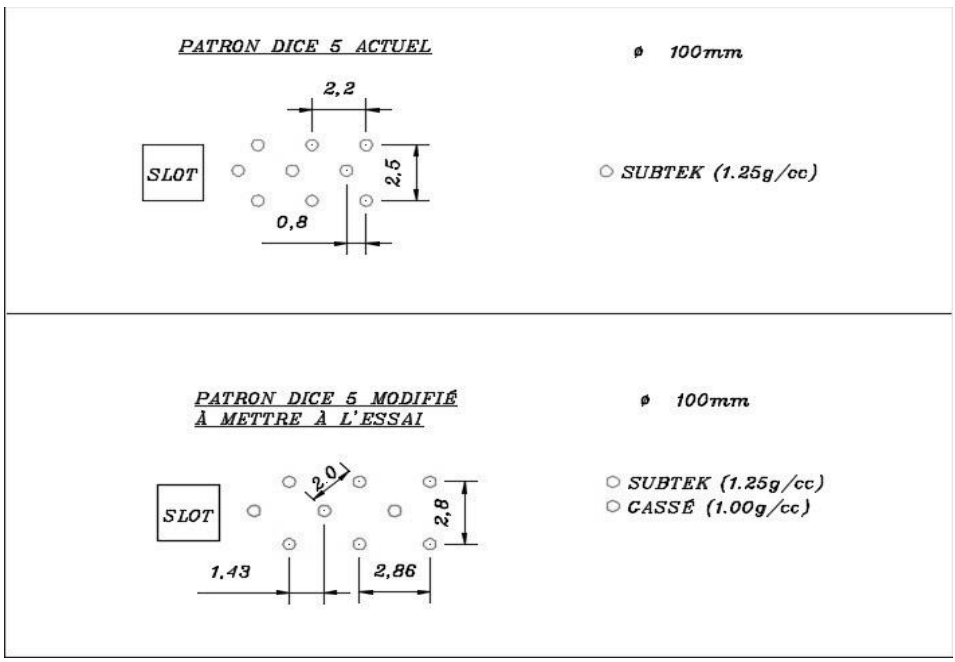

Appendix E: Second image. Difference between the current dice 5 and the modified.

Helsinki Conference Proceedings 2019, R. Holmberg et al

The development of pressure to Young's modulus models for precision presplit blasting

A.J. Konya & C.J. Konya
Precision Blasting Services, Montville, Ohio, USA

ABSTRACT: Precision presplitting has been defined as a new method of presplitting which utilises light explosive loads of less than 0.15 kg/m (0.1 lbs/ft) of borehole and a close spacing of 0.61 m (2 ft) or less. This new method of presplitting has been used on hundreds of construction projects to control overbreak in weak and heavily jointed rock, specifically in construction projects. This paper will look at the mechanisms of how this presplit forms under these light loads and present new models which relate borehole pressure to the rock characteristics, specifically the Young's Modulus with multiple variations in spacing. This gives explosives engineers a new tool to help design this presplit through various borehole diameters, spacing distances, rock types, and structural environments while assuring a smooth neat line is developed with a minimal slow zone.

1 RESEARCH OBJECTIVE

The ability for a mining or construction project to generate smooth walls through the use of explosives is paramount to the operation being economically effective and safe for employees. The use of proper presplitting can reduce the amount of scaling required to 1/10 of that required when traditional blasting is utilised (Paine, Holmes & Clark 1961). This has large economic savings in reduction of manpower ad equipment required and increased excavation capacity. This also leads to a safer project as less rockfalls occur during the scaling process when men and equipment are near the highwall. The minimisation of back-break is not only seen on the face of the excavation, but the reduction in blast damage is metres thick where proper presplits show no degradation of the rock beyond the presplit line (Matheson & Swindells 1981).

While traditional presplit methods can be utilised in hard rock types, they encounter problems when they are applied to weaker rocks. This has led to a false concept that weaker sandstones, shales, mudstones, and siltstones cannot be presplit. However, the method of precision presplitting has been applied to all of these conditions effectively and shown presplits with near perfect walls in full-scale construction projects (Spagna, Konya & Smith 2005). Traditional presplit methods often caused problems with this type of rock as the explosive load was too great and crushing or cratering around the borehole would cause overbreak.

Oftentimes, the structural properties of the geology being blasted also cause back-break

beyond the presplit lines (Worsey, Farmer, & Matheson, 1981; Worsey & Qu, 1987). The solution to minimise the effects of these geologic conditions is to bring the borehole spacing closer together. Traditional presplit design would use 'split-factor' to adjust the explosive load based on a linear relationship with spacing. However, the explosive load to spacing relationship is not linear (Konya & Konya 2017) and this would lead to overloading of the charge in the area. With this being completed in poor geologic conditions, oftentimes with heavy jointing and bedding, the presplit would overbreak the entire region and cause joints and bedding planes to open up from gas penetration.

The mechanisms behind a presplit formation are not well researched and understood. The shock breakage theory is still widely taught and studied (International Society of Explosive Engineers 2016, Salmi & Hosseinzadch 2014) even though this theory has numerous studies showing how it is not applicable and is a false concept (Konya C. 1973, Worsey P. 1981). In fact, under this theory methods such as precision presplitting could not work to produce a presplit. A new theory that the explosive generated gasses in a borehole causes a hoop stress field which causes the presplit fracture to occur (Konya & Konya 2017) would indicate that very small explosive loads could be used, depending on the rock type and structural environment, to generate a fracture without causing any overbreak to the surrounding structure. It has been proposed that this hoop stress field will be a function of the gas pressure and the research on this project will focus on defining this gas pressure in a borehole from detonating explosives to determine if borehole pressures are possible to generate these hoop stress fields.

2 MECHANICS OF PRESPLITTING

In today's blasting industry both shock breakage (Zhang 2016) and gas pressure (Konya & Konya 2017) breakage is presented in modern technical papers focusing on the mechanism behind presplit blasting. Many have also argued that the mechanism behind the presplit is unimportant or academic, which may be true for the traditional case of presplitting which remains the same under almost all circumstances. However, with the advent of precision presplitting the mechanism behind a presplit is of importance as changes to dimensions such as the spacing of boreholes and explosive load in a hole are designed to meet the structural geology and rock properties. Without an understanding of the mechanisms behind a presplit formation a strategic design to eliminate overbreak while allowing for smooth breakage is impossible.

The first large scale explosive presplit was produced on the Niagara Power Project which was completed in 1962. This project was based in dolomite and limestone with a single layer of shale near the bottom of the excavation and had to have smooth walls in order to pour concrete against. During the project, numerous methods of controlled blasting were attempted including line drilling, line drilling with explosive loads in every third hole, modified cushion blasting, decks of dynamites throughout the borehole, and finally presplitting. Presplitting was reported that the only method that produced satisfactory results to minimise overbreak was the presplitting which was accomplished by taping 32 mm (1 ¼ inch) by 100 mm (4 inch) sticks of dynamite on Primacord every 0.30 metres (1 foot). The boreholes were 63 mm (2 ½ inch) to 75 mm (3 inch) in diameter and spaced 0.61 metre (2 feet) apart and stemmed with crushed gravel. This resulted in increased rock excavation and a reduction in scaling by a factor of 10. Additionally, the project had significant savings on concrete costs and increased safety as the walls were cleaned smooth (Paine, Holmes & Clark 1961).

At the time, the project was designed based on the gas pressure generated by the explosive. The engineers assumed that if the gas pressure was kept below the compressive strength of the rock, they would avoid crushing the rock around the borehole. In order to create a break between boreholes the belief was that the borehole pressure had to be above the tensile strength. While this was a bit of a rudimentary theory at its time, however the project was completed and the presplit functioned extremely well. Following the project presplitting was widely accepted as the best and most cost-effective method of overbreak control.

Based on this theory, researchers of presplitting both in a laboratory and practical setting began looking into the decoupling of charges, or the reduction of the diameter of the explosive compared to the diameter of the borehole. This was done to decrease the dynamic gas flow on the borehole wall and to reduce the gas pressure in the borehole (Konya, Britton & Lukovic 1987) preventing large compressive strengths which would lead to overbreak (Day 1982). However, this increase in decoupling ratio also led to minimal shock pressure transmission into the rock mass due to large impedance

mismatches between explosives and air, then air and rock.

With the large increase in research of shock breakage in rock blasting, many authors began to investigate possible effects of shockwave collision between boreholes to develop tensile zones and causing presplit formation (DuPont 1975, Crosby & Bauer 1982). This theory was widespread due to the popularity of the DuPont Blasters Handbook and it is still circulated amongst many leading organisations today (International Society of Explosive Engineers 2016) and researchers (Salmi & Hosseinzadch 2014). This theory was heavily disputed and shown in numerous studies of the day and it was shown that the shockwave has almost no correlation between the dynamic shockwave and the presplit formation, with numerous studies showing that the quasi-static gas pressure in the borehole was responsible for presplit formation (Konya C 1973, Worsey P 1981, Worsey, Farmer & Matheson 1981, Daehnke, Rossmanith & Kouzniak 1996). Additional studies were conducted utilising a propellant charge, Pyrodex, to fire a presplit blast. These propellant charges produced no shockwave as they deflagrate, not detonate, (Akhavan 2011) which completed isolated the gas pressure as the only working energy. Using the same principles as in traditional presplit design (Konya C 1980), the propellant charges produced the exact same results as a presplit blast that was fired with detonating explosives (Konya, Barret & Smith 1986). This proved that presplit mechanisms on a full-scale blast had no reliance on the shockwave generated by detonating explosives.

This led to the development of a precision presplit style of blasting, where extremely light loads of detonating cord are utilised to prevent all breakage except for the breakage between boreholes (Konya C 1982). This design utilised closely spaced borehole of 0.61 metre (2 feet) or less, to minimise the impacts of rock structure on the presplit (Worsey P 1984, Worsey & Qu 1987, Tariq & Worsey 1996). As this design methodology has begun widespread use, new empirical research into the explosive loading based on the rock properties has been developed (Konya & Konya 2015, Konya & Konya 2016, Konya & Konya 2017).

This method of precision presplitting has effectively zero shock energy to form a fracture after accounting for impedance mismatches (Cooper 1996), non-ideal detonation (Cook 1974), and attenuation of the shockwave in the rock mass (Spathis & Wheatley 2016). It has then been theorised that the mechanism behind the presplit formation is due to large hoop stresses which are generated between the boreholes causing a fracture, with no advancement of the fracture from gas penetration (Konya & Konya 2017).

3 PRECISION PRESPLITTING

Precision presplitting is a presplit design technique which was first applied in the 1982 (Konya C 1982) and utilised extremely light loads in closely spaced boreholes to form a presplit with no overbreak in weaker rocks. As it developed, the rock type was considered which dictated variations in the explosive load, with granites requiring a much higher load than a sandstone or siltstone. Those with experience in this method began to have a feel for general ranges that each rock type required based on a 0.61 metre (2 foot) spacing between boreholes, and in a test blast could identify the required load in most rock types. These empirical methods were the basis behind precision presplit design originally, just as they are on traditional presplit design, and relied on the engineer's experience.

The borehole loads were typically so light that no commercially sold presplit powder was available for the application of precision presplitting. The use of dynamite charges on detonating cord was also not applicable as the areas of dynamite would cause significant overbreak. The only available choice to keep the borehole loading light and consistent was detonating cord which in weak rocks, such as mudstones and siltstones, which may be kept under 64 g/m (300 grains/ft). In 2015 the authors began analysing this empirical data from numerous construction projects around the United States to develop equations to estimate the explosive load for a precision presplit based on a rock's Young's Modulus (Konya & Konya 2016). The authors found this to have a good correlation and Figure 1 shows the linear relationship between the explosive load (g/m) and the Young's Modulus (GPa).

The Young's modulus was chosen as the major parameter for this work as it is normally readily available on major construction projects in the United States. Other parameters such as tensile strength would also be of importance, however these are typically not included in most geological reports for contractors on construction projects or in mines. If the Young's modulus of the rock is not known, it can easily be found for a majority of rock types through a literature review as well and

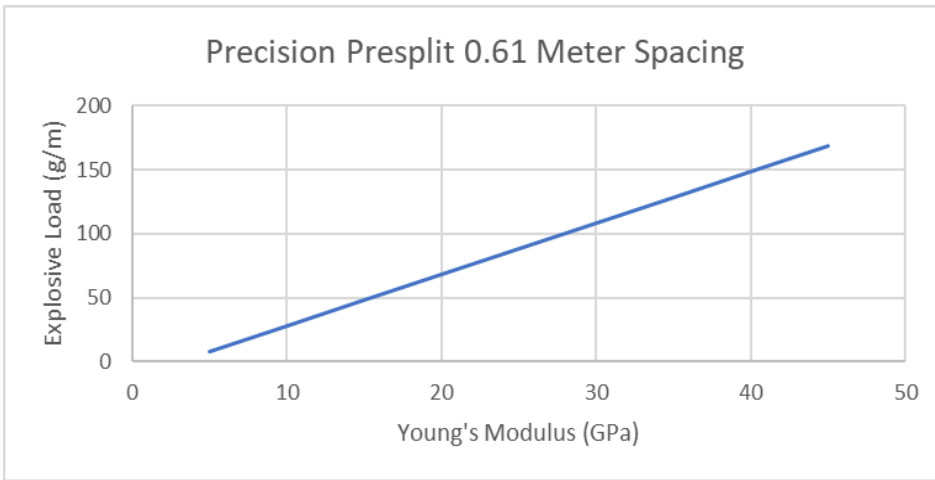

Figure 1. Explosive load to Young's modulus comparison with a 0.61 metre (2 foot) spacing between boreholes.

the Young's modulus does not vary as much as tensile strength. The equation to estimate the explosive load for a 0.61 metre spacing is shown below in Equation 1:

$$EL = 4E - 11.8 \quad (1)$$

Where: EL = Explosive Load (g/m) and E = Young's modulus (GPa)

The next step of the research was to develop a method to design the explosive load at any distance borehole spacing (Konya & Konya 2017). The first step of this was the development of a presplit factor which could be scaled using the Young's modulus of a rock. The Konya Presplit Factor was developed and is shown by Equation 2:

$$K = \left(\frac{40579}{E}\right)^{0.625} \quad (2)$$

Where: K = Konya Presplit Factor

This could then be used in Equation 3 to determine the explosive load for a rock considering any variations in spacing:

$$EL = 2{,}306{,}400 * \left(\frac{S}{K}\right)^2 \quad (3)$$

Where: S = Spacing (metres)

The chart of various rock types explosive load (g/m) versus spacing (metres) is shown in Figure 2.

4 BOREHOLE PRESSURE

The mechanism of breakage being analysed for the precision presplitting is the effect of gas pressurisation of the borehole generating hoop stress fields between boreholes leading to fracture formation. This relies on the proper pressurisation on the borehole and an accurate determination of the inter-borehole pressure. The authors have relied upon stemming studies utilising borehole simulation equipment which could accurately measure the inter-borehole pressure from decoupled charges (Otuonye 1981). The table of pressures has been recreated in Table 1. This pressure data was developed using decoupled PETN charges which were highly decoupled. In addition, this data includes holes that where stemmed and all stemming was retained and holes which had the stemming ejected at some point during the detonation.

The authors have utilised this data to create Equation 4, which can be used to estimate the pressure in a borehole (GPa) based on the explosive load (g/m). This equation has a R^2 value for the data of 0.9696 showing excellent fit even with various stemming ejection conditions. This equation is specifically applicable as a basic equation for precision presplitting and has not been evaluated in various other applications. The authors do not recommend using this as an all-encompassing borehole pressure equation for other charge configurations and methods of

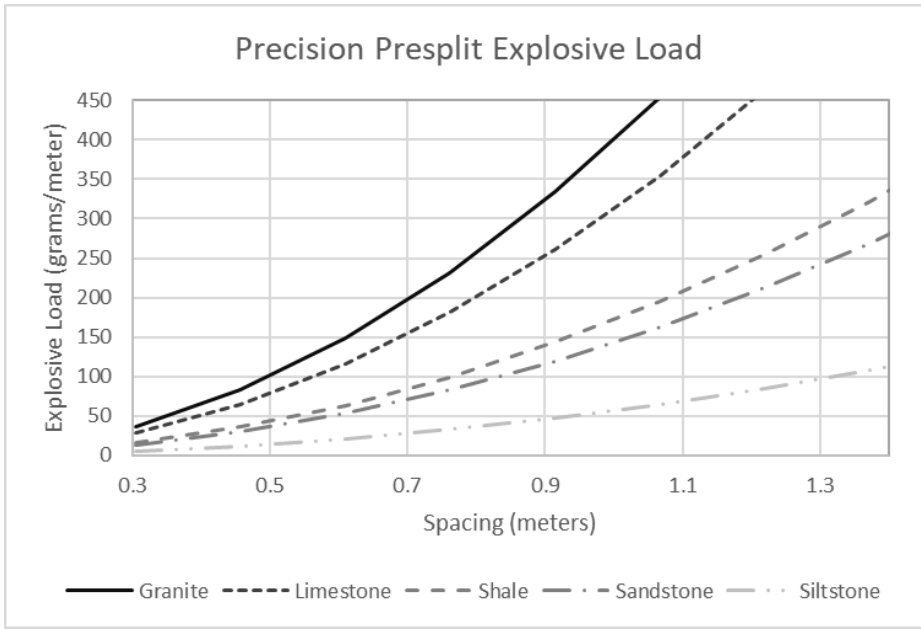

Figure 2. Explosive load variations based on spacing for multiple rock types.

blasting as this equation is based on extreme decoupling with PETN charges and would be unrepresentative of other situations.

Table 1. Recreation of borehole pressure based on charge weight (Otuonye 1981).

Weight of Charge (Grams)	Pressure (PSI)	Weight of Charge (Grams)	Pressure (PSI)
10	9,000	30	27,000
10	11,000	30	28,000
10	10,000	30	27,000
10	10,000	30	26,000
20	19,500	30	27,000
20	17,000	30	25,000
20	18,000	30	30,000
20	15,000	40	37,000
20	19,500	40	37,000
20	19,500	40	36,000
20	19,500	50	50,000
20	13,500	50	51,000

$$P = 0.0009EL - 0.0095 \quad (4)$$

Where: P = Borehole Pressure (GPa)

This equation 4 will then be utilised in accordance with Equation 3 to develop an equation determining the total pressure required for fracturing of various rock types. This will result in Equation 5, which can be utilised to determine the borehole pressure required for a presplit to form based on the spacing of the presplit boreholes.

$$P = 2075\left(\frac{S}{K}\right)^2 \quad (5)$$

Where: P = Pressure (GPa); S = Spacing (m); K = Konya Presplit Factor

This equation has then been used to develop Figure 3 which shows the inter-borehole pressure required to cause a presplit to form in various rock types.

This model gives engineers the ability to change numerous parameters in a presplit blast, such as the stemming length and stemming type in accordance with the retention and ejection borehole pressure models; the explosive type; the decoupling ratio; the loading parameters; etc. in order to obtain proper borehole pressures for fractures to form. This can be considered a low

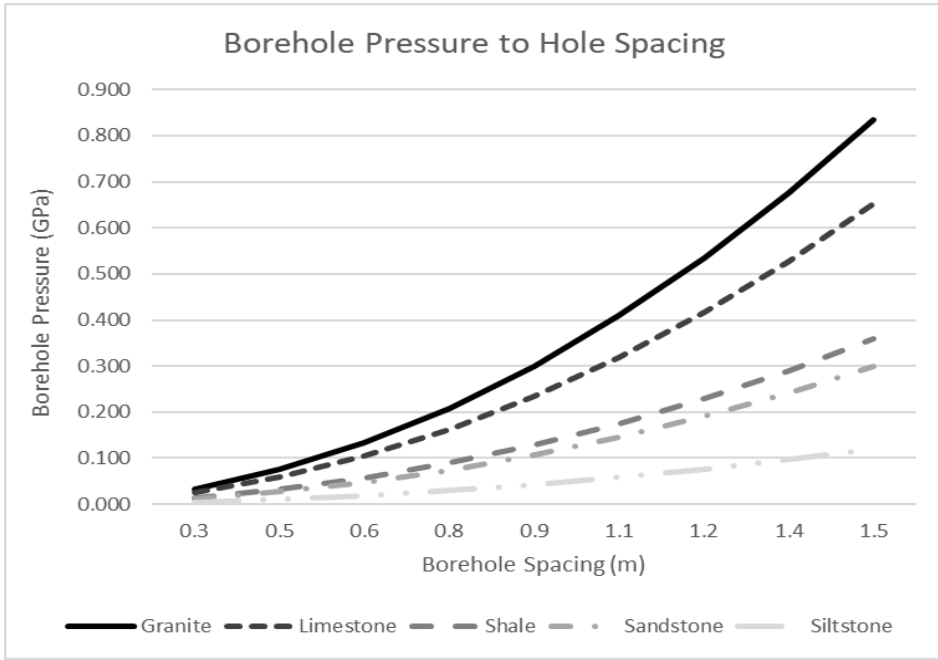

Figure 3. Borehole spacing to borehole pressure based on Equation 5 for various rock types.

level of required pressure to obtain fracture which is slightly above the minimum. The model does slightly overestimate the pressure required for a presplit at close spacings, especially for weak rock, and it is advised that this be utilised for spacings above 0.61 metrE (2 feet).

The authors are currently conducting research using a borehole simulation pressure cannon to further develop the pressure to presplit relationship, particularly at close spacings for weak rock types.

5 CONCLUSION

In this paper a model has been presented to determine a low-level required borehole pressure to cause a fracture to form from a presplit blast. This was completed using previous research projects the authors had completed using empirical data to define explosive loading versus Young' modulus and spacing equations along with research completed collecting data on borehole pressure from extremely decoupled PETN charges in a borehole simulation device.

This indicated that two main parameters are important to determine the pressure required in a presplit; the rock type and the spacing that is between boreholes. The rock type is characterised by the Konya Presplit Factor, which is based on the rock's Young's modulus. Equation 5 can then be utilised to obtain a low-level inter-borehole pressure required for a presplit to form. This can then be utilised by engineers with other inter-borehole pressure models to develop presplit blasts in various rock and hole alignment conditions.

REFERENCES

Akhavan, J. 2011. *The Chemistry of Explosives*. Cambridge: RSC Publishing.

Cook, M.A. 1974. *The Science of Industrial Explosives*. Salt Lake City: IRECO Chemicals.

Cooper, P. 1996. *Explosive Engineering*. New York, New York: VCH Publishers Inc.

Crosby, W. & Bauer, A. 1982. Wall control blasting in open pits. *Mining Engineering*, 34(2), 155-158.

Daehnke, A., Rossmanith, H. & Kouzniak, N. 1996). Dynamic fracture propagation due to blast induced high pressure gas loading. *2nd North American Rock Mechanics Symposium*.

Day, P. 1982. Controlled blasting to minimise overbreak with big boreholes underground. *Proceedings of the Eighth Conference on Explosives and Blasting Technique*, 264-274.

DuPont 1975. *DuPont Blasters Handbook*. DuPont.

International Society of Explosive Engineers 2016. *Blasters Handbook 18th Edition*. International Society of Explosive Engineers.

Konya, A.J. & Konya, C.J. 2017. Precision presplitting. *Proceedings of the Society for Mining, Metallurgy, and Exploration*.

Konya, A. & Konya, C. 2016. Precision presplitting optimisation. *Proceedings of the 42nd International Conference on Blasting and Explosive Technique*.

Konya, A. & Konya, C. 2017. Precision presplitting. *Proceedings of the Society for Mining, Metallurgy, and Exploration.*

Konya, A. & Konya, C. 2017. Precision presplitting - explosive variations with spacing. *Proceedings of the 43rd International Conference on Explosive and Blasting Technique.*

Konya, C. 1973. High speed photographic analysis of the mechanics of presplit blasting. *Proceedings of Sprengtechnick International*.

Konya, C. 1980. Pre-split blasting: theory and practice. *Preprint AIME*, 80-97.

Konya, C. 1982. Seminar on blasting to the Ohio Laborers Union. Mont Vernon, Ohio.

Konya, C. & Konya, A. 2015. Precision presplitting optimisation. *8th Drilling-Blasting Symposium*, (pp. 1-10). Istanbul, Turkey.

Konya, C., Barret, D. & Smith, J.E. 1986. Presplitting granite using Pyrodex, a propellant. *Proceedings of the Twelfth Conference on Explosive and Blasting Technique*, 159-166.

Konya, C., Britton, R. & Lukovic, S. 1987. Charge decoupling and its effect on energy release and transmission for one dynamite and water gel explosive. *Proceedings of the Thirteenth Conference on Explosives and Blasting Technique*.

Matheson, G. & Swindells, C. 1981. Seismic detection and measurement of blast disturbances. *Transport and Road Resarch Laboratoy*.

Otuonye, F. 1981. Effective blasthole stemming. *Department of Civil Engineering.* Columbus: The Ohio State University.

Paine, R., Holmes, D. & Clark, H. 1961. Presplit blasting at the Niagara power project. *The Explosives Engineer*, 72-91.

Salmi, E. & Hosseinzadch, S. 2014. A further study on the mechanisms of pre-splitting in mining engineering. *App Mech Mater*, 553, 476-481.

Spagna, S., Konya, C. & Smith, E. 2005. Utilisation of detonation cord to presplit Pennsylvanian aged sandstone and shale, Grundy, Virginia. *Proceedings of the International Conference on Explosives and Blasting Technique*.

Spathis, A. & Wheatley, M. 2016. Dynamic pressure measured in a water-filled hole adjacent to a short explosive charge detonated in rock. *Blasting and Fragmentation Journal*, 10(1), 33-42.

Tariq, S. & Worsey, P. 1996. An investigation into the effects of some aspects of jointing and single decoupled blast holes on pre-splitting and boulder blasting. *Rock Fragmentation by Blasting - Fragblast* 5, 438.

Worsey, P. 1981. Geotechnical factors affecting the application of presplit blasting to rock slopes. University of Newcastle Upon Tyne.

Worsey, P. 1984. The effect of discontinuity orientation on the success of presplit blasting. *10th Annual Society of Explosive Engineers Conference on Explosives and Blasting Technique*, 197-217.

Worsey, P. & Qu, S. 1987. Effect of joint separation and filling on presplit blasting. *13th Society of Explosive Engineers Conference on Explosives and Blasting Technique.*

Worsey, P., Farmer, I. & Matheson, G. 1981. The mechanics of presplitting in discontinuous rocks. *22nd U.S. Symposium on Rock Mechanics*, 205-210.

Zhang, Z.X. 2016. *Rock fracture and blasting theory and applications*. Elsevier Inc.

Helsinki Conference Proceedings 2019, R. Holmberg et al

Wall control blasting – design and analysis

T.N. Little
Blasting Geomechanics Pty Ltd, Australia

ABSTRACT: This paper is concerned with design and analysis of Wall Control Blasts. The introduction is used to reintroduce the blast management framework and the blast design requirements classification system previously developed by the author. The four categories of approaches to blast design are also outlined. The second section discusses wall control blasting objectives, in terms of profile control and damage control, and performance evaluation. In the third section, line drilling and four wall control blasting techniques are defined. The next section of the paper explores three wall control designs elements: Pre-split design – it is not as easy as people think; Single hole (or row) design – trial and error is too slow; and Blast pattern timing design – poor timing and firing direction can increase damage. Modified production blast design can simplify mining operations and reduce operating costs; and Slope steepening design, if it can be successfully applied, the method can increase the ore reserve and decrease waste volume. Eight conclusions have been formulated based on the current study.

1 INTRODUCTION

1.1 The blast management framework

This paper is a follow-up to the paper published in the 9th EFEE conference held in Stockholm. In that paper (Little 2017) the author showed how the recently developed blast design requirements (BDR) classification scheme could be used to improve the blast design management process, see Figure 1. In the current paper the second component, blast design and analysis, is demonstrated within a wall control blasting context.

1.2 Further development of the BDR classification scheme

The development of the BDR classification scheme began by focusing on ground control blasting (Little 2015) and was extended to all surface blasting applications (Little 2017). The BDR classification scheme was further developed to cater for underground blasting operations and the paper introduces the relatively new concept of 'value-based ore control' (Little & Lovitt 2018). In this paper the author has taken the opportunity to provide an update to the BDR classification scheme to include 'ground improvement' as a technical blasting objective. Note, the overall aim is for the BDR classification scheme to be relevant to all blasting operations in soil or rock on the surface, underground and underwater.

The BDR classification system uses four classification elements: the blast location relative to the earth's surface, the number of different grades of geological materials, the orientation of the free face relative to the blastholes, and the number and type of primary technical blasting objectives. The first three classification elements

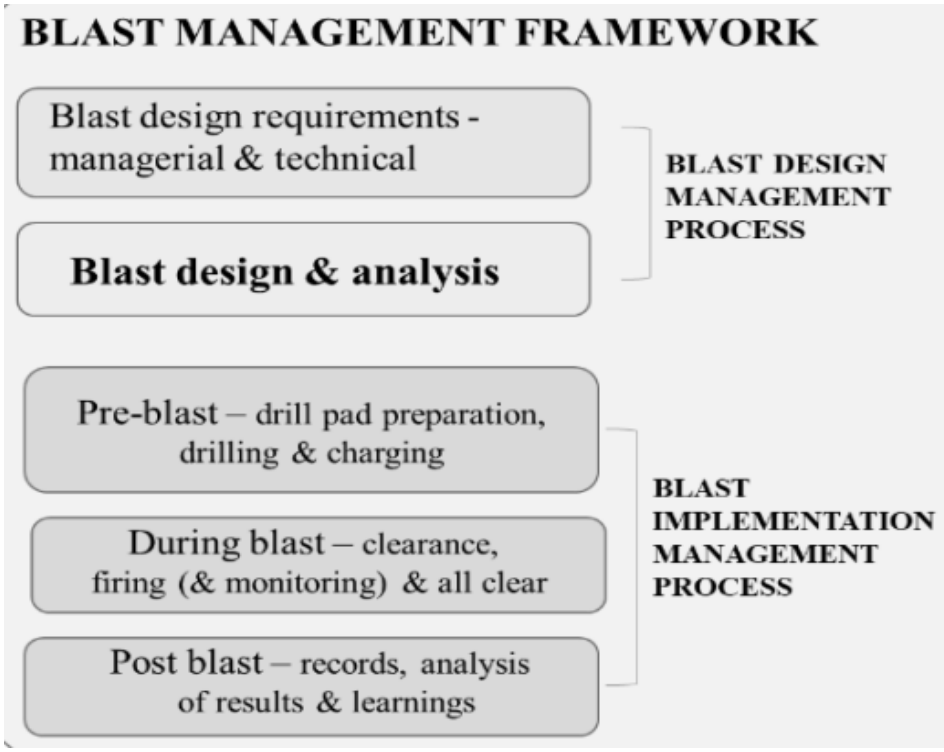

Figure 1. Blast management framework showing the component parts (Little 2017).

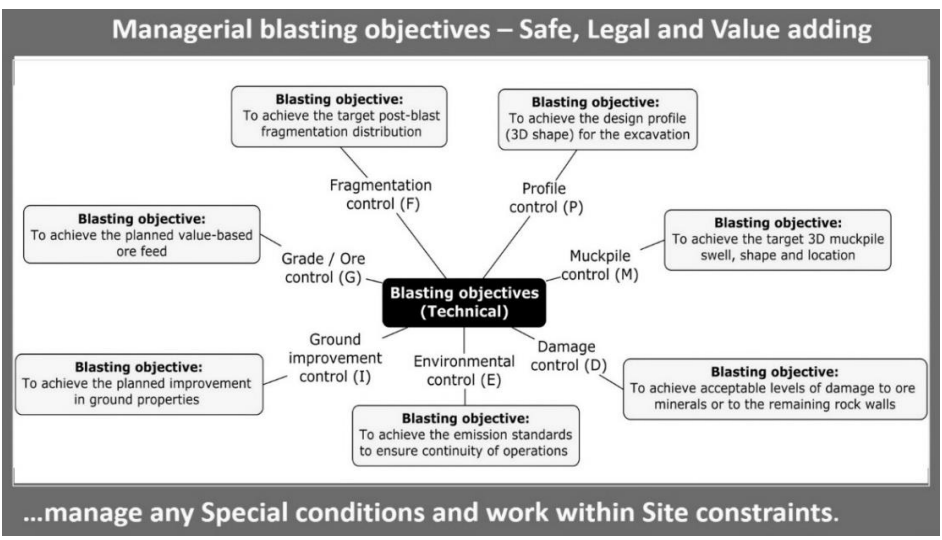

Figure 2. Technical and managerial blasting objectives (modified from Little 2017 & 2018).

Table 1. Technical blasting objectives.

Technical Blasting Objective	Interpretation in soil and rock blasting context
G Grade /Ore control	Reducing unplanned ore loss and unplanned dilution.
F Fragmentation control	Obtaining the desired fragment distribution.
D Damage control	Reducing strength of the remaining rockmass. Reducing damage to valuable minerals.
P Profile control	Reducing overbreak, underbreak and bridging.
M Muckpile control	Obtaining required muck-pile and ore flow characteristics.
E Environmental control	Reducing unwanted blasting emissions e.g. vibration, airblast, fumes, dust, flyrock, water pollution and asset damage.
I Ground Improvement control	Increase density and/or shear strength of weak geomaterial zones. Reduce stress in highly stressed rock volumes.

are objective physical properties and the fourth relates to technical blasting design objectives.

Blasting objectives have been grouped into two categories, managerial and technical, see Figure 2. The premise is that all blasts must satisfy the managerial objectives and hence have not been included in the BDR classification scheme. That is, all blasts must be safe, legal, add value, manage any special conditions and work within site constraints. Note that blast design is the fundamental engineering control to obtain consistent outputs that achieves all relevant blasting objectives.

1.3 Approaches to blast design

The four main approaches to blast design are illustrated in Figure 3.

The experiential approach may be acceptable for one-off shot-firing tasks but is not suitable for mine blasting. Benchmarking from similar sites can be a good starting position.

Trial blasting is a sound approach to blast design as feedback on the performance of the design is rapidly received (in days). It should be noted that design feedback for slope engineering can takes years to decades.

Empirical methods, such as rules of thumb or blasting indices, can be used as a first pass design or as a broad-brush audit check. A number of empirical fragmentation distribution models are

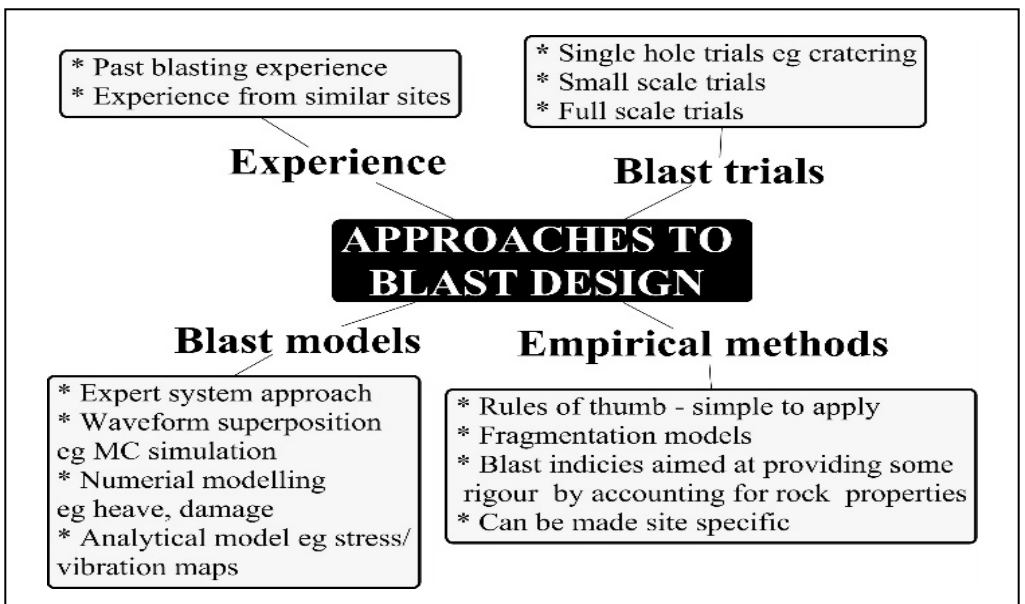

Figure 3. Approaches to blast design.

available and commonly used. Customised or site-specific blast ability indices can be developed and used successfully.

Blast model assisted design is the approach considered to be the 'state of the art' and is demonstrated in this article.

2 WALL CONTROL OBJECTIVES

2.1 Wall control blasting objectives

Wall control blasts involve both profile control and damage control blasting objectives. A BDR classification for a typical wall control blast will take the following form: S_SG_VF_PDO

Where: S – Surface blast, SG – single grade of material (i.e. ore or waste), VF – vertical or sub-vertical free face, and PDO – profile and damage control technical objectives in priority order. Note, some wall control applications may set a priority of damage ahead of profile (DPO).

2.2 Profile control blasting objectives

Figure 4 shows the range of profile control techniques. Pre-split, post-split, and line drilling (and guide hole) are not - discussed here as they are addressed in Section 3.

Fracture control aims to control the generated fracture direction and length. It can be achieved by modifying the- blasthole shape, charge shape or charge configuration. The shock wave reflecting device placed in the toe of a blasthole is a new and novel approach used in contour (profile control) blasting for dam engineering in China (Lu *et al.* 2018).

When assessing the performance of profile control technique results, a face achievement (Df) rating can be used. The assessment involves evaluating: bench face angle (50% weighting), bench width (40%) and toe position (10%). The percentage in brackets is the weighting system sometimes used. A more rigorous approach has been developed (Seery *et al.* 2007 and Juldyz 2019) called Excavation Compliance Indicator (ECI). Juldyz (2019) concluded that, every deposit has its own litho-structural characteristics and mining practices that could directly or indirectly affect design achievement. Design achievement tolerances should be applied to the bench face angle, crest and toe elements based on equipment size and operational practices; i.e. ECI tolerances and weightings should be deposit-specific.

2.3 Damage control blasting objectives

Figure 5 illustrates the main damage control blasting techniques. They work in association with profile control techniques and it is critical they do not compromise them. For example, if the trim blast takes out the pre-split line the mine is wasting money, may not achieve design and is

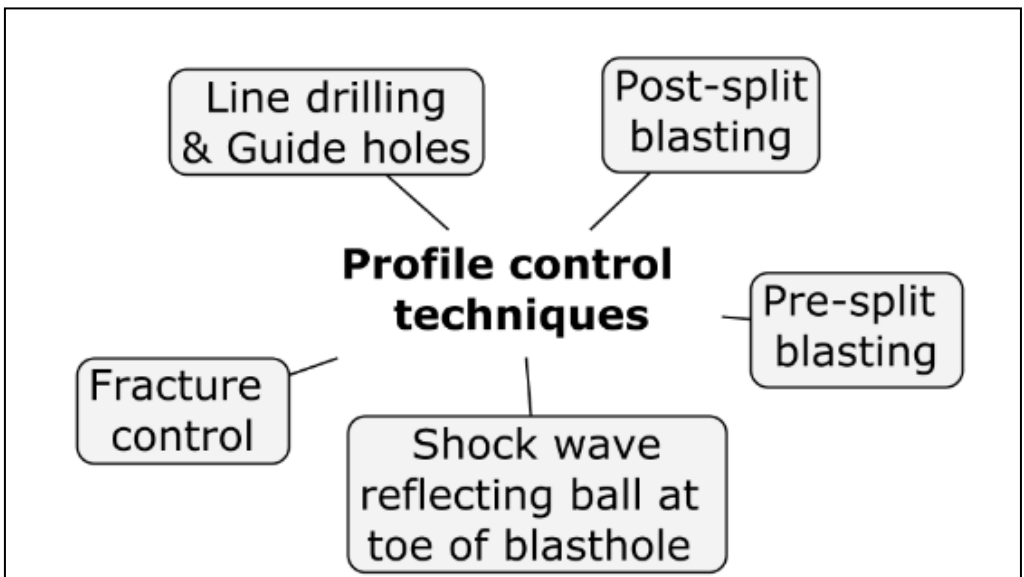

Figure 4. Profile control techniques.

Table 2. Wall control blasting techniques.

Method and illustrative cross section	Features
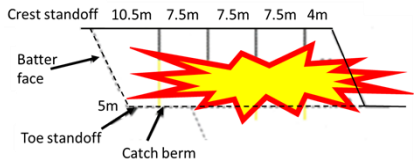 Method 1 Buffer (Stand-off) blasting	Buffer blasting can be used in weak rock masses and has the following general features: Toe standoffs is critical Blasthole diameter can be same as production holes Charge in buffer rows can be reduced Excavation equipment digs to hard BDR classification S_SG_VF_DPFO
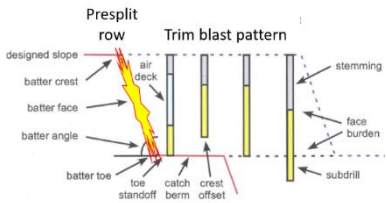 Method 2 Pre-split blasting	Pre-split or mid-split blasting works best in massive rock with tight joints and has the following general features: Smaller diameter blastholes and closely spaced Loaded with decoupled charges to reduce blasthole pressure Blastholes are fired prior (milliseconds or days) to the first hole in the adjacent pattern Unstemmed unless mine is airblast sensitive BDR classification: S_SG_VF_PDO
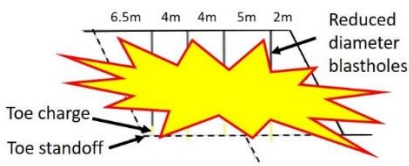 Method 3 Trim blasting	Trim blasting can be used in a wide variety of rock masses and has the following general features: Generally, uses smaller diameter blastholes and can be used with or without pre-split The balance between charge weight and standoff is critical but the balance between charge diameter and stand-off distance is even more critical Can be free faced or choked or reverse fired BDR classification: S_SG_VF_DPFO
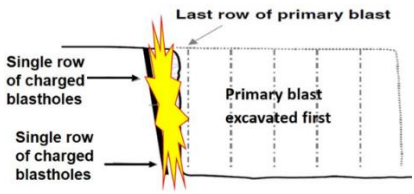 Method 4 Post-split blasting	Post-Split blasting is not often used and has the following general features: Row of closely spaced holes along the final wall Light and well distributed charges used Blastholes drilled and fired after primary blast is excavated (Dynamic post-split has also been used) Critical that damage from primary blast not to extend beyond post-split line BDR classification: S_SG_VF_PDO
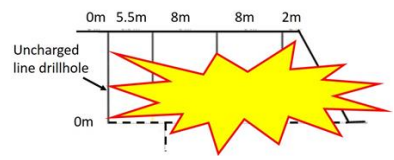 Method 5 Line drilling	Line drilling can be used in most ground and has the following general features: Line of closely spaced unloaded holes drilled along the final limit This weakened zone helps guide the excavation of the slope BDR classification: Not applicable

potentially creating a rockfall hazard. These damage control techniques are all discussed and addressed in Section 3 of this paper.

When assessing the performance of damage control a face condition (Fc) assessment can be used. It involves evaluating: percent of visible half-barrels (20%), intact rock breakage (15%), open joints (10%), loose material on the face (10%), face profile [in section] (20%), and crest condition (10%). For more detail see Walliams *et al.* (2009) and Figure 15 in this paper.

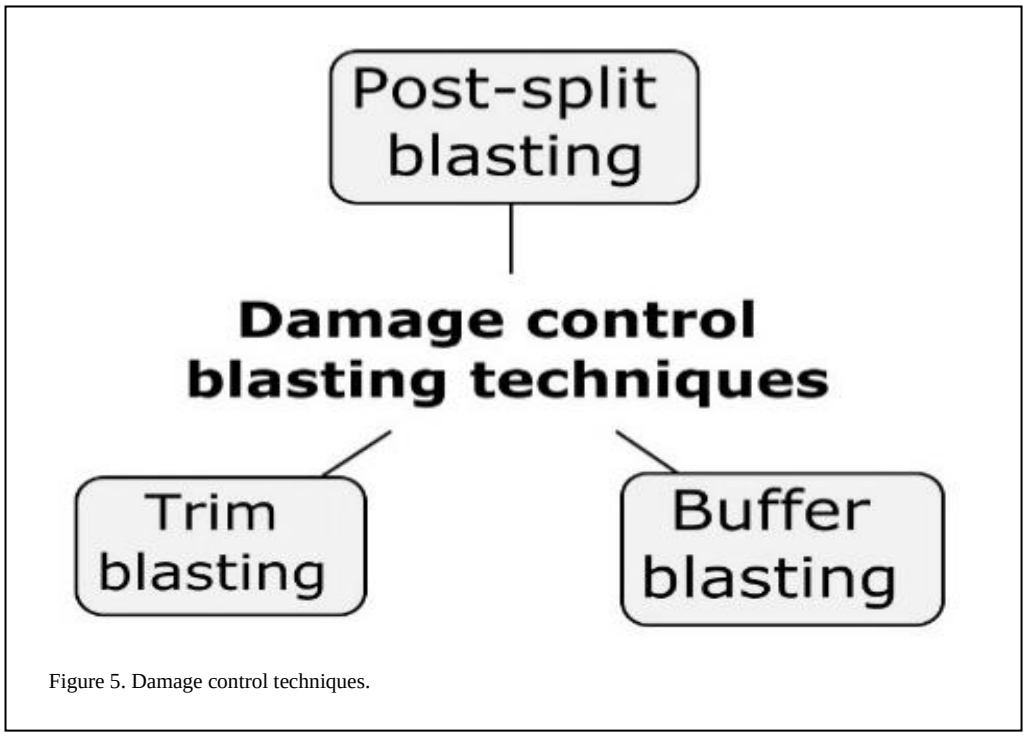

Figure 5. Damage control techniques.

3 WALL CONTROL BLASTING TECHNIQUES

Wall control blasting terms are uniform across companies, states and countries. Even the term 'wall control blasting' has many aliases, for example, limits blasting, controlled blasting, contour blasting, perimeter blasting and smooth-wall blasting. To ensure that readers are clear, the wall control blasting terms used in this paper are defined in Table 2. In short: a buffer blast uses stand-off to avoid damage and the wall is formed by the excavating equipment; a pre-split blast defines the profile and the thin damage zone attenuates vibrations; a trim blast attempts to balance the charge diameter and stand-off distance; and a post- split blast uses a single row of closely spaced holes along the final wall and shots to a free face. Line drilling is an alternative to pre-splitting and is not classified as a blasting technique.

4 WALL CONTROL BLAST DESIGN AND ANALYSIS

In this section the design features of five wall control applications are discussed. They are: pre-split design; single blasthole (or row) design; timing design; modified production blast design; and slope steepening design. In this paper the terms overbreak (crest loss, face loss etc) and underbreak (floor toe, bench toe or cling-on) are used for post blast geometric features that can be measured using surveying techniques and these provide feedback profile and damage control performance.

4.1 Pre-split design and analysis

Despite what some engineers may think the design of a pre-split blast is not a simple matter. The first decision is to decide if pre-split blasting is worthwhile at a particular mine site. Some key questions are:

– what are the objectives to be targeted? In a hard rock environment it may be to achieve the design profile, achieve acceptable damage levels and / or provide a platform for slope steepening. In a throw blasting coal environment it may be to reduce the likelihood of rockfall / slope failure hazard for mining underneath the face, provide a face that leads to faster dragline recovery during off-line key digging or chap cutting, enable a consistent front row burden in the next bench for engineering control

(Lewandowski *et al*. 1996).

- what are the benefits expected? Improved safety by lowering the probability of rockfall, improved stability by reducing rock mass damage. Blair (2015b) showed that the vibration reduction due to pre-split formation was statistically meaningful and a reduction of 40 per cent was estimated.
- what is the feasibility of a pre-split being effective? If a pre-split is considered to be a thin damage zone then it should be possible to create such a zone in most rock masses.
- do the benefits outweigh the additional costs?

Once a decision to employ a pre-split row has been made a number of design elements need to be determined. They are:

- hole diameter and spacing
- blasthole inclination and length
- timing design and firing direction
- how are tight corners to be handled?
- explosive type, configuration and coupling

Table 3 discusses pre-split design approaches.

Table 3. Pre-split design approaches

Design approach	Pre-split design comments
Experience	Can use experience from similar site as a design starting position.
Blast trials	Trial and error can be used to refine the pre-split design. Blasting trials needed to confirm design developed by all other design approaches
Empirical methods	Rule of thumb, for example spacing equals 8-13 hole diameters. Empirical equations two dimensional static theory only valid for static loads.
Blast models	MC waveform superposition - See Fig 7 for an example output. ELFEN/ MBM/ SoH modelling – See Fig 8 for an example output. HSBM / SMB modelling – See Fig 9 for an example output.

Figure 6 illustrates the results obtained for a 100-hole pre-split line (2 m spacing) predicted from a waveform superposition model. Initiation point at northern-most hole. Note, VPPV is on a log scale. The pre-split on the left was fired with detonating cord and on the right groups of 5 holes with 17 ms delays were modelled.

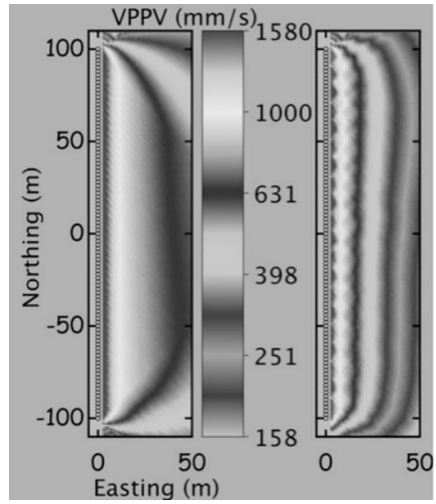

Figure 6. Monte Carlo waveform superposition modelling used to determine vibration radiation patterns (source: Blair & Little 2019).

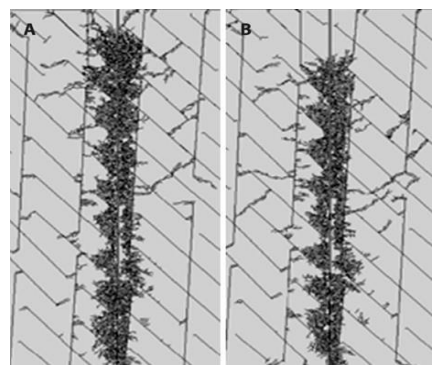

Figure 7. Damage patterns along pre-split blasthole from MBM model (A) 2 m collar, (B) 4 m collar (source: Battison *et al.* 2015).

A HSBM model was set up to reproduce the pre-split blast design. Illustrated in Figure 8 are the results when the hole

diameter (D) is 100 mm and the charge diameter (d) is 45 mm, leading to a decoupling ratio (D^2/d^2) of 5.

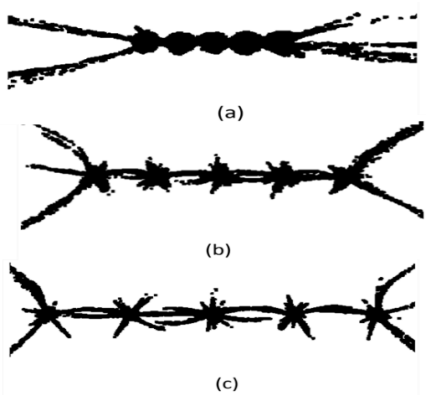

Figure 8. Modelled pre-splits (a) 0.8 m, (b) 1.5 m and (c) 2.0 m.

The results (Etchells *et al.* 2013) of studies shown in Figure 8-a indicate that the spacing of 0.8 m is too close and results in localised damage. Expanding the spacing to 1.5 m (Figure 8-b) leads to less damage at the central holes and straighter cracks in between the holes. The damage at the ends extends at a much more oblique angle into the face. If the spacing is expanded further to 2 m (Figure 8-c) there tends to be excessive bowing of the fractures between the holes.

Table 4. Single hole (row) design approaches.

Design approach	Single hole (row) design comments
Experience	Can use experience from similar site as a design starting position.
Blast trials	Trial and refinement can be used but is tedious. Blasting trials needed to confirm designs developed by all other design approaches.
Empirical methods	Rule of thumbs for burden and spacing can be used. Approaches based on charge weight scaling
Blast models	Analytical Damage Model (ADM). See Figures 11 and 12. Heelan solution coupled with charge weight scaling. (Blair & Minchinton 2006, Blair 2015b, Couceiro *et al.* 2018)

4.2 Single hole (row) impacts

Wall control blasts need to be designed so that each blasthole (or row) does not unduly damage the wall behind the design limit or if pre-splits are developed the blast does not take them out.

This is especially critical for row of holes closest to the wall, but is also important for the buffer rows and the first production row of blastholes. At many mine sites, the charge weight/standoff-distance is set by an extensive trial and refinement process. Marklund *et al.* (2007) discussed such an approach used at Aitik Mine in Sweden. Figure 9 illustrates the predicted damage zones for a number of different charge diameters. The figure also illustrates the dimensions of damage types for strong and weak rock.

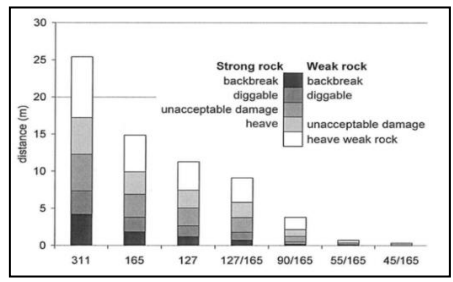

Figure 9. Bar chart of charge diameter and damage dimensions for the Aitik Mine.

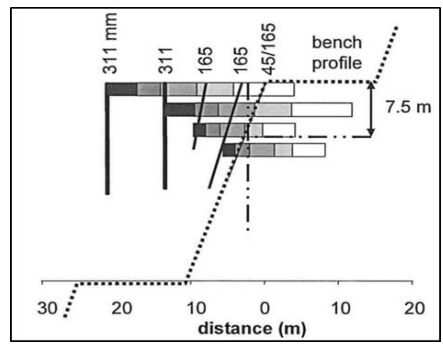

Figure 10. Damage prediction applied to a wall control blast design (Marklund *et al.* 2007).

An alternative dynamic stress approach was developed and reported by Blair 2015a. That work describes the development of an Analytical Damage Model (ADM) based on an exact solution under the assumption of viscoelastic material. The model takes full account of: the rock mass elastic/viscoelastic properties, the explosive type, the geometry, and primer location. The output is a prediction of dynamic stress for direct comparison with the unconfined compressive strength of the local rock mass. Figure 11 illustrates a detailed dynamic stress radiation from a single blasthole.

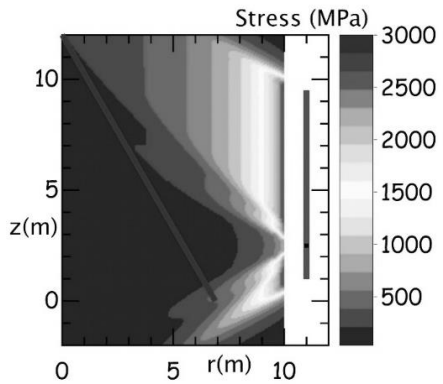

Figure 11. Dynamic stress radiation from a single blasthole (source: Blair & Little 2019).

According to the ADM, for a sufficient length of charge column in a given surrounding rock mass, the only way to alter the damage standoff distance is to: alter the diameter of the charge column; alter the explosive type; or use a pre-split or any combination of these design elements.

The ADM modelling can be used to determine:

- toe and collar standoffs for batter, buffer and production blasthole (rows)
- standoff distance charts for blast design
- burden and spacing distances
- investigate air decking effects
- appropriate primer location(s) to direct dynamic stress radiation patterns
- angled blasthole radiation patterns.

4.3 Timing design

When the charge weight/distance configuration has been determined for each blasthole (row) using the ADM, the next step is to determine the behaviour of a delayed sequence of such

Table 5. Timing design approaches.

Design approach	Timing design comments
Experience	Can use experience from similar site as a design starting position.
Blast trials	Trial and refinement can be used for timing but is tedious. Blasting trials needed to confirm designs developed by all other design approaches.
Empirical methods	Rule of thumbs for timing generally focus on fragmentation and muckpiles, so are of limited use for wall control blasting.
Blast models	MC waveform superposition - See Fig 15 for an example output at a single monitoring point.

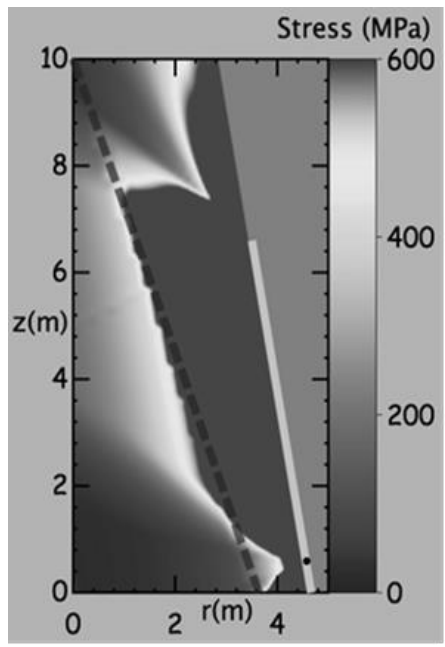

Figure 12. Radiation of peak dynamic stress from a batter blasthole with pre-split in place.
This predicts reduced damage at the wall line and beyond.

blastholes. The delay sequence introduces two main influences: waveform superposition and vibration screening.

Waveform superposition: Superposition occurs if multiple blastholes fire relatively close in time such that their extended vibration waveforms overlap. It should be appreciated that superposition allows both constructive and destructive interference of waveforms, i.e. superposition can produce either large peak levels or small peak levels (even smaller than peaks from individual blastholes). In a statistical sense, however, the outcome of superposition is biased towards an increase of peak levels simply because there is a high probability that reinforcement will occur at least somewhere along the extended waveforms. This simple addition of waveforms from each blasthole is the basis of all waveform superposition model.

In order to minimise the potential for timing design of a blast pattern to cause damage, the Monte Carlo waveform superposition model (MCWSM) can be used to determine the most appropriate delay sequence. The MCWSM takes a measured waveform from a single (seed) blasthole and uses this, as well as other information, to construct a model for a delayed sequence of such measured seeds. One timing design is given in Figure 13. The results of modelling for three different firing patterns are presented in Figure 14 and they show a 40 percent reduction from 50 mm/s to 30 mm/s.

Three improvements to the MCWSM were reported by Blair (2012). The improvements are:

- an improved method for adding random fluctuations to seed waveforms
- the development of a seed waveform that continually varies with distance
- the ability to account for 3D distances

The MCWSM can also be used to:

- compare the vibration maps from trim blast and modified production blast
- model the appropriate delay sequence and spatial layout of blasthole
- produce a VPPV map within in around the pattern

Vibration screening: Vibration screening occurs when any initiating blasthole has its travel path to the wall disrupted by damaged ground from previously fired holes. This disruption will reduce the wall impact due to the initiating blasthole. Blair (2015b) concluded that vibration screening is real, measurable and has a significant influence on

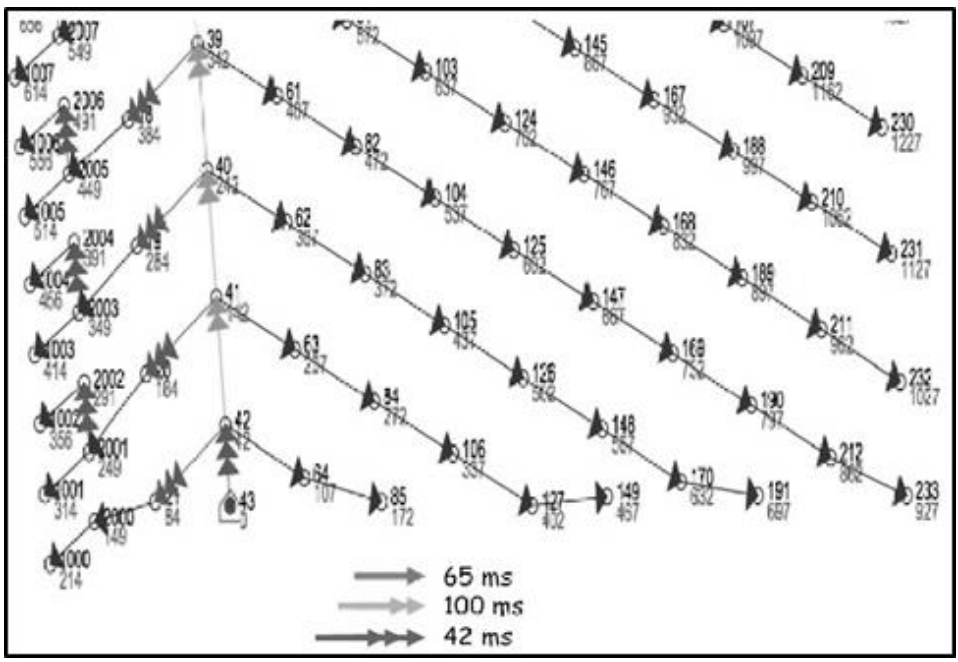

Figure 13. Tie-in design for the preferred firing pattern (100 ms x 65 ms).

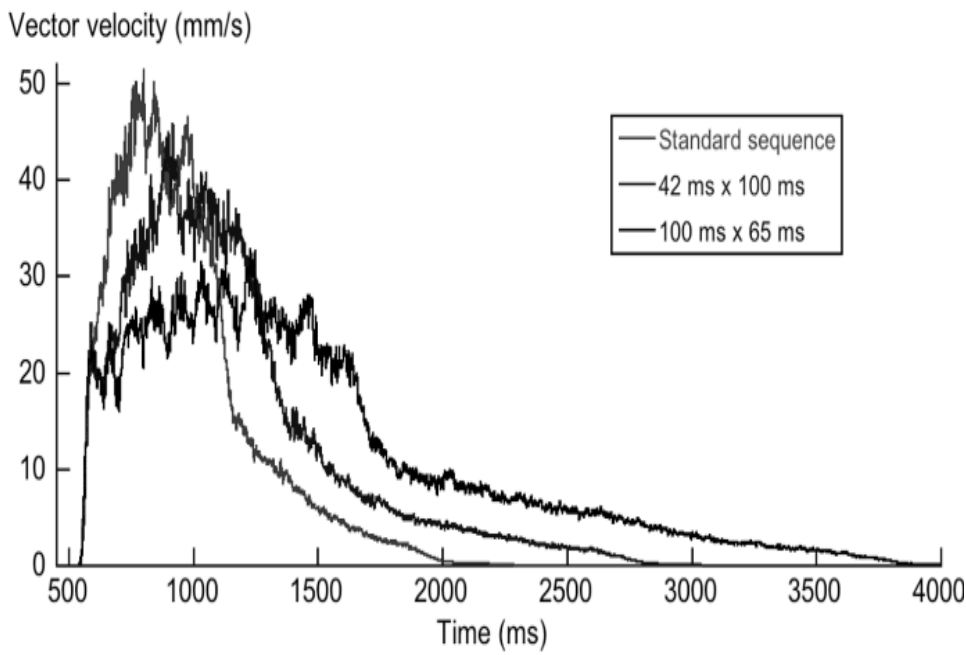

Figure 14. Model predictions for averaged vector velocity waveforms at particular monitoring location.

blast vibration. It is thus worthwhile considering this phenomenon as a tool to reduce vibration impact to a pit wall. To that end reverse firing is discussed in the Section 5.2.

5 WALL CONTROL BLAST APPLICATION

5.1 Wall control blast applications

The author has identified four main application areas for wall control blasting. From a risk continuum perspective (Blair & Little 2019) the first application is 'hazard reduction' and can be termed 'elimination of blast induced wall failure'. This will necessarily involve obtaining a good understanding of the geometry, geology and major structures to identify vulnerable locations. Also critical is an investment in slope monitoring equipment and an analysis capability to provide feedback to blasting operations.

The second application involves 'variation management' and can be termed 'wall design

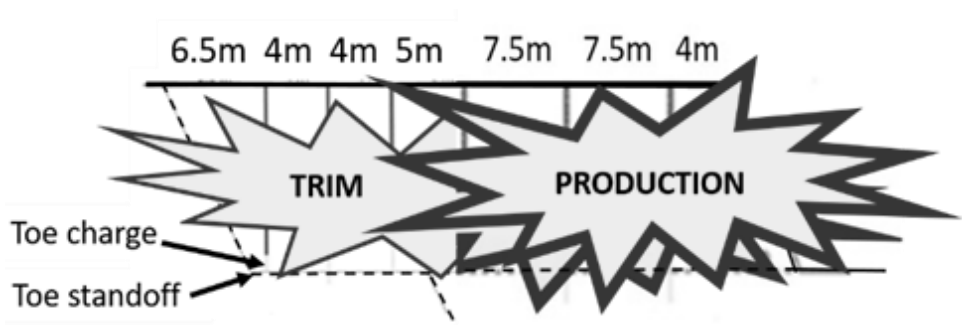

Figure 15. Wall control blasting evaluation chart.

achievement'. In addition to the requirements outlined in the first application a design achievement programme requires a higher level of quality assurance and quality control (QA/QC) and wall performance evaluation.

Figure 15 shows an overview of one such evaluation system (Williams *et al.* 2009).

The third application also involves a 'variation management' option that involves undertaking a hybrid 'modified production blast'. Section 5.2 is dedicated to discussing the design and analysis of such a blasting strategy.

The fourth application is an 'opportunity seeking' option termed 'wall or slope steepening' and is discussed in Section 5.3.

5.2 Modified Production Blasting

In this paper a modified production blast (MPB) is taken to be a hybrid made up of a trim blast close to a final wall and a production blast further away from the wall region. Such a blast would have a BDR classification: S_SG_VF_DPGFMO. This requires a complex multi-objective blast design which can only be achieved as the first two priority objects (damage and profile control) are required near the wall and the next three objectives (grade, fragmentation and muckpile control) are relevant to the production blast region away from the walls. When designing MPBs it is important to understand reverse firing, this will be discussed later in this sub-section. Figure 16 illustrates the hybrid nature of a modified production blast.

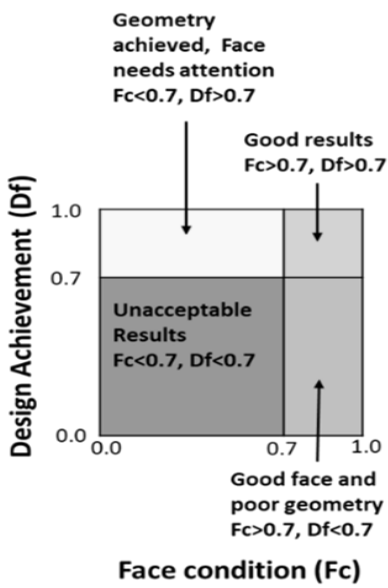

Figure 16. Modified production blast.

Features of the MPB are:

- trim and production blast fired together
- can be fired with or without pre-split
- trim section fired first as shield blast
- production section can be fired first
- can have trim sections on two or more sides (wall to wall blasting)

Figure 17 illustrates a very large (10.7 Mt) modified production blast. This blast employed multi-point initiation fired around the perimeter of the pit and the central production blast was then fired. This design aimed to reduce the vibrations impact (protect the wall) from the production holes by screening by the damage zone created by the perimeter trim blasts.

Reserve firing: This involves firing the blastholes closest to the wall first. These holes then provide a damage zone that screens the vibration from the next-closest row, which, in turn, provides a damage zone for the third-fired row and so on. Thus, previous rows shield the wall from subsequent rows.

The reverse firing dilemma: Reverse firing is a dilemma for mine operators. It has the potential to reduce vibration impact to a pit wall but, if implemented poorly, it has the potential to impart significant vibration to the wall, especially from the closest row because it is fired in undamaged ground. A correct implementation can only be obtained by balancing the influences of vibration (or stress) impact and screening. Thus, there is a trade-off to be considered when reverse firing. Holes firing in a row close to the wall will need to be undercharged to avoid wall damage. However, if they have too little charge, then the ground damage they create is negligible. In this case, their screening influence for subsequent rows is also negligible and the advantage of reverse firing is lost. Furthermore, this would result in poor fragmentation close to the wall.

A variant of reverse firing: This involve initiating the blast in the third row from the wall. This reduces the impact of the holes in the row close to the wall because they are firing in ground that now has some global damage due to the previously fired third and second rows. The fourth and all subsequent rows have a significant damage zone between themselves and the wall, and combined with increasing distances, have little potential for wall damage. This variant version of reverse firing (initiation point two or three rows off the wall) was successfully used between 1998

Figure 17. Shot W22A 203 fired on 20/02/2017 (from https://www.miningreview.com.au).

and 2010 at a large open pit mine in Western Australia.

Some purported benefits of an MPB are:

- increase in pattern size possible (up to 5 times)
- reduce number of blasting days (up to a half)
- decrease movements of digging units
- decreased reliance on auxiliary machines for pattern preparations
- increase in drilling and charging productivity due to less moving of machines and work areas
- truck / shovel productivity increased

Some checks that need to be made for MPB:

- check that the trim section is carefully designed and monitored to ensure no additional adverse impact on the walls compared with a dedicated trim blast
- check that the production section is carefully designed and monitored to ensure no adverse impacts on value-based ore control

5.3 Slope steepening – design and analysis

Slope steepening as an application of wall control blasting is an opportunity available to some mining operations. The most common method of slope steepening and is mainly done by stacking two or three benches together and reducing the overall berm width and increasing the inter-ramp angles. Such an approach requires a strategic decision to be made and this decision would be based on an evaluation that steeper slopes will result in significant economic benefit, and that the organisation has the capacity to achieve a steeper slope in a safe manner. Figure 18 illustrates the pit and bench stack terminology useful when describing a slope steepening programme.

Prior to embarking on a slope steepening programme the technical teams involved should be able to demonstrate that they have achieved the existing design consistently over an extended period of time. Also, that the teams have built up reliable geological and structural databases, have developed robust standards of QA/QC and have invested in slope monitoring and damage assessment technology.

Three examples are given in this sub-section. The first example illustrates that each bench in a double or triple bench stack can have different operational targets. The second example illustrates that wall control blasting involves an ongoing extensive programme of trials and refinements over a long period of time and can be described as a journey. Lessons learnt over that journey are also presented. The third example was chosen to illustrate the significant benefits that a wall steepening programme can deliver.

5.3.1 First example linking blasting objective and operational targets

The first case example is from Mexico and based on the work of Cebrian *et al. (*2018). This recently published study was selected to illustrate that the design of a wall control should be directly linked to the blasting objective and operational targets, Figure 19 clearly indicate this concept.

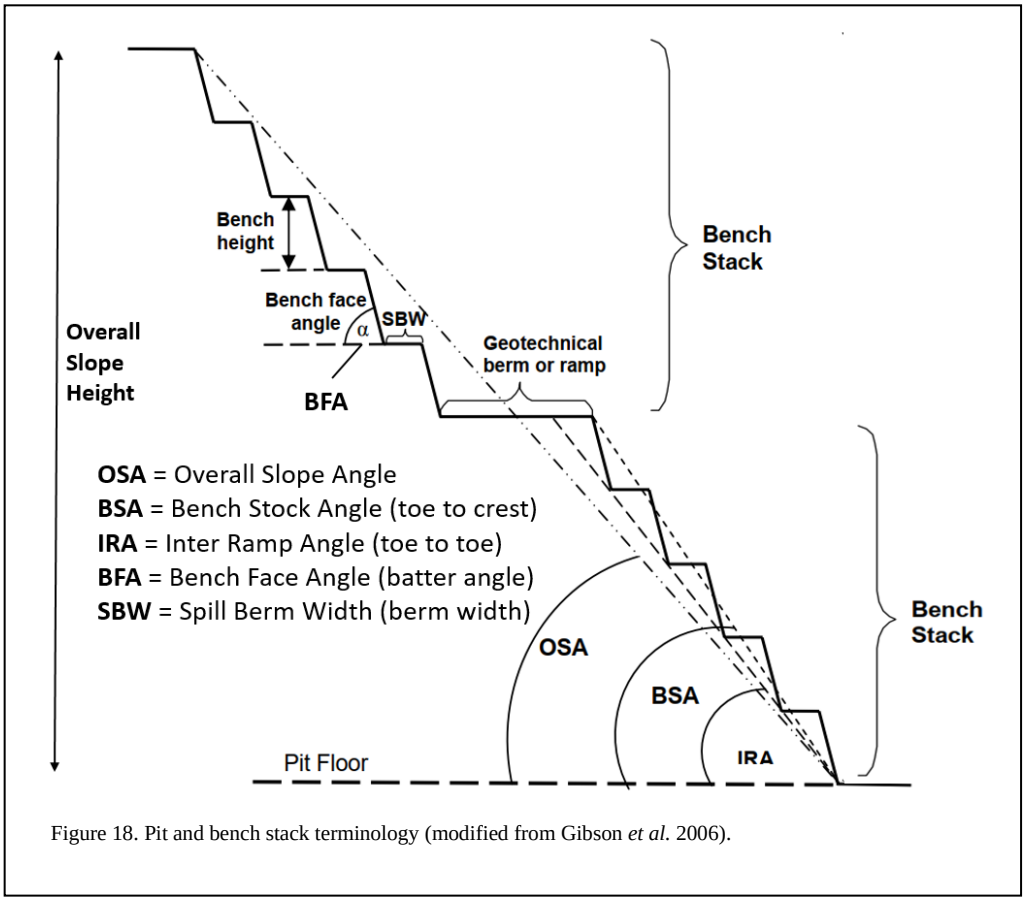

Figure 18. Pit and bench stack terminology (modified from Gibson *et al.* 2006).

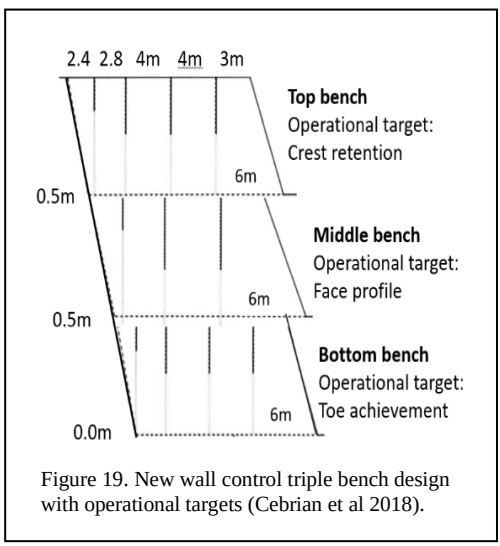

Figure 19. New wall control triple bench design with operational targets (Cebrian et al 2018).

The main features of the wall control blast design illustrated here are:

- inclined full triple bench pre-split blast
- decrease of energy of first buffer row using air decks to avoid damage in crests
- decrease burden of first buffer row
- decrease the offset of first buffer row and eliminate the offset of buffer row in bottom blast to achieve the toe
- sub-drill eliminated at bottom blast to avoid damage in future crest or berm
- rows limited to four or less

5.3.2 Second example learning from design considerations

The second example is from the Newmont Boddington mine in Western Australia (Graff *et al.* 2016). The discussion focuses on design considerations and then on what has been learnt. The wall control blasting techniques developed at Boddington involve an ongoing extensive programme of trials and refinements over a long period of time and is described as a journey.

The design journey:

- 2005 feasibility study recommended triple stacked 12 m benches with 85 degree batters and 12 m catch berms, IRA = 64^0
- 2008 initial wall control programmes focussed on development of an effective pre-split
- 2010 a changed configuration using a double bench of 24 m, 90 degree batter and 14.5 m berms, IRA= 59^0
- 2012 a changed to a double bench of 24 m, with 70^0 batter for the top bench, followed by a 90^0 bottom bench, berm width was reduced to 8.3 m to maintain an IRA=59^0
- 2013 a changed to a triple bench of 36 m, with 70^0 batter for the top bench, followed by a 90^0 bottom two benches. berm width was increased to 15.2 m to maintain an IRA=59^0
- 2015 reductions in crest loss and improved batter conditions have enabled wall-steepening trials to commence in late 2015

The utilisation of free faced trim blasts was the single largest change to be implemented in wall control at Boddington. The concept for free faced trim blasts is shown in Figure 20 along with other key aspects of the drill design.

The lessons learnt from the Boddington programme are now:

5.3.2.1 Cross-functionality

Cross functionality:

- build a strong multi-disciplinary team that work well together, are open to change, and have the ability to share knowledge, learn, and innovate
- conduct weekly pit inspection by a key group of drill & blast engineers and geotechnical engineers to critically evaluate wall control drilling and blasting results, identify areas of concern, and recommend refinements to designs

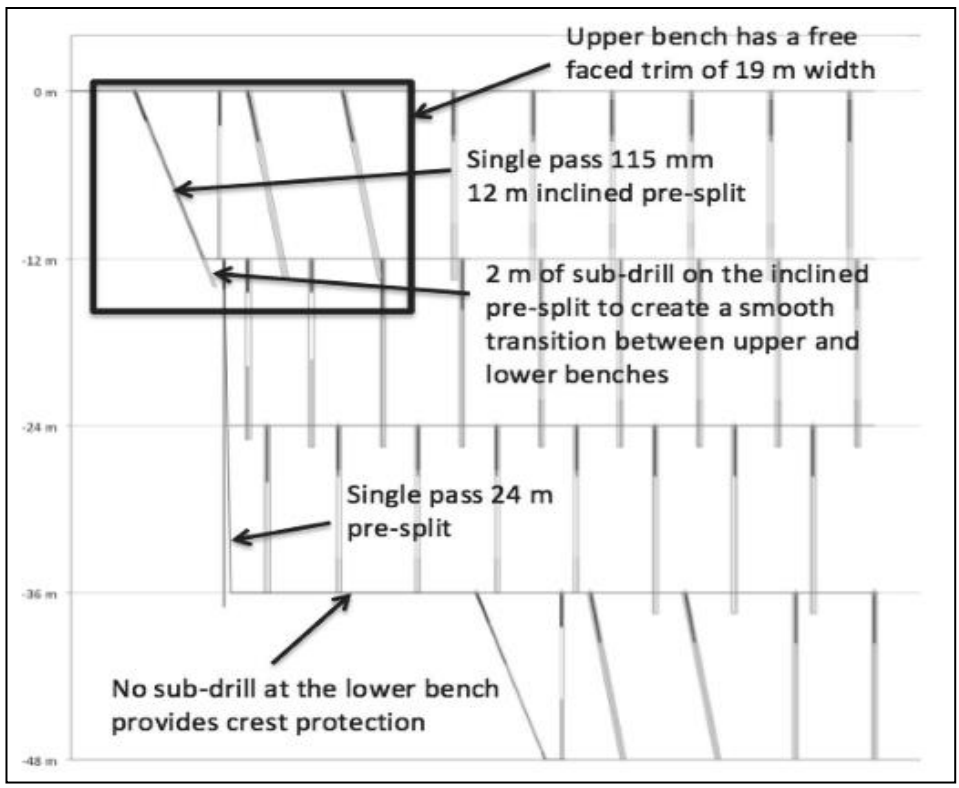

Figure 20. Section view showing key aspects of the drill design (Graff *et al.* 2016).

5.3.2.2 Overarching strategy

Overarching strategy:

- a strategy and procedure driven approach to wall control refinement (development, implementation, monitoring, evaluation, and refinement) is required, and all changes documented
- sound walls in difficult ground conditions requires a carefully chosen set of parameters all working well together
- implicit in the strategy is the commitment to continuous improvement, and ongoing internal and external peer review of the operating considerations, this process may take a number of years to complete

5.3.2.3 Embracing change

Embracing change:

- Efforts to move away from this accepted method, equipment, and parameters took time, involved careful stakeholder engagement and a commitment to innovate.
- Design is an iterative process. As part of this process it is important not to over-complicate, be able to acknowledge when something is not working, have review and stop points, and

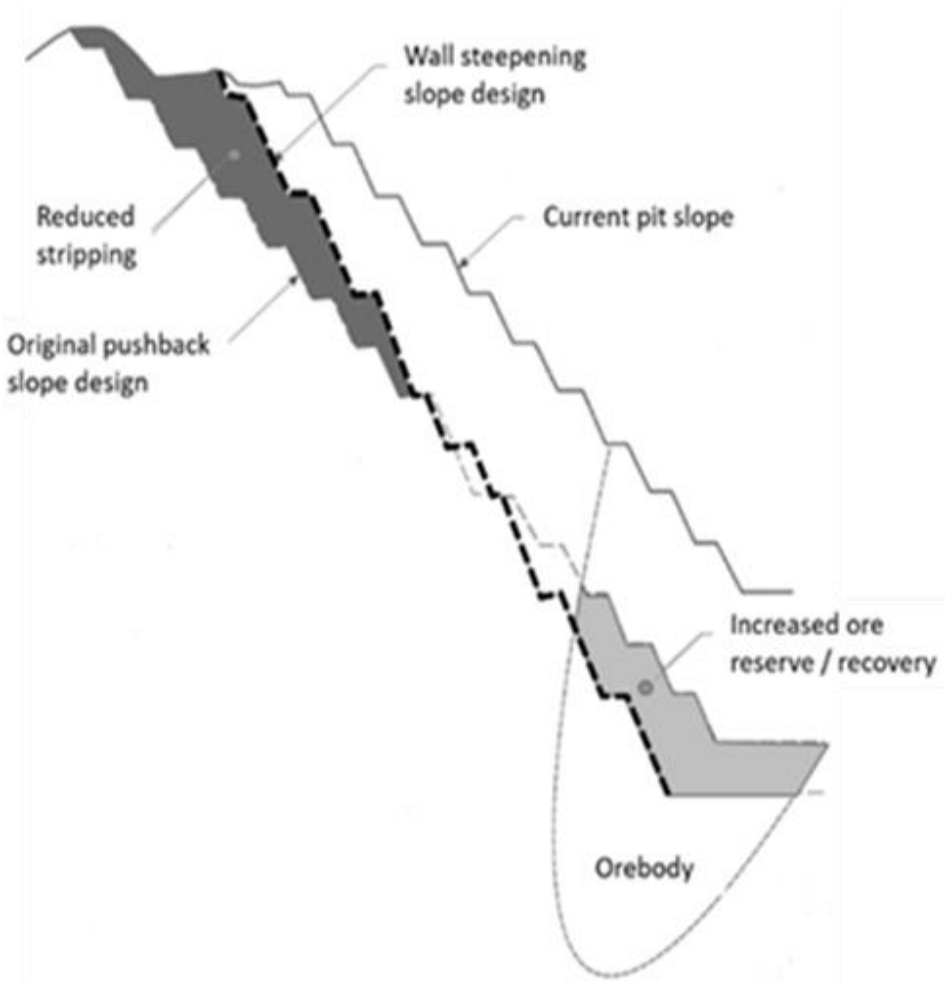

Figure 21. Generic sloped steepening application showing potential benefits (after Williams *et al.* 2009).

understand when to go ‘back to basics’. Persistence, resilience, and an openness to change is required.

A fundamental aspect of any steepening trial is whether the steeper configuration can reliably provide the required rockfall protection. An incremental approach to wall-steepening has been adopted, the initial trial is a 60.8 degree inter-ramp angle (Graf *et al.* 2006).

5.3.3 Third example slope optimisation

The third example involves a slope optimisation study to safely steepen the western wall of the Golden Pike cutback at Kalgoorlie Consolidated Gold Mines (KCGM) Fimiston Pit in Western Australia (Bungard *et al.* 2016). The purpose of including this example is to highlight the potential benefits of a wall steepening programme. Figure 22 illustrates some potential generic benefit of a slope steepening programme. The main economic benefits are reduced waste volumes and increased ore reserve. From a sustainability perspective such benefits can lead to improved resource utilisation. The optimised slope design exceeds 700 m in height, with a maximum overall slope angle of 52°, putting it near the limit of global experience.

Table 6. West wall slope design parameters by rock type, (Bungard *et al.* 2016).

Domain rock type	Bench face angle (°)	Bench height (m)	Bench width (m)	Inter-ramp angle (°)
Weathered / oxide	50	20 (2×10)	10	37
Golden Mile Dolerite	75 @ 10 m 1m step-in 90 @ 20 m	30 (3×10)	11.5	63
Paringa Basalt	75	30 (3×10)	10	59
Black Flag Beds	75	30 (3×10)	10	59

To build a case for a steeper slope design, KCGM undertook a campaign of data collection and analysis-which culminated in the successful completion of batter steepening trials within selected geotechnical domains. The optimised design incorporates a 75/90° bi-angle batter face, to achieve steeper inter-ramp slopes while maintaining sufficient safety berm catch capacity.

The steepened slope design parameters that are being implemented are summarised in Table 6. The steepened batter design incorporates an 11.5 m berm producing a 63° inter-ramp slope angle. These design parameters will be implemented up to a maximum inter-ramp height of 300 m, in line with previous experience at Fimiston.

KCGM claim the opportunity of the updated ‘life-of-mine’ design pit shell steepens the west wall to a maximum overall slope angle of 52^{o} and deepens the pit by 50 m to 720 m. Also, the new pit design based on these parameters adds approximately 630,000 ounces to mine reserves and approximately 12 months to the mine schedule. On the downside for each 30 m batter stack mined to the steeper configuration, there has been an increase in cable bolt meterage of 15–20% compared to base case levels on the Golden Pike west wall. Bungard *et al.* (2016) stated that the significant issue of pre-split downhole deviation leading to toe flare was overcome by the drilling of vertical holes and improved drill implementation. The wall steepening project would not have been successful without having overcome this issue.

6 CONCLUSIONS

Based on the current study the author draws the following eight conclusions.

A blast management framework developed by the author has been used to put wall control blast design and analysis into context. The framework is simple and generic and its use by others is encouraged.

The BDR classification system has been developed to improve the blast design process. Blast design is the fundamental engineering control to obtain consistent output that achieves the results demanded by the relevant managerial and technical blasting objectives.

The design of wall control blasts must explicitly address both profile and damage control objectives. This could be achieved over a period of time by trial and refinement. However, the approach outlined in this paper, using blast modelling has proved to be quicker, less prone to misinterpretation, and, importantly, it allows for optimisation.

The four main approaches to blast design are experience based, blast trial based, empirical methods and the use of blast models.

Pre-split blasting is not straight forward and for optimisation it requires a combination of design analysis effort and field trials to assist the design process.

Timing design can be used to reduce vibration levels by preventing waveform crowding. The delay sequence introduces two main influences: waveform superposition and vibration screening. Reverse firing (shield blasting) can be used when the charge weight/distance configuration has been determined for each blasthole (row).

Modified production blasts are hybrid blasts consisting of a trim blast pattern close to the wall, coupled with a production blast pattern away from wall areas. From a design perspective they have more complex blasting objectives, but can rely on the spatial separation involved.

Embarking on a slope steepening programme requires a strategic decision to be made. If the critical success factors are in place such an undertaking can be rewarding for the people involved and value enhancing for the mining company. Such a design journey may require a number of years.

REFERENCES

Battison, R., Esen, S., Duggan, R., Henley, K. & Dare-Bryan, P. 2015. Reducing crest loss at Barrick Cowal Gold Mine. *Proceeding of 11th Int. Symp. on Rock Fragmentation by Blasting*. 24-26 August 2015, Sydney, Australia.

Blair, D. and Minchinton, A. 2006. Near field blast vibration models. *Proc. 8th Int. Symp. on Rock Fragmentation by Blasting, Fragblast* 8, Santiago, Chile, pp. 152-159.

Blair, D.P. 2015a. The free surface influence on blast vibration. *Int J of Rock Mechanics and Mining Sciences*, Vol 2 (77), pp. 182 - 191.

Blair, D.P. 2015b. Wall control blasting. *Keynote address in proceeding of 11th Int Symp on Rock Fragmentation by Blasting*. 24-26 August 2015, Sydney, Australia.

Blair, D.P. 2018. Vibration modelling and mechanisms for wall control blasting. *Proceeding of 12th Int Symp on Rock Fragmentation by Blasting.* Luleå Sweden 11-13 June 2018.

Blair, D.P. & Little, T.N. 2019. Advanced wall control blasting short course. Version 8 April. Published by Blast Geomechanics Pty Ltd.

Bungard, G.P., Gleeson, A. & Basson, F.R.P. 2016. Slope steepening of the Golden Pike west wall at Fimiston Pit. *The First Asia Pacific Slope Stability in Mining (APSSIM) Conference*, held in Brisbane, Australia, 6-8 September 2016.

Cebrian, B., Rocha, M., Morales, B., Castanon, J.L. & Floyd, J. 2018. Full wall control blasting optimisation. *J Explosives Engineering* Volume 35 Number 4. ISEE publication.

Etchells, S.J., Sellers, E.J. & Furtney J. 2013. Understanding the blast damage mechanisms in slopes using observations and numerical modelling. *Proceedings of the 2013 Int Symp on Rock Slope Stability in Open Pit Mining and Civil Engineering* (Editor: Phil Dight ACG). 25-27 September, Brisbane, Australia.

Gibson, W.H., de Bruyn, I.A. & Walker, D.J.H. 2006. Considerations in the optimisation of bench face angle and berm width geometries for open pit mines. *Proc. South African Institute of Mining and Metallurgy* (SAIMM) Int Symp on Stability of Rock Slopes in Open Pit Mining and Civil Eng, 557-578.

Graf, C.C. & Sullivan, R. 2016. A journey of wall control improvement at Boddington Gold. *The First Asia Pacific Slope Stability in Mining (APSSIM) Conference.* Held in Brisbane, Australia, 6-8 September 2016.

Juldyz, A. 2019. Use of the excavation compliance indicator at the Oyu Tolgoi copper–gold mine, Mongolia. *Proceeding of Mining Geomechanical Risk conference*. J Wesseloo (ed.) Australian Centre for Geomechanics, Perth, pp 337-350.

Lewandowski, T., Luan Mai, V.K. & Danell, R.E. 1996. Influence of discontinuities on pre-splitting effectiveness. *Proceedings of 5th Int. Symp. on Rock Fragmentation by Blasting.* 25-29 August 1996, Montreal, Quebec, Canada.

Little, T.N. 2015. Classification and development in grade current blasting for surface mines. *Proceedings of 11th Int Symp on Rock Fragmentation by Blasting*. 24-26 August 2015, Sydney, Australia.

Little, T.N. 2017. Blast design requirements classification system for blast purposes. *Proceedings of EFEE 9th World Conference on Explosive and Blastin*g, Stockholm, Sweden.

Lu, W., Yan, P., Hu, Y., Zhang, Y., Chen, M. & Gao, Q. 2018. A review of dam foundation excavation techniques in China. *Proceeding of 12th Int. Symp. on Rock Fragmentation by Blasting*. Luleå Sweden 11-13 June 2018.

Marklund, P-I., Sjoberg, J., Ouchterlony, F. & Nilsson, N. 2007. Improved blasting and bench slope design at the Aitik Mine. *Proceedings of the 2007 Int Symp on Rock Slope Stability in*

Open Pit Mining and Civil Engineering. 12-14 September, Perth, Australia.

Seery, J. & Lapwood, J. 2007. Use of an excavation compliance indicator to assess conformance to slope design. In Y Potvin (ed.), *Proceedings of the 2007 Int Sym on Rock Slope Stability in Open Pit Mining and Civil Engineering*, Australian Centre for Geomechanics, Perth, pp. 431–437.

Williams, P., Floyd, J., Chitombo, G. & Maton, T. 2009. Design implementation. In J Read & P Stacey (eds), *Guidelines for Open Pit Slope Design*, CSIRO Publishing, Collingwood, pp 265–326.